

DOKUZ EYLÜL UNIVERSITY
GRADUATE SCHOOL OF NATURAL AND APPLIED SCIENCES

**REACTIVE POWER COMPENSATION IN
DISTRIBUTION SYSTEM**

by
Ali Eren KOCAMIŞ

January, 2009
İZMİR

REACTIVE POWER COMPENSATION IN DISTRIBUTION SYSTEM

**A Thesis Submitted to the
Graduate School of Natural and Applied Sciences of Dokuz Eylül University
In Partial Fulfillment of the Requirements for the Degree of Master of Science
in Electrical-Electronically Engineering, Applied Electronically Program**

**by
Ali Eren KOCAMIŞ**

January, 2009

İZMİR

M. Sc THESIS EXAMINATION RESULT FORM

We have read the thesis entitled **REACTIVE POWER COMPENSATION IN DISTRIBUTION SYSTEM** completed by **ALİ EREN KOCAMIŞ** under supervision of **PROF. DR. EYÜP AKPINAR** and we certify that in our opinion it is fully adequate, in scope and in quality, as a thesis for the degree of Master of Science.

.....
Prof. Dr. Eyüp AKPINAR

Supervisor

.....

(Jury Member)

.....

(Jury Member)

Prof. Dr. Cahit HELVACI
Director
Graduate School of Natural and Applied Sciences

ACKNOWLEDGEMENTS

I express my deepest gratitude to my advisor Prof. Dr. Eyüp AKPINAR for his guidance and support in every stage of my research. The technique background and the research experience I have gained under his care will be valuable asset to me in the future.

This thesis was carried out as a part of project, ‘Türkiye Elektrik Sisteminde Güç Kalitesine Etki Eden Değişkenleri ve Güç Akışını İzleme, Problemlerin Tespiti, Değerlendirilmesi ve Karşı Önlemlerin Hayata Geçirilmesi Projesi’ sponsored by Turkish Scientific and Research Council (TÜBİTAK) under contract no. 105G129 (106G012). I would like to thank them for their financial support.

I also would like to thank my parents for their understanding and never ending support throughout my life.

Ali Eren KOCAMIŞ

REACTIVE POWER COMPENSATION IN DISTRIBUTION SYSTEM

ABSTRACT

In this thesis, thyristor controlled reactor is designed and analyzed to compensate the reactive power demand in balanced and unbalanced loads. The arc furnaces in the region of Aliğa-İzmir are considered the load in this type.

This system is preferred in the application of reactive power compensation if the load is varying faster such that the traditional reactive power compensation algorithms having mechanical contactors are not fast enough. The system proposed here is used either with a fix capacitor or with the passive filter circuit.

Simulations are carried out in MATLAB / Simulink and PSCAD. The application software is converted from MATLAB into TMS320F2812 eZdsp. The system is built at 3 kVAR rating in the Electrical Machines Laboratory. The PSPICE program is also used to design electronic circuit implemented in this work.

Keywords : TCR, Compensation, DSP F2812

ELEKTRİK ENERJİ DAĞITIM SİSTEMLERİNDE REAKTİF GÜÇ KOMPANZASYONU

ÖZ

Bu tezde, dengeli ve dengesiz yüklerde ihtiyaç duyulan reaktif gücü kompanze etmek için thristör kontrollü reaktörlerin tasarımı ve analizleri yapılmıştır. Yük olarak Aliğa-İzmir bölgesindeki ark ocakları göz önünde bulundurulmuştur.

Hızlı değişen yüklerde reaktif güç kompanzasyonunda bu sistemlerin kullanılması tercih edilmektedir. Mekanik kontaklar kullanılarak yapılan klasik kompanzasyonlar bu tarz hızlı değişen sistemler için yeterince hızlı değildir. Bu sistemlerin fix kapasitörler ya da pasif filtrelerle kullanılması önerilmektedir.

Simülasyon kısmı MATLAB/simulink ve PSCAD ortamlarında yapıp uygulama yazılımı MATLAB'ten çevrilerek TMS320F2812 DSP kitine yüklenip laboratuvar çalışması yapıldı. 3kVAR lık sistem elektrik makineleri laboratuvarında oluşturuldu. Bu çalışmada kullanılan elektronik devrelerin tasarımında PSPICE programı kullanılmıştır.

Anahtar Sözcükler: TKR(Thristör Kontrollü Reaktör), Kompanzasyon, DSP F2812

CONTENTS

	Page
M. Sc THESIS EXAMINATION RESULT FORM	ii
ACKNOWLEDGEMENTS	iii
ABSTRACT	iv
ÖZ	v
CHAPTER ONE-INTRODUCTION	1
CHAPTER TWO-THEORY OF THRISTOR CONTROLLED REACTOR	4
2.1 Principles Of TCR	4
2.2 Analysis Of Load Compensation.....	7
2.3 Load Compensation In Terms Of Symmetrical Components	20
CHAPTER THREE-SIMULATION OF THRISTOR-CONTROLLED REACTOR AND CIRCUITS FOR APPLICATON	33
3.1 Modeling And Simulation TCR In PSCAD	33
3.1.1 Balanced Condition	35
3.1.2 Unbalanced Condition	40
3.2 Modeling And Simulation TCR In MATLAB	44
3.2.1 Balanced Condition	45
3.2.2 Unbalanced Condition	49
3.3 Harmonic Analysis	53
3.4 Current And Voltage Measurement Sensors And Circuits	62
3.5 Pulse Drive Circuit	63
3.6 Zero Crossing Detection	64
3.7 Phase Delay Circuit In PSPICE.....	67
3.8 Zero Crossing Circuit With Phase Delay.....	68

CHAPTER FOUR-EXPERIMENTAL RESULTS OF TCR.....	71
CHAPTER FIVE-PASSIVE FILTER ANALYSIS	82
5.1 Passive Filter Analysis In PSCAD	84
5.1.1 Passive Filter Analysis Of Plant1 In PSCAD	84
5.1.2 Passive Filter Analysis Of Plant2 In PSCAD	87
5.2 Frequency Response Of Passive Filters In Plant1 And Plant2	90
CHAPTER SIX-CONCLUSION.....	95
REFERENCES	96

CHAPTER ONE

INTRODUCTION

In an ideal AC power system, the voltage and current waveforms should be free from harmonics, frequency should be constant at each measurement point and the power factor should be unity.

If the reactive power of the load is changing rapidly, fast response compensators are required. This is typically the case of FC-TCR (Fixed Capacitor – Thyristor Controlled Reactor). The ability of an FC-TCR compensator is to change its reactive power within theoretical time of half a period.

The TCR are also used to regulate the transmission voltage at a given terminal and to provide power factor correction. Also, when load is unbalanced, TCR provides reactive power compensation to balance the demand of load. The compensation requirements reduce reactive power demanded by the source. Figure 1.1 shows the load drawing the reactive power (inductive) which is generated from capacitor block. But when these capacitors generate reactive power more than demand of load, this reactive power will flow through source. This leading power factor at the source can be brought to unity with the help of TCR.

The theory of the reactive power measurement and determination of the susceptances of the phases are given in (Miller, 1982) in detail. (Tosato, Quiaia, & Rabach, 1989), the system is modeled in package programs for simulation which consist of FC, TCR and arc furnaces. The theoretical approach and the computer modeling have been compared too. The control strategy is based on unbalanced supply voltage conditions for the compensation (Farias, de Oliveira, Silveria, & Miskulin, 1991). New formulations to evaluate the necessary TCR phase susceptances under unbalanced voltage condition are also provided (Farias, & others, 1991). (Lee, & Kim, 2007), the system is implemented in a laboratory which consists of capacitor bank, TCR and variable load. A fully controlled TCR is described and implemented using a digital signal processing chip ADMC401. Where controls

method guarantees that the compensation process will perform within $\frac{1}{4}$ cycle of the fundamental line period where line frequency is 60 Hz. (Gyugyi, & Taylor, 1980), the operating and performance characteristics of two basic types of Thyristor-Controlled Reactor, one with a fixed capacitor bank and the other with synchronously switching capacitor (TSC) banks, are presented with regard to power transmission system applications.

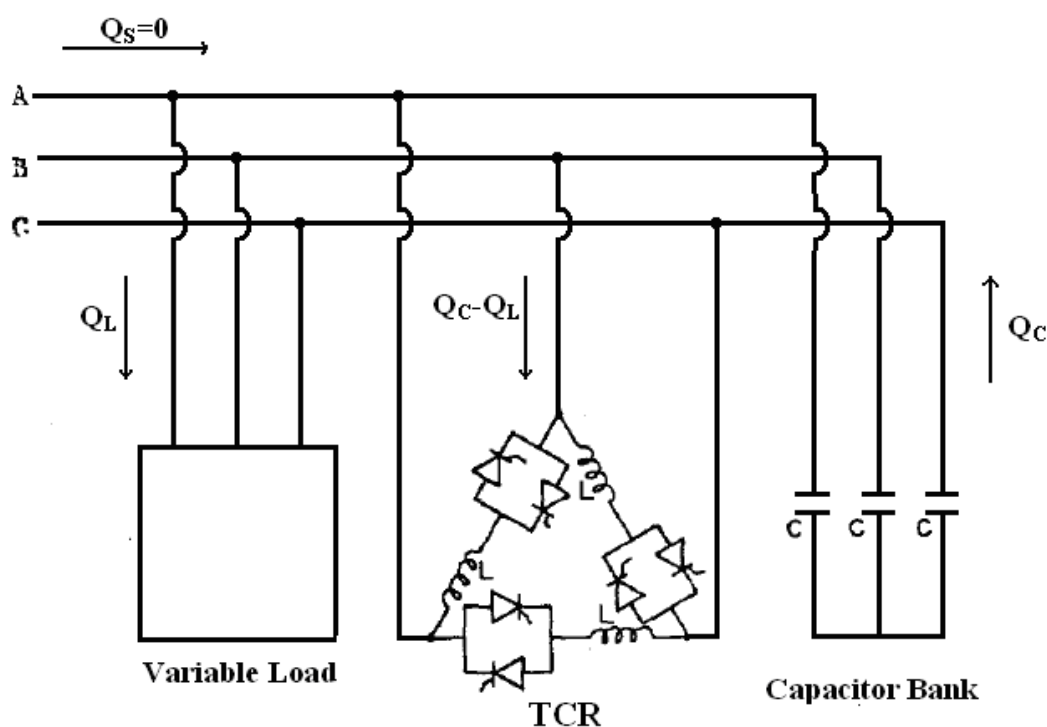


Figure 1.1 Variable load, TCR and capacitor bank.

Content of the thesis can be summarized briefly as follows;

In chapter two, the basics of TCR are explained and the useful equations are derived. It is proved that how the unbalanced loads are converted to balanced loads with the help of TCR.

In chapter three, the PSCAD and MATLAB package programs are used to prepare a model for simulation. The results are compared for verification of correct analysis. Then the MATLAB/Simulink program is converted to the ones required for the DSPF2812 in chapter four.

In chapter five, given the passive filter analysis is done for steel industry (named Plant1 and Plant2 in this thesis). The passive filters generate the reactive power under fundamental frequency of voltage and current while they filter out the harmonic current at different frequencies. This reactive power is usually absorbed by the help of TCR unit in steel industry.

Chapter six is concerned on conclusions of the research done in the topic of thesis.

CHAPTER TWO

THEORY OF THYRISTOR CONTROLLED REACTOR

2.1 Principles Of TCR

Two oppositely poled thyristors in series with an inductance are shown in figure 2.1. If the thyristors are gated into conduction precisely at the peaks of the supply voltage, full conduction results in the reactor.

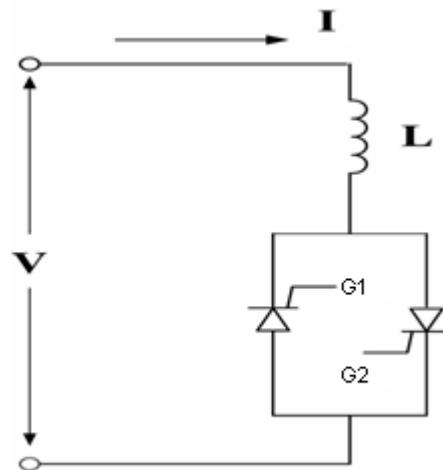


Figure 2.1 Equivalent circuit of TCR.

Let us define,

$$I = \frac{V}{X_L} = \frac{V}{\omega L} \quad (2-1)$$

Here, V is RMS value of source voltage, L is the inductance in Henry and ω is the supply frequency in rad/s.

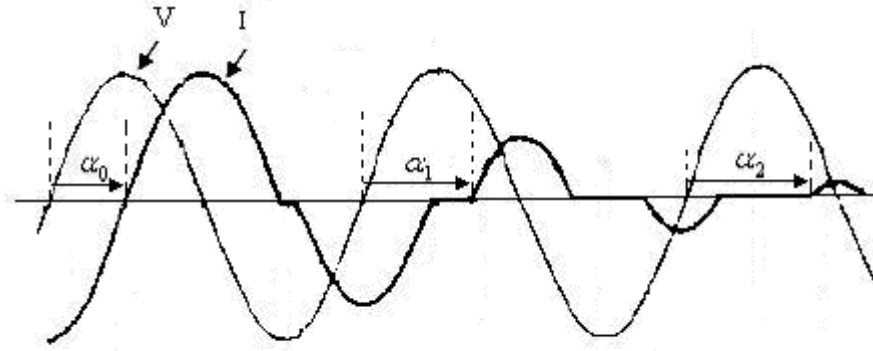


Figure 2.2 Current and voltage waveform when different angle.

The current lags the voltage by 90° , hence, thyristor starts conducting from maximum of voltage. When the gating is delayed by α and this angle changes 90 to 180, the rms value of current waveform can be controlled as being shown in figure 2.2.

The effect of increasing the delay angle is to reduce the fundamental harmonic component of the current. This is equivalent to an increase in the inductance of the reactor, reducing its reactive power as well as its current.

The instantaneous current i is given by (Acha, Agelidis, Anaya-Lara, & Miller, 2002).

$$i(t) = \begin{cases} \frac{\sqrt{2} \cdot V}{X_L} (\cos(\alpha) - \cos(\omega t)) & \alpha \leq \omega t \leq \alpha + \sigma \\ 0 & \alpha + \sigma \leq \omega t \leq \alpha + \pi \end{cases} \quad (2-2)$$

The fundamental component is found by Fourier analysis and is given by (Acha, & others, 2002).

$$I_1 = \frac{\sigma - \sin \sigma}{\pi X_L} V \quad \text{A rms} \quad (2-3)$$

σ is the conduction angle, related to α by the equation,

$$\sigma = 2(\pi - \alpha) \quad (2-4)$$

Let us define

$$\frac{I_1}{V} = B_L(\sigma) \quad (2-5)$$

Where $B_L(\sigma)$ is changeable fundamental frequency susceptance controlled by the conduction angle according to the law (Acha, & others, 2002).

$$B_L(\sigma) = \frac{\sigma - \sin(\sigma)}{\pi X_L} \quad (2-6)$$

The maximum value of B_L is $\frac{1}{X_L}$, when $\sigma = \pi$.

2.2 Analysis Of Load Compensation

Wye connected impedances is shown in figure 2.3. Impedances are not equal to each other and complex. Supply voltages are assumed to be balanced.

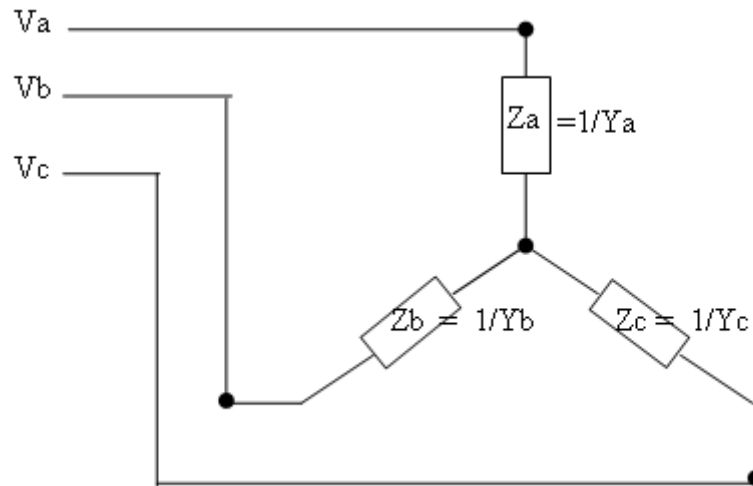


Figure 2.3 Three phase wye connected unbalanced load represented by impedances.

Here,

$$V_a = V$$

$$V_b = KV$$

$$V_c = K^2 V \quad (2-7)$$

$$\text{Where } K = e^{-\frac{j2\pi}{3}}$$

Delta connected admittances are shown in figure 2.4. Wye connected network is converted to delta connected network.

When converting from a wye to equivalent delta, the following equations are used:

$$Z_{ab} = \frac{Z_a * Z_b + Z_b * Z_c + Z_c * Z_a}{Z_c} \quad (2-8)$$

$$Z_{bc} = \frac{Z_a * Z_b + Z_b * Z_c + Z_c * Z_a}{Z_a} \quad (2-9)$$

$$Z_{ca} = \frac{Z_a * Z_b + Z_b * Z_c + Z_c * Z_a}{Z_b} \quad (2-10)$$

$$Z_a = \frac{1}{Y_a}, Z_b = \frac{1}{Y_b}, Z_c = \frac{1}{Y_c} \quad (2-11)$$

Substituting the equation (2-11) into (2-8):

$$Z_{ab} = \frac{Y_a + Y_b + Y_c}{Y_a * Y_b} \quad (2-12)$$

$$Y_{ab} = \frac{1}{Z_{ab}} = \frac{Y_a * Y_b}{Y_a + Y_b + Y_c} \quad (2-13)$$

Similarly, Y_{bc} and Y_{ca} admittances can be found.

$$Y_{bc} = \frac{Y_b * Y_c}{Y_a + Y_b + Y_c} \quad (2-14)$$

$$Y_{ca} = \frac{Y_c * Y_a}{Y_a + Y_b + Y_c} \quad (2-15)$$

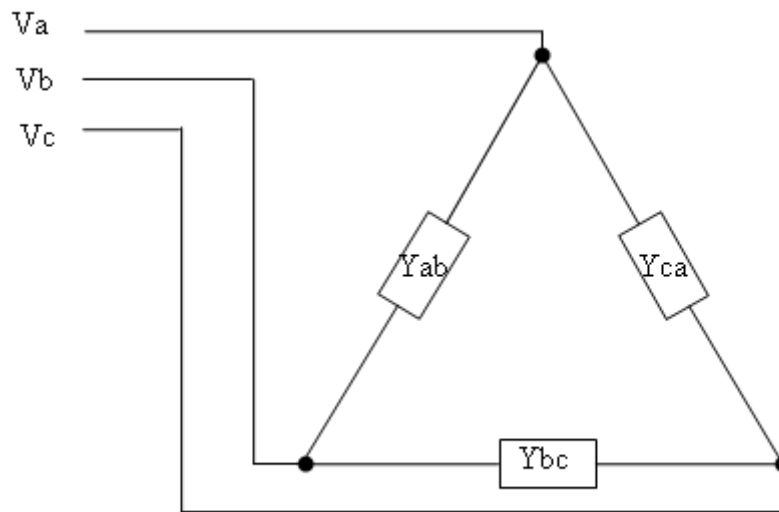


Figure 2.4 Delta equivalent admittances converted from wye connected impedances.

The admittances Y_{ab} , Y_{bc} and Y_{ca} are unequal. And Y_{ab} , Y_{bc} and Y_{ca} are composed of real and reactive parts.

$$Y_{ab} = G_{ab} + jB_{ab} \quad (2-16)$$

$$Y_{bc} = G_{bc} + jB_{bc} \quad (2-17)$$

$$Y_{ca} = G_{ca} + jB_{ca} \quad (2-18)$$

Firstly, the reactive part of admittances can be cancelled when the compensating susceptance connected in parallel with admittances, shown in figure 2.5.

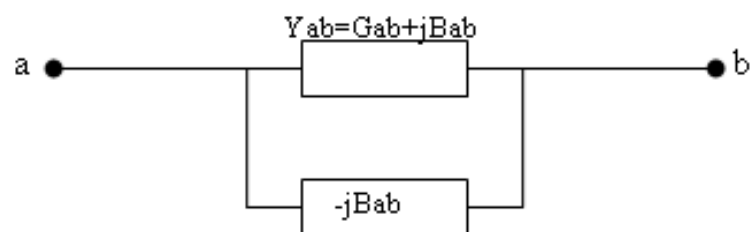


Figure 2.5 Cancelled reactive part of admittances by $-B_{ab}$.

The reactive part of admittances is B_{ab} which is cancelled by $-B_{ab}$ and then admittance is only equal real admittance (G_{ab}).

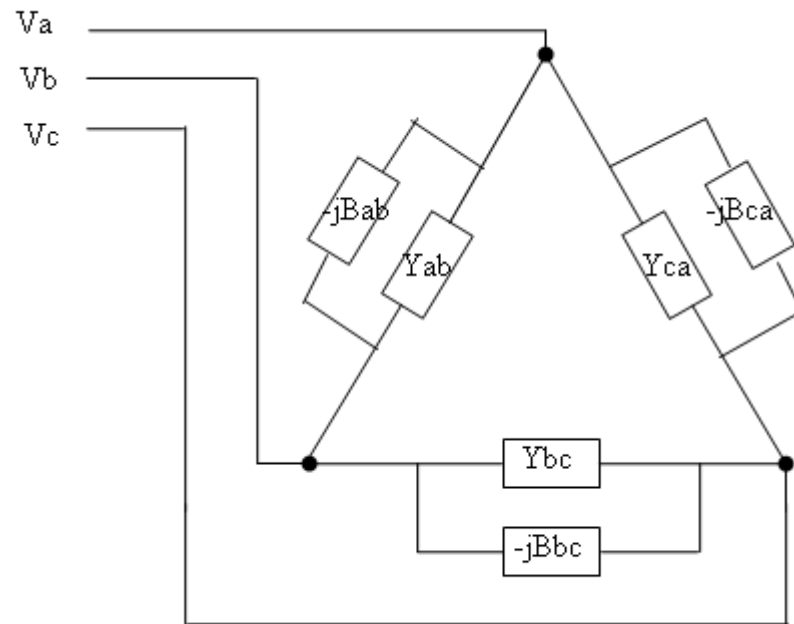


Figure 2.6 Compensating susceptance connected in parallel with admittances.

In figure 2.6, the compensating susceptances are connected in parallel to admittances.

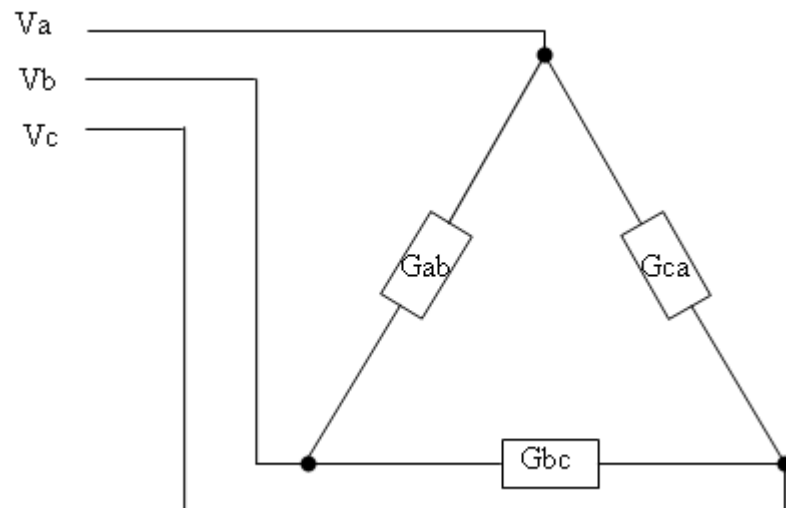


Figure 2.7 Real and unbalanced load with unity power factor.

The load given in figure 2.7 will further be balanced by using the same compensator.

The three load admittances can be compensated separately as if they were three single phase loads. Consider for example phase ab. It is clear that the load on the ac supply becomes balanced if a capacitive susceptance is connected between phase a and c, and an inductive susceptance is connected between phase b and c as shown figure 2.9 (a).

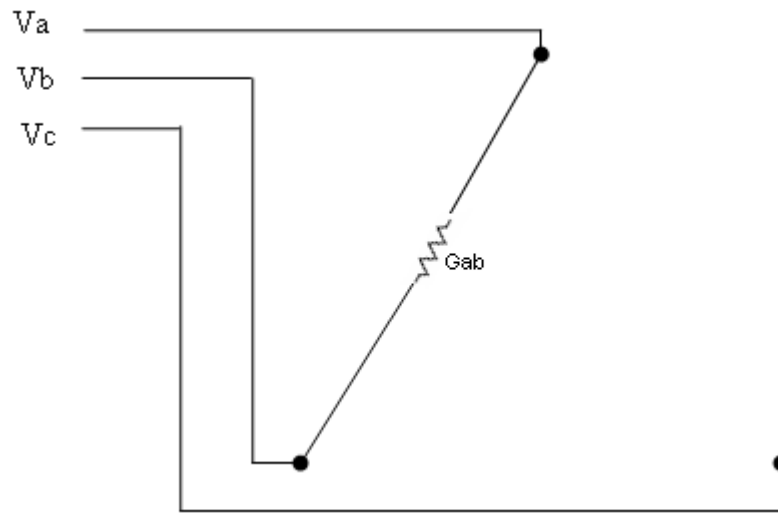


Figure 2.8 Single phase unbalanced load.

In order to obtain a balance single phase real (resistive) load, G_{ab} , two susceptances (inductive and capacitive), B_{ab}^{bc} and B_{ab}^{ca} can be inserted into the circuit;

Capacitive susceptance;

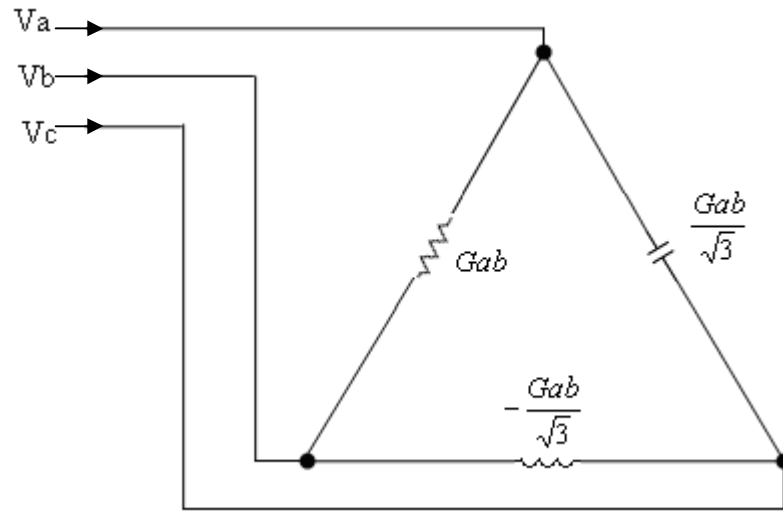
$$B_{ab}^{ca} = j \frac{G_{ab}}{\sqrt{3}} \quad (2-19)$$

Inductive susceptance;

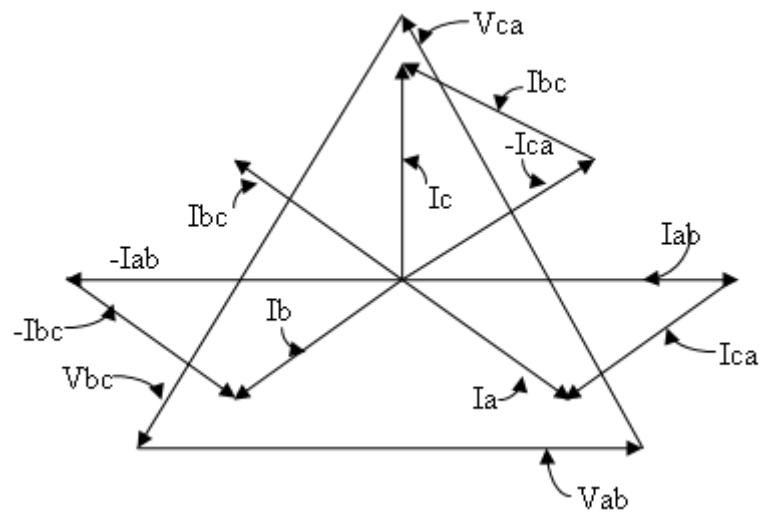
$$B_{ab}^{bc} = -j \frac{G_{ab}}{\sqrt{3}} \quad (2-20)$$

In figure 2.9 (a), the currents of delta connected load branch are unbalanced, but reactive power is not drawn from the supply because the capacitor (between phase a and c) generates the reactive power and the reactor (between phase b and c) absorbs

this reactive power so that the reactive power is neither generated nor absorbed in the supply.



(a)



(b)

Figure 2.9 (a) Positive sequence balancing of the single-phase unity power factor.
 (b) Phasor diagram of single phase unity power factor.

In figure 2.9 (b), where a phasor diagram illustrates how two (capacitive and inductive) susceptances transform the single phase real load into a balanced three phase real load.

The relation between line currents and load phase currents are shown equation (2-21), (2-22) and (2-23).

$$I_a = I_{ab} + I_{ca} = V_a * G_{ab} \quad (2-21)$$

$$I_b = -I_{ab} - I_{bc} = V_b * G_{ab} \quad (2-22)$$

$$I_c = I_{bc} - I_{ca} = V_c * G_{ab} \quad (2-23)$$

After compensation the compensated load may be represented as three wye connected resistor, shown in figure 2.10 (Miller, 1982).

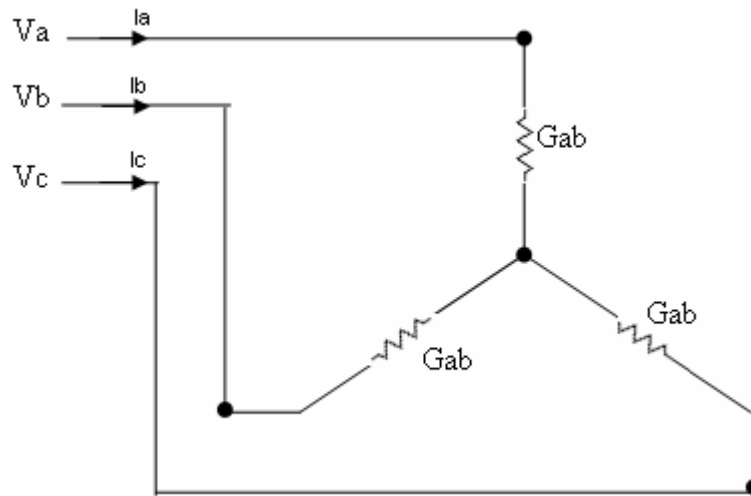


Figure 2.10 Compensated load.

A procedure similar to that outlined above can be followed to compensate the load admittances in phases bc and ca. First, susceptances B_{bc} and B_{ca} are cancelled by two compensating susceptances of opposite sign, $-B_{bc}$ and $-B_{ca}$, respectively. Second, the conductances, G_{bc} and G_{ca} are balanced two pairs of susceptances (capacitive and inductive) respectively.

$$B_{bc}^{ca} = -j \frac{G_{bc}}{\sqrt{3}} \quad (2-24)$$

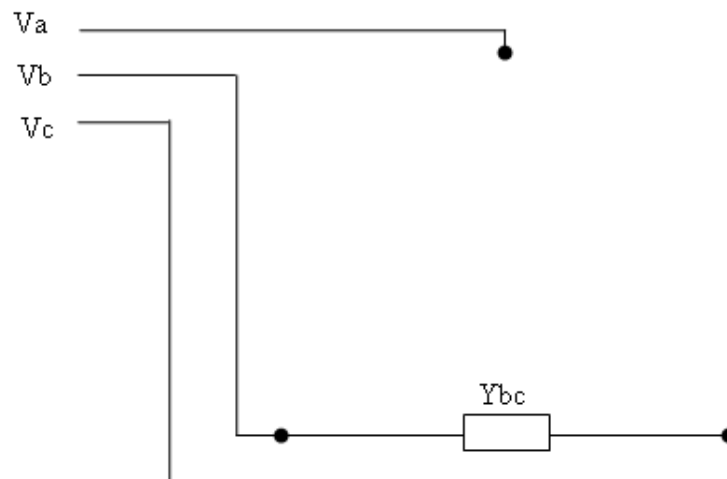
$$B_{bc}^{ab} = j \frac{G_{bc}}{\sqrt{3}} \quad (2-25)$$

And

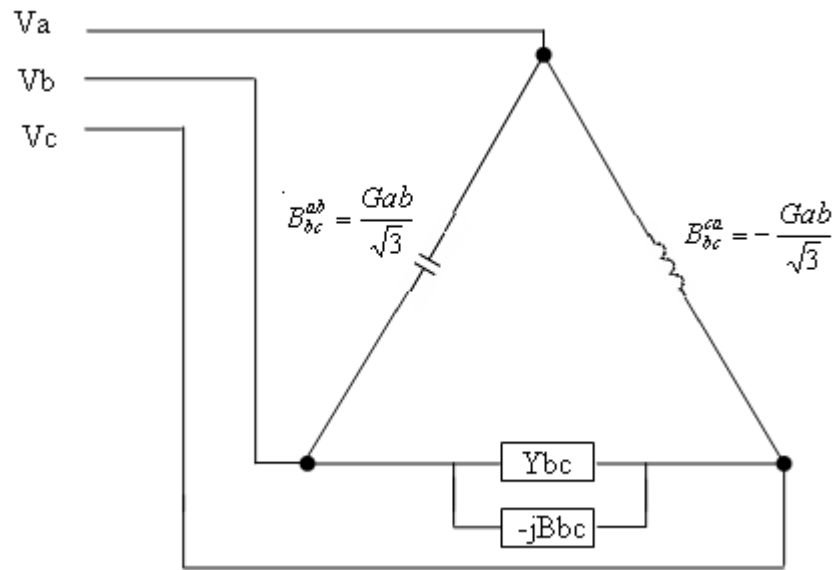
$$B_{ca}^{ab} = -j \frac{Gca}{\sqrt{3}} \quad (2-26)$$

$$B_{ca}^{bc} = j \frac{Gca}{\sqrt{3}} \quad (2-27)$$

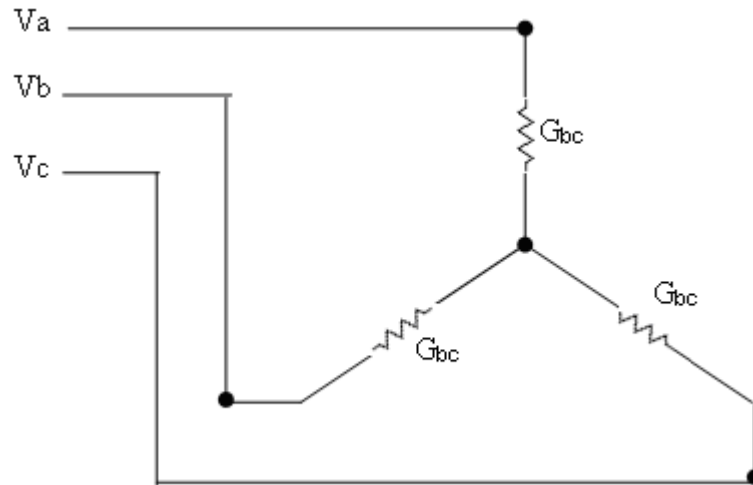
The compensation steps of admittances Y_{bc} is show figure 2.11. Where first imaginary part of Y_{bc} is cancelled and capacitive susceptance is connected between phase a and b and inductive susceptance is connected between phase a and c. Thus we transform the single phase real load into a balanced three phase real load.



(a)



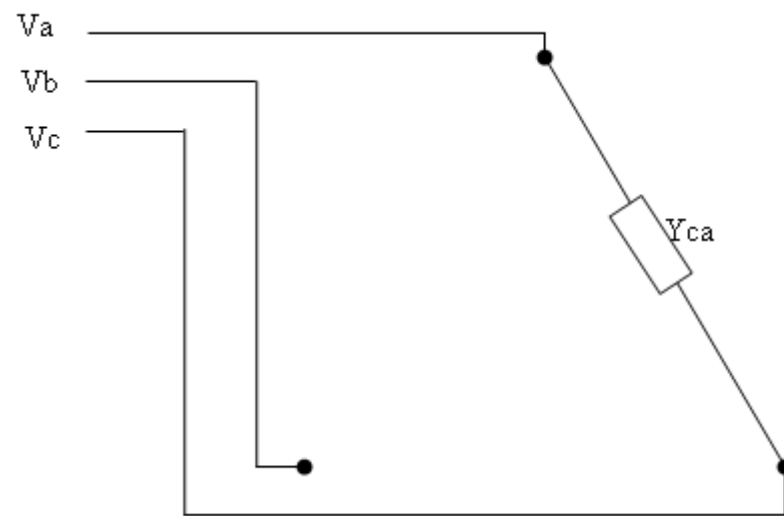
(b)



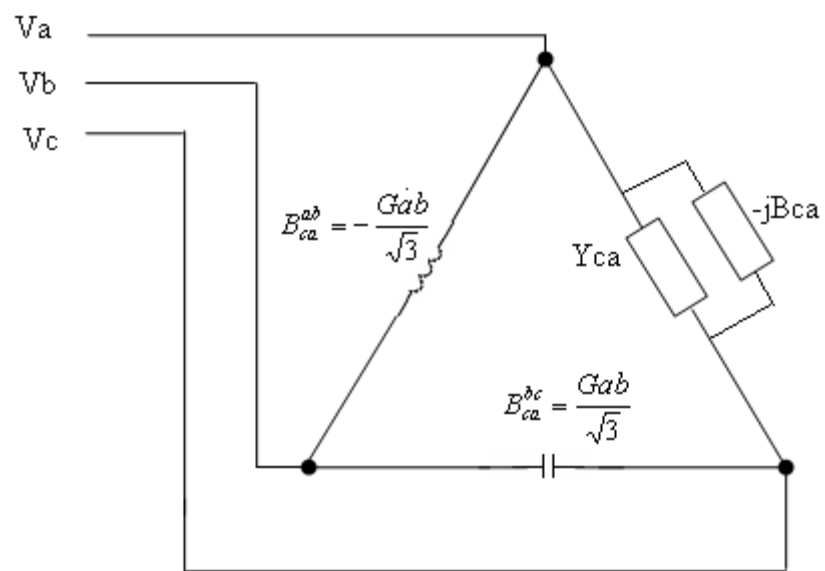
(c)

Figure 2.11 (a) Single phase, bc, unbalanced load, (b) positive sequence balancing of the single-phase unity power factor, (c) compensated load

Lastly, it is clear that the compensation steps of admittances Y_{ca} is show figure 2.12 where first imaginary part of Y_{ca} is cancelled and capacitive susceptance is connected between phase b and c and inductive susceptance is connected between phase a and b . Thus we transform the single phase real load into a balanced three phase real load.



(a)



(b)

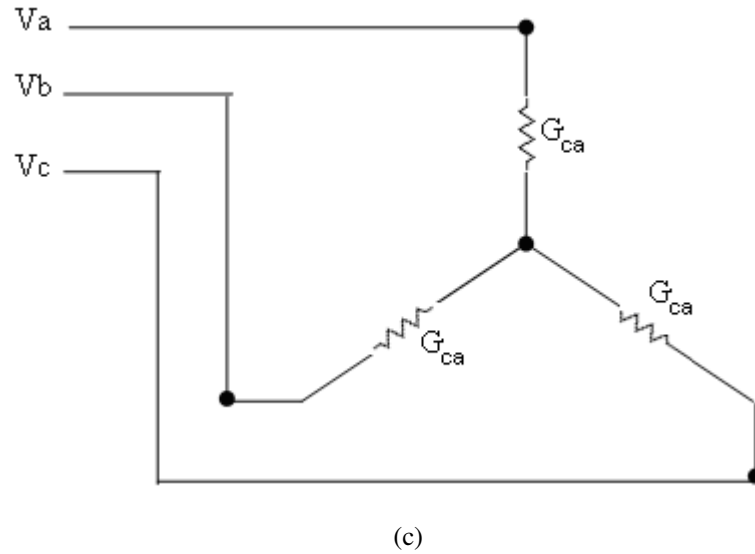


Figure 2.12 (a) single phase, ca, unbalanced load, (b) Positive sequence balancing of the single-phase unity power factor, (c) compensated load.

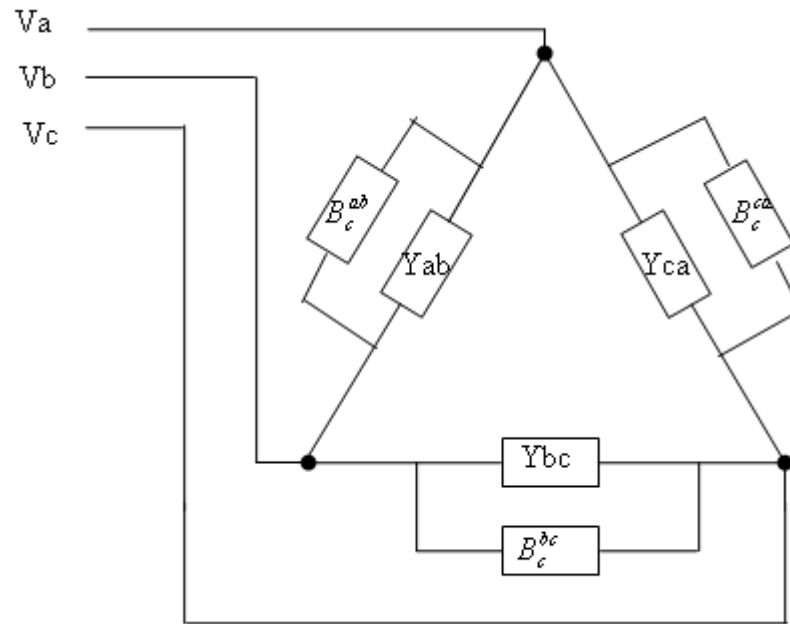
Complete compensation of the three phase load is readily obtained by adding all compensating susceptances in each phase as illustrated in figure 2.13. Thus, the resultant compensating susceptance B_c^{ab} , B_c^{bc} and B_c^{ca} are total of the susceptances of individual phases.

$$B_c^{ab} = -B_{ab} + B_{bc}^{ab} + B_{ca}^{ab} \quad (2-28)$$

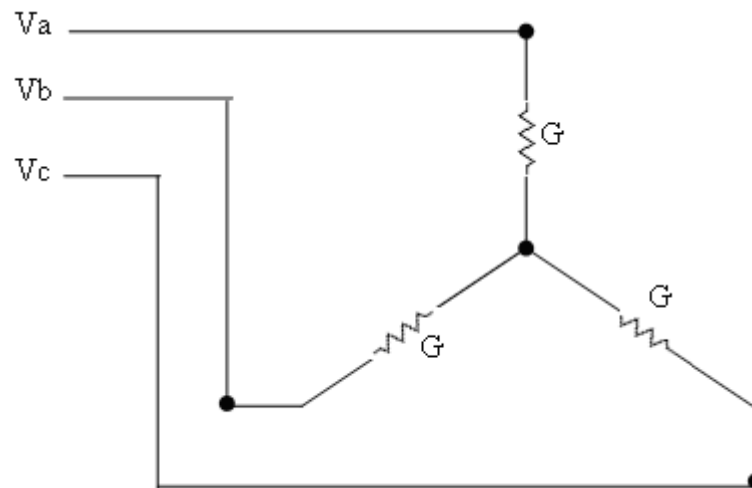
$$B_c^{bc} = -B_{bc} + B_{ca}^{bc} + B_{ab}^{bc} \quad (2-29)$$

$$B_c^{ca} = -B_{ca} + B_{ab}^{ca} + B_{bc}^{ca} \quad (2-30)$$

Where superscript (c) stands for 'compensating'.



(a)



(b)

Figure 2.13 Application of principles of single phase load compensation to an unbalanced three phase load.

Here, G is total of G_{ab} , G_{bc} and G_{ca} (Miller, 1982), which are the compensating admittance.

First, compensating susceptances of between phase a and b. Substituting the equation (2.25) and (2.26) into (2.28):

$$B_c^{ab} = -B_{ab} + \frac{Gbc}{\sqrt{3}} - \frac{Gca}{\sqrt{3}} \quad (2-31)$$

Second, compensating susceptances of between phase b and c. Substituting the equation (2.20) and (2.27) into (2.29):

$$B_c^{bc} = -B_{bc} - \frac{Gab}{\sqrt{3}} + \frac{Gca}{\sqrt{3}} \quad (2-32)$$

Last, compensating susceptances of between phase c and a. Substituting the equation (2.19) and (2.24) into (2.30):

$$B_c^{ca} = -B_{ca} + \frac{Gab}{\sqrt{3}} - \frac{Gbc}{\sqrt{3}} \quad (2-33)$$

As a result, an arbitrary ungrounded unbalanced linear three phase load can be transformed into a balanced three phase load without changing the real power exchange between load and source.

2.3 Load Compensation In Terms Of Symmetrical Components

The delta equivalent of the load, defined by admittances Y_{ab} , Y_{bc} , and Y_{ca} is used again for convenience, and compensator, defined by compensating susceptances B_c^{ab} , B_c^{bc} and B_c^{ca} , as shown in figure 2.14.

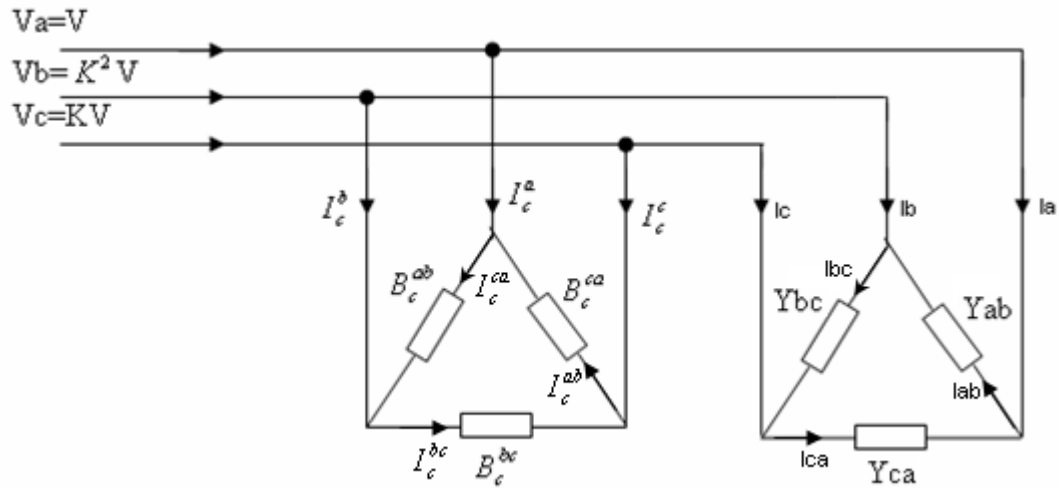


Figure 2.14 Three phase unbalanced load and connected with parallel compensator.

The source voltages are assumed balanced with a positive phase rotation, that is

$$V_a = V \quad (2-34)$$

$$V_b = K^2 V \quad (2-35)$$

$$V_c = KV \quad (2-36)$$

Where,

$$K = e^{\frac{j2\pi}{3}} \quad (2-37)$$

Line to line voltages are:

$$V_{ab} = V_a - V_b = V - K^2V = (1 - K^2)V \quad (2-38)$$

$$V_{bc} = V_b - V_c = K^2V - KV = (K^2 - K)V \quad (2-39)$$

$$V_{ca} = V_c - V_a = K V - V = (K - 1)V \quad (2-40)$$

The currents drawn by the delta load branches are:

$$I_{ab} = Y_{ab} * V_{ab} = Y_{ab} * (1 - K^2)V \quad (2-41)$$

$$I_{bc} = Y_{bc} * V_{bc} = Y_{bc} * (K^2 - K)V \quad (2-42)$$

$$I_{ca} = Y_{ca} * V_{ca} = Y_{ca} * (K - 1)V \quad (2-43)$$

Line currents are:

$$I_a = I_{ab} - I_{ca} \quad (2-44)$$

$$I_b = I_{bc} - I_{ab} \quad (2-45)$$

$$I_c = I_{ca} - I_{bc} \quad (2-46)$$

Substituting the equation (2-41) and (2-43) into (2-44):

$$\begin{aligned} I_a &= Y_{ab} * (1 - K^2)V - Y_{ca} * (K - 1)V \\ &= [Y_{ab} * (1 - K^2) - Y_{ca} * (K - 1)]V \end{aligned} \quad (2-47)$$

Substituting the equation (2-41) and (2-42) into (2-45):

$$\begin{aligned} I_b &= Y_{bc} * (K^2 - K)V - Y_{ab} * (1 - K^2)V \\ &= [Y_{bc} * (K^2 - K) - Y_{ab} * (1 - K^2)]V \end{aligned} \quad (2-48)$$

Substituting the equation (2-42) and (2-43) into (2-46):

$$\begin{aligned} I_c &= Yca^*(K-1)V - Ybc^*(K^2-K)V \\ &= [Yca^*(K-1) - Ybc^*(K^2-K)]V \end{aligned} \quad (2-49)$$

The symmetrical components in terms of the three line currents are given by

$$\begin{bmatrix} I^0 \\ I^+ \\ I^- \end{bmatrix} = \frac{1}{\sqrt{3}} \begin{bmatrix} 1 & 1 & 1 \\ 1 & K & K^2 \\ 1 & K^2 & K \end{bmatrix} \begin{bmatrix} I_a \\ I_b \\ I_c \end{bmatrix} \quad (2-50)$$

Here, I^0 , I^+ and I^- are the reference phasors of the zero, positive and negative sequence currents sets, respectively (Miller, 1982).

The currents (zero, positive and negative sequence) can be found from equation (2-50).

$$I^0 = \frac{I_a + I_b + I_c}{\sqrt{3}} \quad (2-51)$$

$$I^+ = \frac{I_a + KI_b + K^2I_c}{\sqrt{3}} \quad (2-52)$$

$$I^- = \frac{I_a + K^2I_b + KI_c}{\sqrt{3}} \quad (2-53)$$

The zero positive and negative sequence currents are obtained. Substituting the equation (2-47), (2-48) and (2-49) into (2-51), the zero sequence component of load current can be obtained as follows;

$$\frac{\sqrt{3}I^0}{V} = [Y_{ab}*(1-K^2) - Y_{ca}*(K-1) + Y_{bc}*(K^2-K)] + \quad (2-54)$$

$$[-Y_{ab}*(1-K^2) + Y_{ca}*(K-1) - Y_{bc}*(K^2-K)] = 0$$

Substituting the equation (2-47), (2-48) and (2-49) into (2-52), the positive sequence component of load current can be obtained as given below;

$$I^+ = \frac{[Y_{ab}*(1-K^2) - Y_{ca}*(K-1)]V}{\sqrt{3}} + \quad (2-55)$$

$$\frac{K[Y_{bc}*(K^2-K) - Y_{ab}*(1-K^2)]V}{\sqrt{3}} +$$

$$\frac{K^2[Y_{ca}*(K-1) - Y_{bc}*(K^2-K)]V}{\sqrt{3}}$$

$$I^+ = \frac{[Y_{ab}*(1-K^2)(1-K) + Y_{ca}*(K-1)(K^2-1)]V}{\sqrt{3}} + \quad (2-56)$$

$$\frac{[Y_{bc}*(K^2-K)(K-K^2)]}{\sqrt{3}}$$

$$I^+ = \frac{[3*Y_{ab} + 3*Y_{bc} + 3*Y_{ca}]V}{\sqrt{3}} = [Y_{ab} + Y_{bc} + Y_{ca}]V\sqrt{3} \quad (2-57)$$

Substituting the equation (2-47), (2-48) and (2-49) into (2-53), the negative sequence component of load current can be obtained as below;

$$I^- = \frac{[Y_{ab}*(1-K^2) - Y_{ca}*(K-1)]V}{\sqrt{3}} + \quad (2-58)$$

$$\frac{K^2[Y_{bc}*(K^2-K) - Y_{ab}*(1-K^2)]V}{\sqrt{3}} +$$

$$\frac{K[Y_{ca}*(K-1) - Y_{bc}*(K^2-K)]V}{\sqrt{3}}$$

$$= -[Y_{ab}*K^2 + Y_{bc} + Y_{ca}*K]V\sqrt{3}$$

When $Y_{ab} = Y_{bc} = Y_{ca}$ (balanced load), ($K^2 + K + 1 = 0$), there is no negative sequence current (Miller, 1982).

The symmetrical components of the line currents to a delta connected reactive compensator are given similarly by

$$I_c^{ab} = jB_c^{ab} * V_{ab} = jB_c^{ab} * (1 - K^2)V \quad (2-59)$$

$$I_c^{bc} = jB_c^{bc} * V_{bc} = jB_c^{bc} * (K^2 - K)V \quad (2-60)$$

$$I_c^{ca} = jB_c^{ca} * V_{ca} = jB_c^{ca} * (K - 1)V \quad (2-61)$$

The compensator line currents are:

$$I_c^a = I_c^{ab} - I_c^{ca} \quad (2-62)$$

$$I_c^b = I_c^{bc} - I_c^{ab} \quad (2-63)$$

$$I_c^c = I_c^{ca} - I_c^{bc} \quad (2-64)$$

We find compensator line currents. Substituting the equation (2-59) and (2-61) into (2-62):

$$\begin{aligned} I_c^a &= jB_c^{ab} * (1 - K^2)V - jB_c^{ca} * (K - 1)V \\ &= j[B_c^{ab} * (1 - K^2) - B_c^{ca} * (K - 1)]V \end{aligned} \quad (2-65)$$

Substituting the equation (2.59) and (2.60) into (2.63):

$$\begin{aligned} I_c^b &= jB_c^{bc} * (K^2 - K)V - jB_c^{ab} * (1 - K^2)V \\ &= j[B_c^{bc} * (K^2 - K) - B_c^{ab} * (1 - K^2)]V \end{aligned} \quad (2-66)$$

Substituting the equation (2.60) and (2.61) into (2.64):

$$\begin{aligned} I_c^c &= jB_c^{ca} * (K-1)V - jB_c^{bc} * (K^2 - K)V \\ &= j[B_c^{ca} * (K-1) - B_c^{bc} * (K^2 - K)]V \end{aligned} \quad (2-67)$$

$$\begin{bmatrix} I_c^0 \\ I_c^+ \\ I_c^- \end{bmatrix} = \frac{1}{\sqrt{3}} \begin{bmatrix} 1 & 1 & 1 \\ 1 & K & K^2 \\ 1 & K^2 & K \end{bmatrix} \begin{bmatrix} I_c^a \\ I_c^b \\ I_c^c \end{bmatrix} \quad (2-68)$$

We will find zero, positive and negative sequence of compensator currents from equation (2-68).

$$I_c^0 = \frac{I_c^a + I_c^b + I_c^c}{\sqrt{3}} \quad (2-69)$$

$$I_c^+ = \frac{I_c^a + KI_c^b + K^2I_c^c}{\sqrt{3}} \quad (2-70)$$

$$I_c^- = \frac{I_c^a + K^2I_c^b + KI_c^c}{\sqrt{3}} \quad (2-71)$$

Substituting the equation (2.65), (2.66) and (2.67) into (2.69):

$$\begin{aligned} I_c^0 &= j \frac{[B_c^{ab} * (1 - K^2) - B_c^{ca} * (K - 1) + B_c^{bc} * (K^2 - K)]V}{\sqrt{3}} \\ &+ j \frac{[-B_c^{ab} * (1 - K^2) + B_c^{ca} * (K - 1) - B_c^{bc} * (K^2 - K)]V}{\sqrt{3}} \end{aligned} \quad (2-72)$$

$$I_c^0 = 0 \quad (2-73)$$

Substituting the equation (2.65), (2.66) and (2.67) into (2.70):

$$\begin{aligned}
I_c^+ &= j \frac{[B_c^{ab} * (1 - K^2) - B_c^{ca} * (K - 1)]V}{\sqrt{3}} \\
&+ j \frac{[K[B_c^{bc} * (K^2 - K) - B_c^{ab} * (1 - K^2)]V]}{\sqrt{3}} \\
&+ j \frac{[K^2[B_c^{ca} * (K - 1) - B_c^{bc} * (K^2 - K)]V]}{\sqrt{3}}
\end{aligned} \tag{2-74}$$

$$\begin{aligned}
I_c^+ &= j \frac{[3 * B_c^{ab} + 3 * B_c^{bc} + 3 * B_c^{ca}]V}{\sqrt{3}} \\
&= j[B_c^{ab} + B_c^{bc} + B_c^{ca}]V\sqrt{3}
\end{aligned} \tag{2-75}$$

Substituting the equation (2.65), (2.66) and (2.67) into (2.71):

$$\begin{aligned}
I_c^- &= j \frac{[B_c^{ab} * (1 - K^2) - B_c^{ca} * (K - 1)]V}{\sqrt{3}} \\
&+ j \frac{[K^2[B_c^{bc} * (K^2 - K) - B_c^{ab} * (1 - K^2)]V]}{\sqrt{3}} \\
&+ j \frac{K[B_c^{ca} * (K - 1) - B_c^{bc} * (K^2 - K)]V}{\sqrt{3}}
\end{aligned} \tag{2-76}$$

$$\begin{aligned}
I_c^- &= j \frac{[B_c^{ab} * (-3K^2) + B_c^{bc} * (-3) + B_c^{ca} * (-3K)]V}{\sqrt{3}} \\
&= -j[B_c^{ab} * K^2 + B_c^{bc} + B_c^{ca} * K]V\sqrt{3}
\end{aligned} \tag{2-77}$$

The compensated load will be balanced if its negative sequence current is zero, requiring that $I^- + I_c^- = 0$. This equations yields the real part, $\text{Re}[I^- + I_c^-]$, and imaginary part, $\text{Im}[I^- + I_c^-]$, to be equal to zero.

The reactive part of positive sequence current will be cancelled for power factor correction.

The compensation requirements (load balancing and there is not negative sequence current) can be formulated mathematically as follows:

$$\text{Im}[I^+ + I_c^+] = 0 \quad (2-78)$$

Substituting the equation (2.75) into (2.78):

$$\text{Im}[I^+] + \text{Im}[j[B_c^{ab} + B_c^{bc} + B_c^{ca}]V\sqrt{3}] = 0 \quad (2-79)$$

$$\text{Im}[I^+] + [B_c^{ab} + B_c^{bc} + B_c^{ca}]V\sqrt{3} = 0 \quad (2-80)$$

$$B_c^{ab} + B_c^{bc} + B_c^{ca} = -\frac{\text{Im}[I^+]}{V\sqrt{3}} \quad (2-81)$$

$$\text{Im}[I^- + I_c^-] = 0 \quad (2-82)$$

Substituting the equation (2.77) into (2.82):

$$\text{Im}[I^-] + \text{Im}[-j[B_c^{ab} * K^2 + B_c^{bc} + B_c^{ca} * K]V\sqrt{3}] = 0 \quad (2-83)$$

$$\text{Im}[I^-] + \left[\frac{B_c^{ab}}{2} - B_c^{bc} + \frac{B_c^{ca}}{2} \right] V\sqrt{3} = 0 \quad (2-84)$$

$$B_c^{ab} - 2 * B_c^{bc} + B_c^{ca} = -\frac{2 * \text{Im}[I^-]}{V\sqrt{3}} \quad (2-85)$$

$$\text{Re}[I^- + I_c^-] = 0 \quad (2-86)$$

Substituting the equation (2.77) into (2.86):

$$\text{Re}[I^-] + \text{Re}[-j[B_c^{ab} * K^2 + B_c^{bc} + B_c^{ca} * K]V\sqrt{3}] = 0 \quad (2-87)$$

$$\operatorname{Re}[I^-] + \left[-\frac{\sqrt{3} * B_c^{ab}}{2} + \frac{\sqrt{3} * B_c^{bc}}{2} \right] V \sqrt{3} = 0 \quad (2-88)$$

$$-B_c^{ab} + B_c^{ca} = -\frac{2}{3V} \operatorname{Re}[I^-] \quad (2-89)$$

Equations (2.81), (2.85) and (2.89) are solved for $B_c^{ab}, B_c^{ca}, B_c^{bc}$.

First, B_c^{bc} is obtained:

$$B_c^{bc} = \frac{1}{3\sqrt{3}V} (-\operatorname{Im}I^+ + 2\operatorname{Im}I^-) \quad (2-90)$$

Second, B_c^{ca} is obtained, substituting the equation (2-90) into (2-81):

$$B_c^{ab} + B_c^{ca} = -\frac{\operatorname{Im}[I^+]}{V\sqrt{3}} - \frac{1}{3\sqrt{3}V} (-\operatorname{Im}[I^+] + 2\operatorname{Im}[I^-]) \quad (2-91)$$

$$B_c^{ca} = -\frac{1}{3\sqrt{3}V} (\operatorname{Im}[I^+] + \operatorname{Im}[I^-] + \sqrt{3} \operatorname{Re}[I^-]) \quad (2-92)$$

Last, B_c^{ab} is obtained, substituting the equation (2-92) into (2-89):

$$B_c^{ab} = -\frac{1}{3\sqrt{3}V} (\operatorname{Im}[I^+] + \operatorname{Im}[I^-] - \sqrt{3} \operatorname{Re}[I^-]) \quad (2-93)$$

Now Ia, Ib and Ic are obtained by taking the inverse of equation (2-50) as shown in equation (2-94).

$$\begin{bmatrix} I_a \\ I_b \\ I_c \end{bmatrix} = \frac{1}{\sqrt{3}} \begin{bmatrix} 1 & 1 & 1 \\ 1 & K^2 & K \\ 1 & K & K^2 \end{bmatrix} \begin{bmatrix} I^0 \\ I^+ \\ I^- \end{bmatrix} \quad (2-94)$$

From equation (2-92)

$$I_a = \frac{I^+ + I^-}{\sqrt{3}} \quad (2-95)$$

From equation (2-95)

$$I^+ + I^- = \sqrt{3}I_a \quad (2-96)$$

From equation (2-92)

$$I_b = \frac{K^2 * I^+ + K * I^-}{\sqrt{3}} \quad (2-97)$$

From equation (2-97)

$$K^2 * I^+ + K * I^- = \sqrt{3}I_b \quad (2-98)$$

From equation (2-92)

$$I_c = \frac{K * I^+ + K^2 * I^-}{\sqrt{3}} \quad (2-99)$$

From equation (2-99)

$$K * I^+ + K^2 * I^- = \sqrt{3}I_c \quad (2-100)$$

$$\sqrt{3} \operatorname{Re}[I^-] = \sqrt{3} \operatorname{Im}[j * I^-] \quad (2-101)$$

Equations (2.96), (2.98), (2.100) and (2.101) are solved for I^+ , I^- and substituting equation of I^+ , I^- into (2.90), (2.92) and (2.93):

$$B_c^{ab} = -\frac{1}{3V} (\text{Im}[I_a] + \text{Im}[K * I_b] - \text{Im}[K^2 I_c]) \quad (2-102)$$

$$B_c^{bc} = -\frac{1}{3V} (-\text{Im}[I_a] + \text{Im}[K * I_b] + \text{Im}[K^2 I_c]) \quad (2-103)$$

$$B_c^{ca} = -\frac{1}{3V} (\text{Im}[I_a] - \text{Im}[K * I_b] + \text{Im}[K^2 I_c]) \quad (2-104)$$

And multiplying equation (2.102), (2.103) and (2.104) with V .

$$B_c^{ab} = -\frac{1}{3V^2} (\text{Im}[V * I_a] + \text{Im}[V * K * I_b] - \text{Im}[V * K^2 I_c]) \quad (2-105)$$

$$B_c^{bc} = -\frac{1}{3V^2} (-\text{Im}[V * I_a] + \text{Im}[V * K * I_b] + \text{Im}[V * K^2 I_c]) \quad (2-106)$$

$$B_c^{ca} = -\frac{1}{3V^2} (\text{Im}[V * I_a] - \text{Im}[V * K * I_b] + \text{Im}[V * K^2 * I_c]) \quad (2-107)$$

Substituting the equation (2.34), (2-35) and (2-36) into (2-105), (2-106) and (2-107):

$$B_c^{ab} = \frac{1}{3V^2} (\text{Im}[V_a * I_a^*] + \text{Im}[V_b * I_b^*] - \text{Im}[V_c * I_c^*]) \quad (2-108)$$

$$B_c^{bc} = \frac{1}{3V^2} (-\text{Im}[V_a * I_a^*] + \text{Im}[V_b * I_b^*] + \text{Im}[V_c * I_c^*]) \quad (2-109)$$

$$B_c^{ca} = \frac{1}{3V^2} (\text{Im}[V_a * I_a^*] - \text{Im}[V_b * I_b^*] + \text{Im}[V_c * I_c^*]) \quad (2-110)$$

Let us relate,

$$\text{Im}[V * I^*] = \frac{1}{T} \int v(-\frac{\pi}{2}) * i^* dt \quad (2-111)$$

Where $v_a(-\frac{\pi}{2})$, $v_b(-\frac{\pi}{2})$ and $v_c(-\frac{\pi}{2})$, represent the signal v_a , v_b and v_c phase shifted by $-\frac{\pi}{2}$ electrical radians at the fundamental frequency. Where T is the period. This expression can be interpreted as a reactive power averaged over one complete cycle. Thus the first “reactive power” terms in equation are;

$$\text{Im}[V_a * I_a^*] = \frac{1}{T} \int v_a(-\frac{\pi}{2}) * i_a^* dt \quad (2-112)$$

$$\text{Im}[V_b * I_b^*] = \frac{1}{T} \int v_b(-\frac{\pi}{2}) * i_b^* dt \quad (2-113)$$

$$\text{Im}[V_c * I_c^*] = \frac{1}{T} \int v_c(-\frac{\pi}{2}) * i_c^* dt \quad (2-114)$$

In practice the phase voltages can be immediately derived from diagram relating line to neutral voltages to line to line voltages. Since,

$$\begin{aligned} V_{ab} &= -j\sqrt{3}V_c \\ V_{bc} &= -j\sqrt{3}V_a \\ V_{ca} &= -j\sqrt{3}V_b \end{aligned} \quad (2-115)$$

Let,

$$\begin{aligned}
v_a\left(-\frac{\pi}{2}\right) &= \frac{v_{bc}}{\sqrt{3}} \\
v_b\left(-\frac{\pi}{2}\right) &= \frac{v_{ca}}{\sqrt{3}} \\
v_c\left(-\frac{\pi}{2}\right) &= \frac{v_{ab}}{\sqrt{3}}
\end{aligned} \tag{2-116}$$

Finally by substituting the equation (2-112), (2-113) and (2-114) and (2-116) into (2.108):

$$B_c^{ab} = \frac{1}{3\sqrt{3}V^2} \frac{1}{T} \int (v_{bc} * i_a + v_{ca} * i_b - v_{ab} * i_c) \tag{2-117}$$

Substituting the equation (2-112), (2-113) and (2-114) and (2-116) into (2.109):

$$B_c^{bc} = \frac{1}{3\sqrt{3}V^2} \frac{1}{T} \int (-v_{bc} * i_a + v_{ca} * i_b + v_{ab} * i_c) \tag{2-118}$$

Substituting the equation (2-112), (2-113) and (2-114) and (2-116) into (2.110):

$$B_c^{bc} = \frac{1}{3\sqrt{3}V^2} \frac{1}{T} \int (v_{bc} * i_a - v_{ca} * i_b + v_{ab} * i_c) \tag{2-119}$$

CHAPTER THREE
SIMULATION OF THRISTOR-CONTROLLED REACTOR AND CIRCUITS
FOR APPLICATON

3.1 Modeling And Simulation TCR In PSCAD

The model of the load and TCR is obtained in the PSCAD as follows;

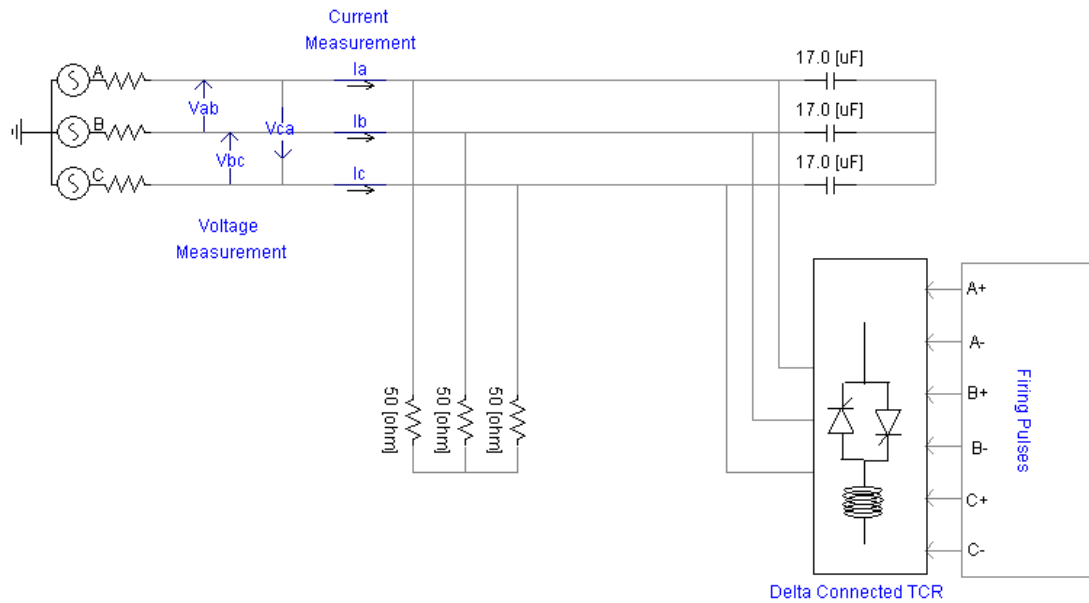


Figure 3.1 Delta connected TCR connected with parallel to system.

The line currents (I_a , I_b , I_c) and phase to phase voltages (V_{ab} , V_{bc} , V_{ca}) are measured from system as shown figure 3.1. Reactive power is calculated with these measurements. Firing angles are obtained from look up table which consisting of values equation (3-1). These angles are converted to time as delay.

$$B_{TCR} = \frac{2(\pi - \alpha) + \sin(2\alpha)}{\pi} \quad (3-1)$$

B_{TCR}	α
-1.0	179
0.0	179
0.015	161.89
0.05	149.79
0.15	138.08
0.25	128.94
0.4	119.5
0.6	108.32
1.0	88
1.5	88

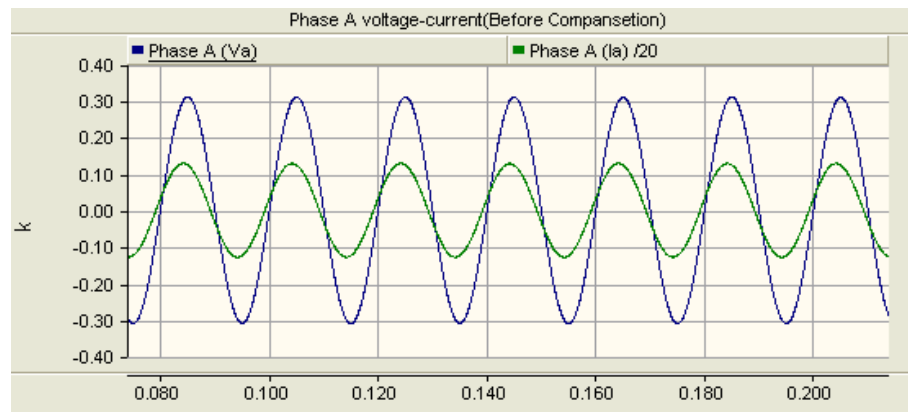
Figure 3.2 Look up table in reactive power calculation.

Three phase loads supplied by the source may be balanced or unbalanced. In the first case, the load is considered balanced and in the second case the load is assumed to be unbalanced.

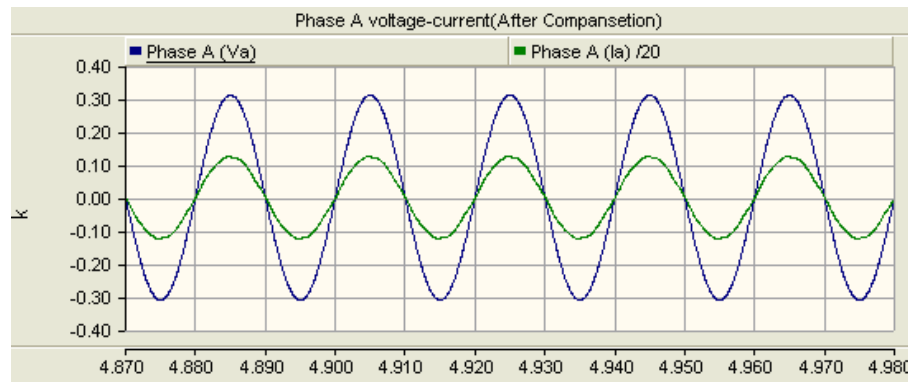
3.1.1 Balanced Condition

When the loading is identical in all phases, this condition is assumed to be balanced. So, peak value of per phase current equal to each other on source as shown figure 3.3.

Figures 3.3, 3.4 and 3.5 show the phase voltages and currents during the compensation under balanced loading conditions.



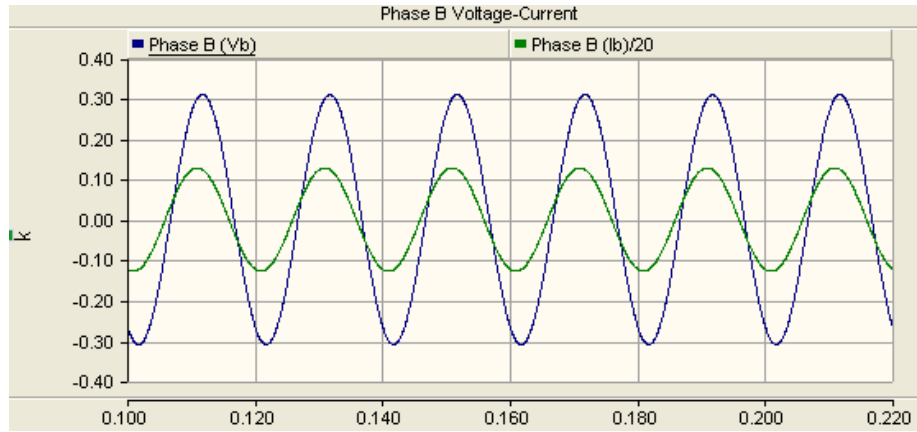
(a)



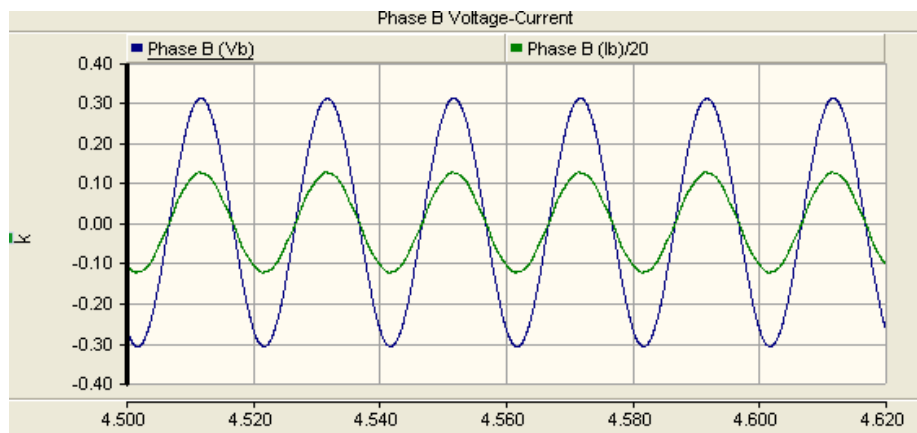
(b)

Figure 3.3 Current and voltage waveform phase a , (a) before compensation, (b) after compensation.

It is clear that after compensation the phase voltage and current are in phase, while the current leads the voltage before compensation.



(a)



(b)

Figure 3.4 Current and voltage waveform phase b (a) before compensation (b) after compensation.

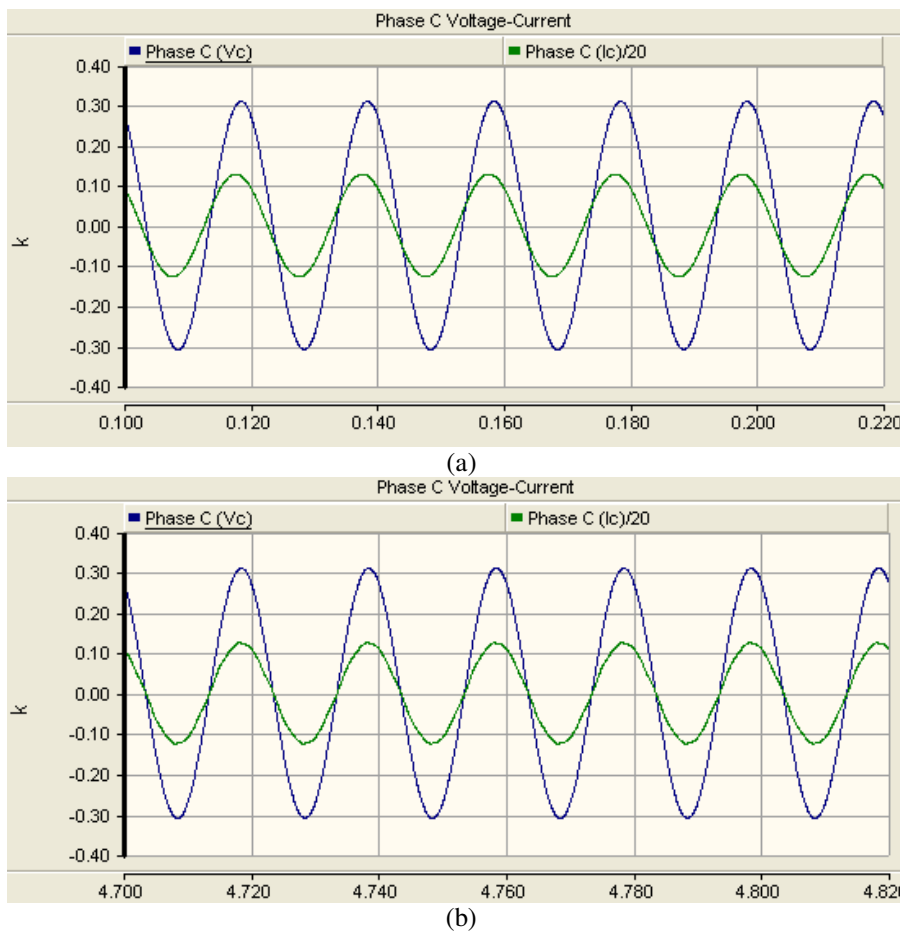


Figure 3.5 Current and voltage waveform phase c (a) before compensation (b) after compensation.

Figure 3.6 shows the line current of the reactor. This current is not purely sinusoidal and it contains some amount of harmonics.

When the firing angles of thyristors are increase from 90 to 180 degrees, amount of distortion increases in the line currents of the reactor.

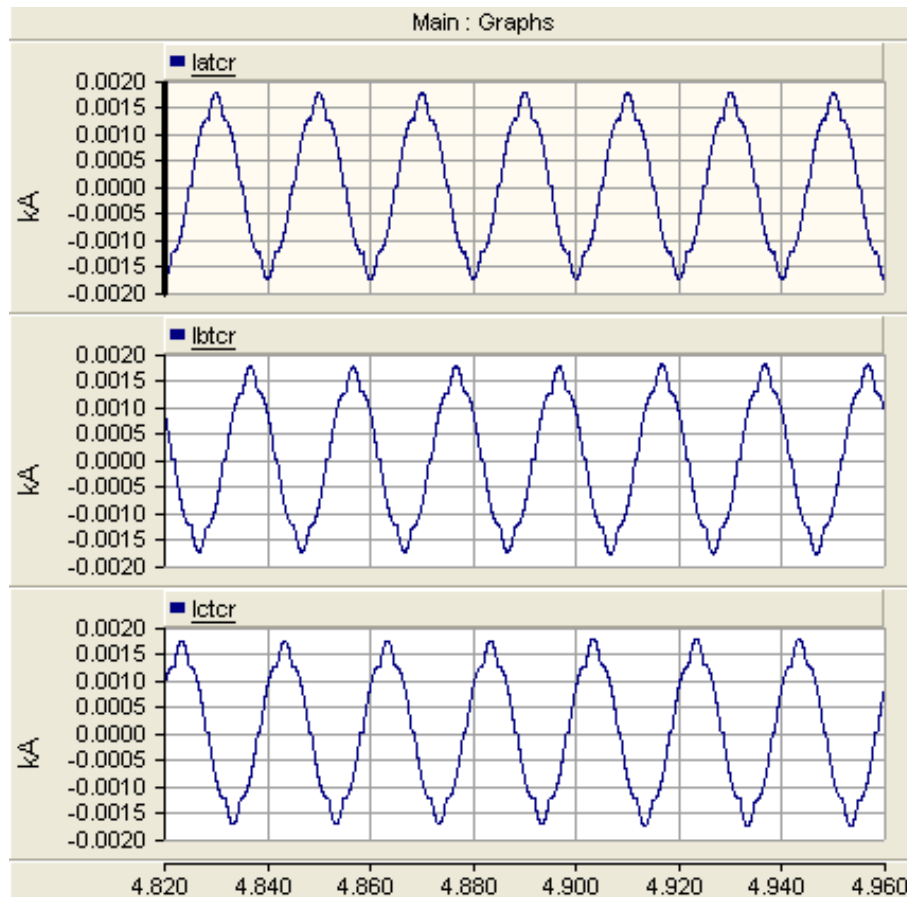


Figure 3.6 Per phase current in TCR.

If the firing angles vary from 90 to 180, TCR current waveform becomes less sinusoidal.

Here, when the angle is equal to 90 degree, amount of TCR phase current is maximum. Also, when the angle is equal to 180 degree, amount of TCR phase current is minimum.

The waveforms given in figure 3.7 are obtained while the firing angle is 120°.

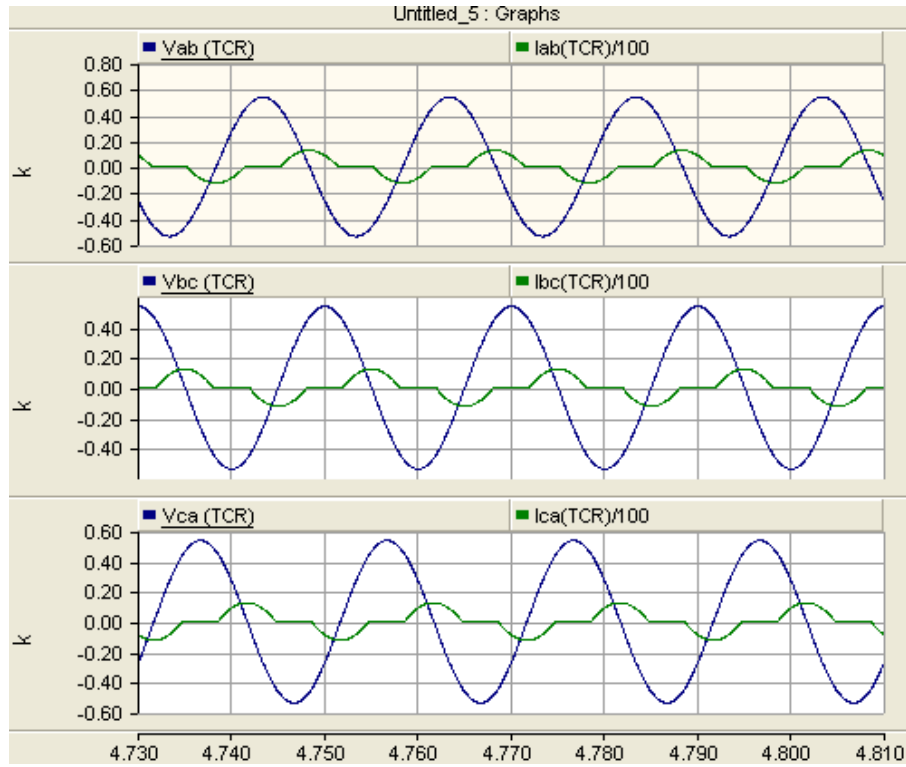


Figure 3.7 Phase to phase voltages and TCR currents. Here the firing angle is about 120.

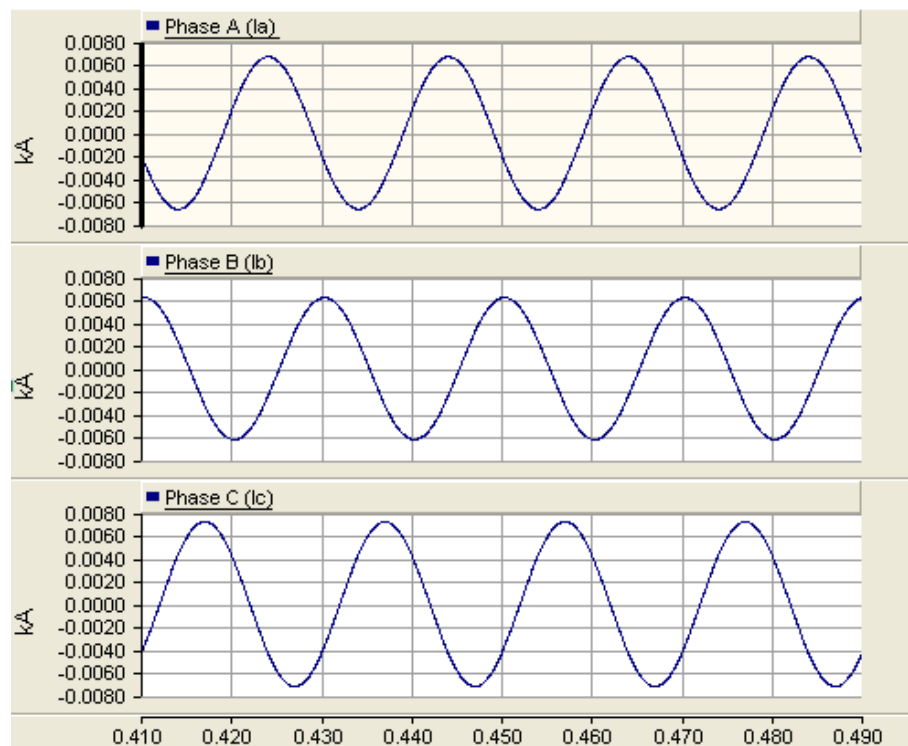
3.1.2 Unbalanced Condition

In this case, the loading condition is changed and the capacitor of each phase is set to different values. These values are given below;

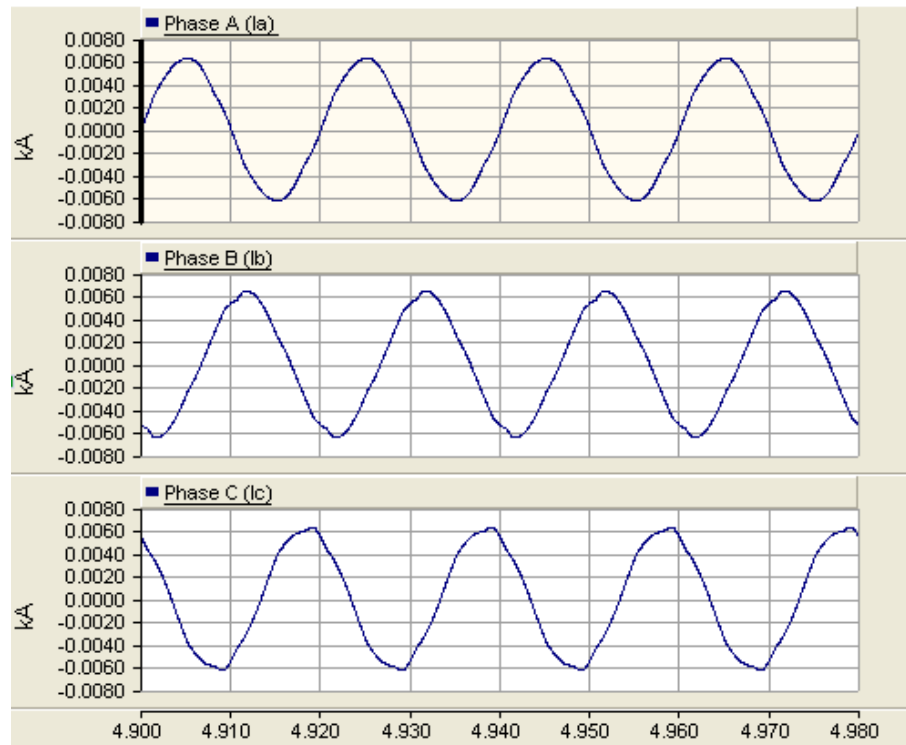
$$\begin{aligned} C_a &= 17 \mu F \\ C_b &= 27 \mu F \\ C_c &= 37 \mu F \end{aligned} \quad (3-2)$$

Figure 3.8 shows the phase currents during compensation. It is clear that the peak values of currents have different values before compensation and they are sinusoidal. After compensation peak values are almost same while they are non sinusoidal.

The TCR circuit injects some harmonics in the line and they appear in the line currents.



(a)



(b)

Figure 3.8 Per phase current waveform (a) before compensation (b) after compensation.

Figure 3.9 and 3.10 show the line and phase currents of TCR unit, respectively. Since the TCR circuit is connected in delta, the 3rd harmonic and multiples are not injected to line.

It is clear that the value of phase current of TCR is different at each phase. Since the load draws different value of reactive power in per phase, the TCR responds to this demand with different value of currents as being shown in figure 3.9.

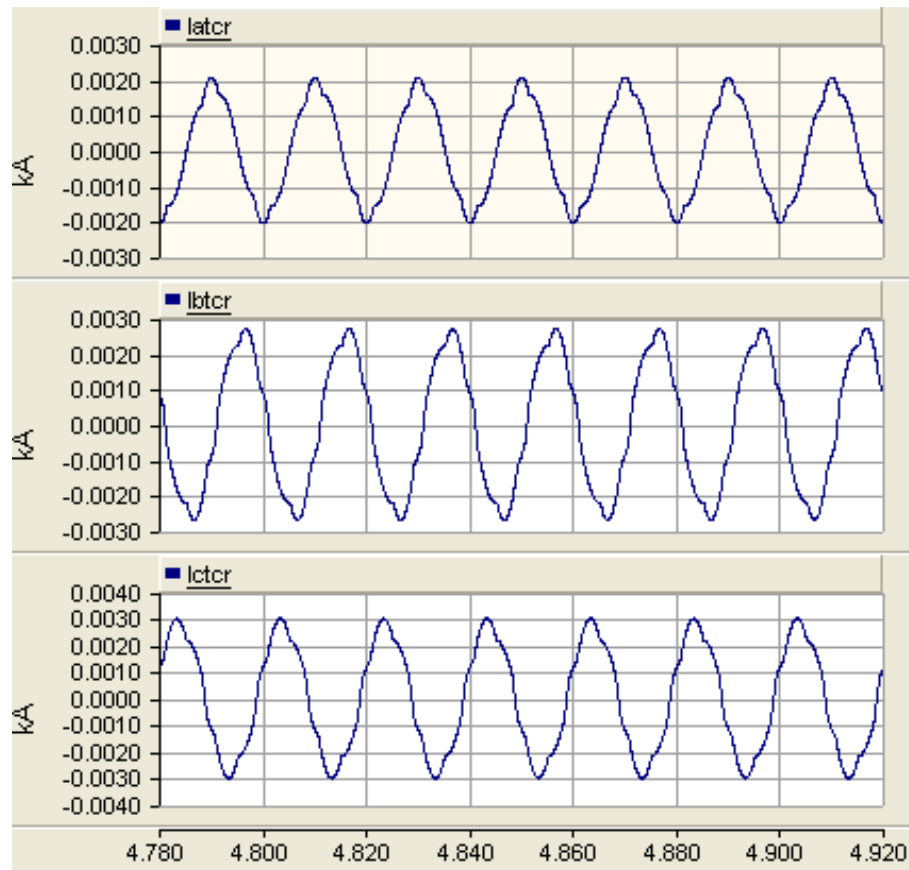


Figure 3.9 Line currents of TCR unit.

The line currents of source are balanced due to the response of TCR circuit under unbalanced loading case. It is clearly observed from figure 3.10 that the balance condition is created by the TCR unit responding at different firing angle of the phases.

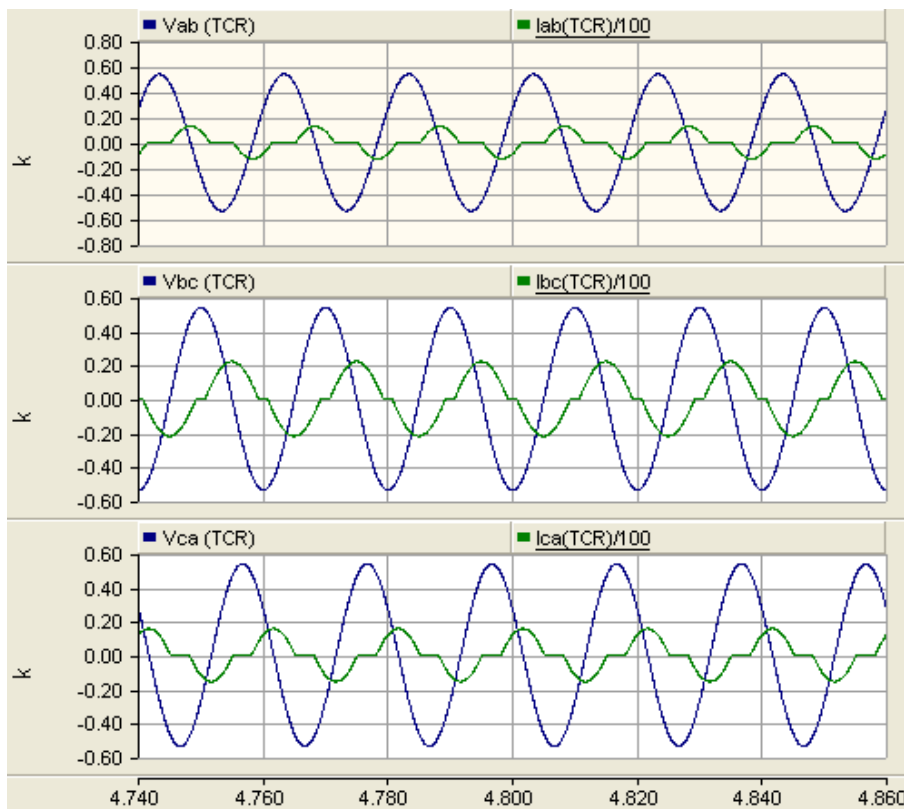


Figure 3.10 Phase to phase voltages and phase current of TCR unit.

As a result, amount of reactive power which is generated by the capacitor equals that of absorbed by the TCR.

3.2 Modeling And Simulation TCR In MATLAB

The circuit is also modeled in MATLAB package program, because this package has DSP toolbox that can be used to prepare the program for DSP unit. The model is given in figure 3.11 and detail of TCR circuit is depicted in figure 3.12.

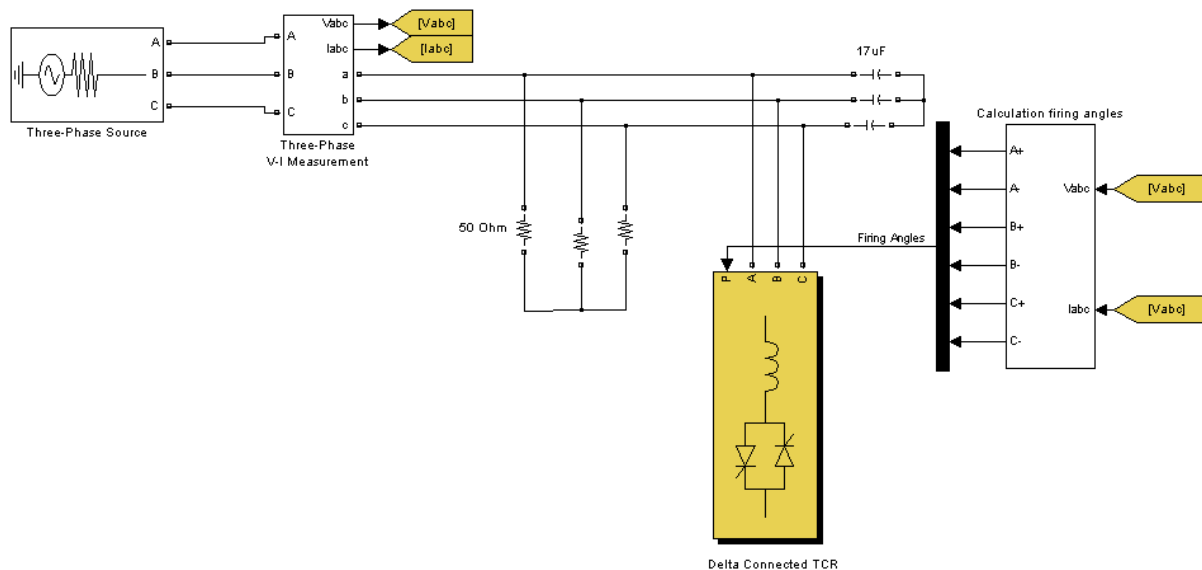


Figure 3.11 Delta connected TCR connected with parallel to system.

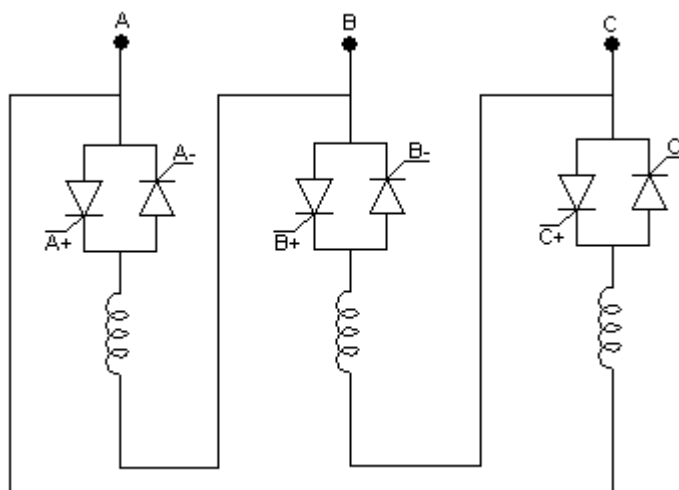


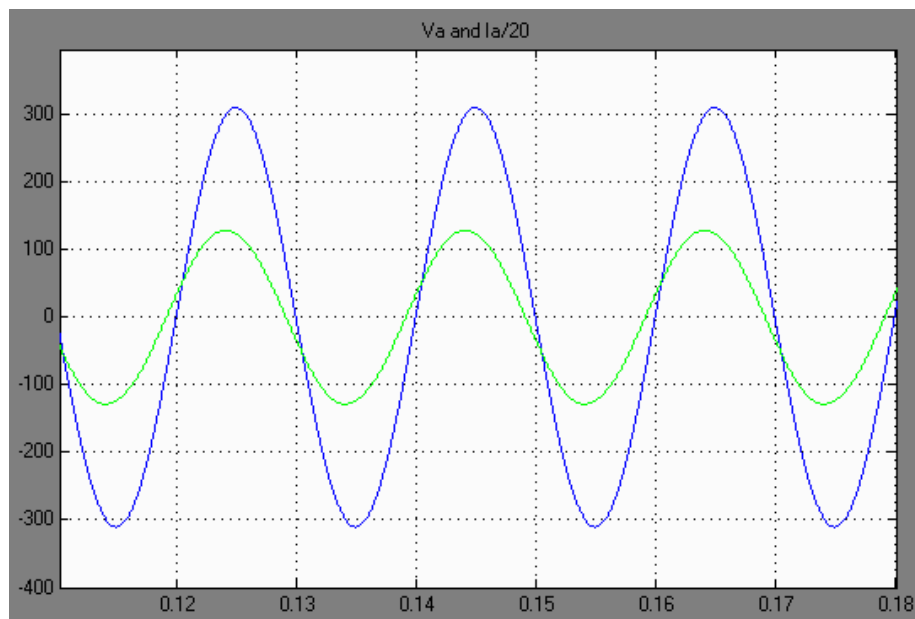
Figure 3.12 Delta connected TCR .

The results of PSCAD and MATLAB are identical, hence, the results show that the logic is correct and applicable in the DSP. DSP uses the digital model in MATLAB. Because of this reason, all the blocks are performed in digital form (not continuous).

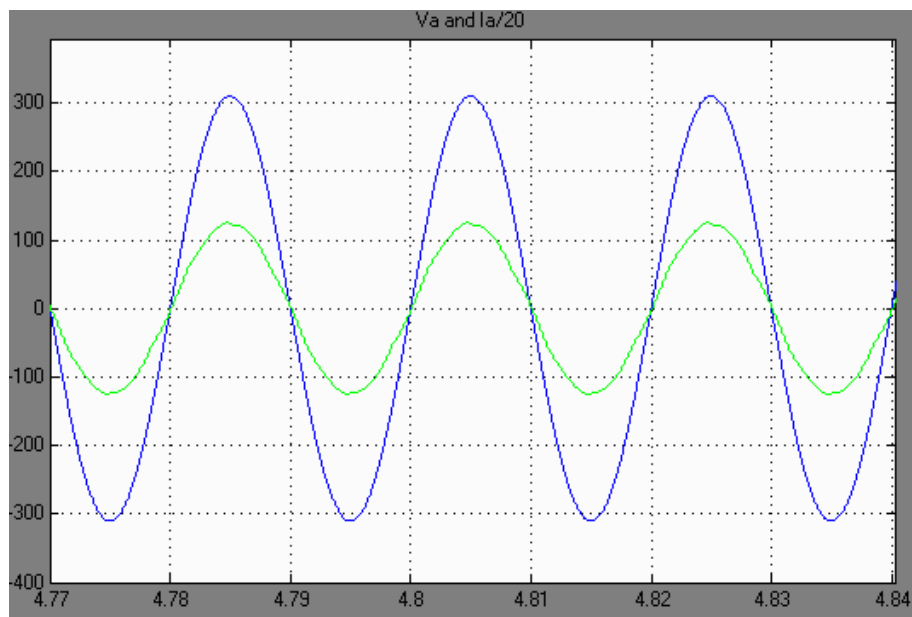
3.2.1 Balanced Condition

When the load equals each other per phase, this condition is balanced. So per phase current peak value is equal to each other as shown figure 3.13.

Figures 3.13, 3.14 and 3.15 show the phase voltages and currents during the compensation under balanced loading conditions.



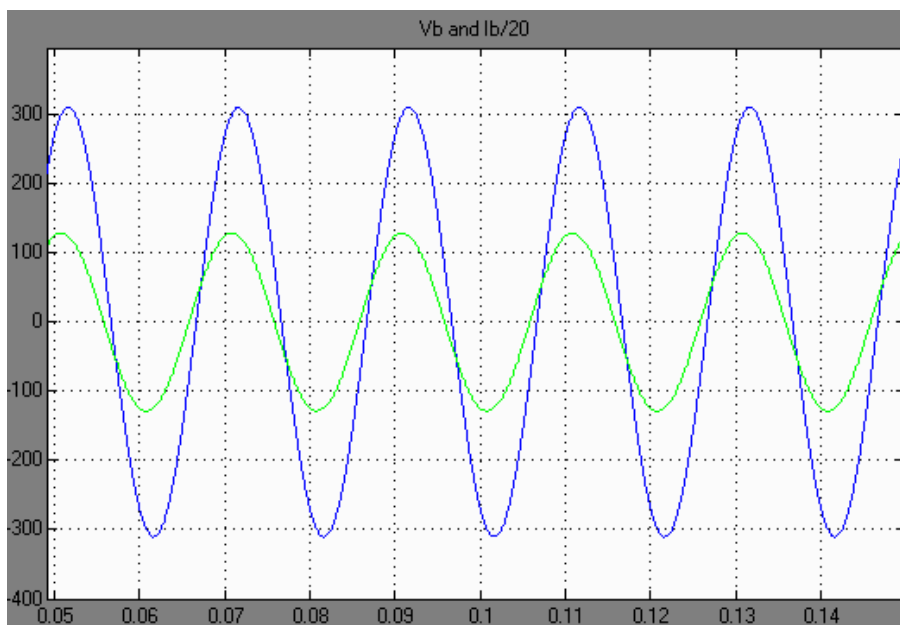
(a)



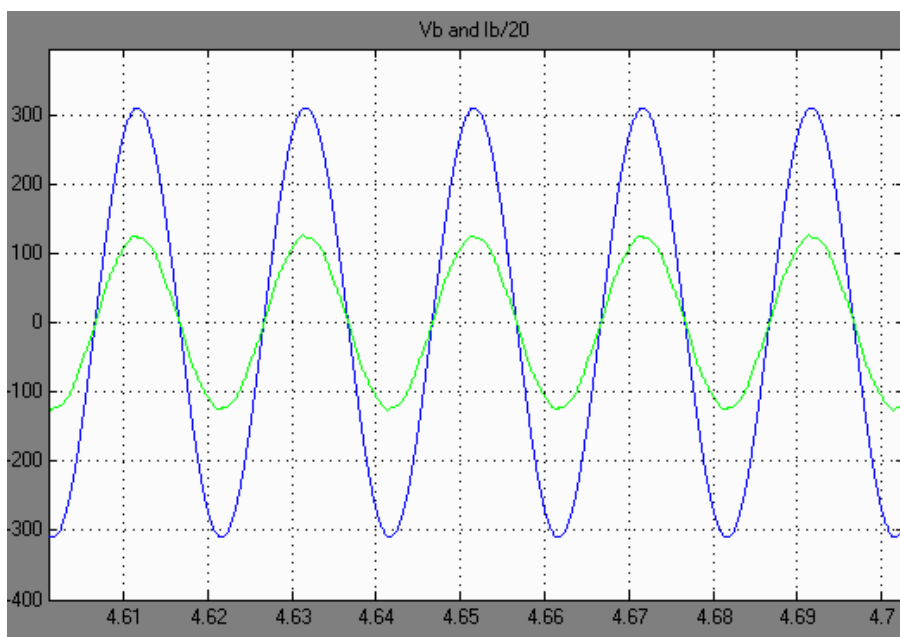
(b)

Figure 3.13 current and voltage waveform phase a (a) before compensation (b) after compensation.

It is clear that after compensation the phase voltage and current are in phase, while the current leads the voltage before compensation.

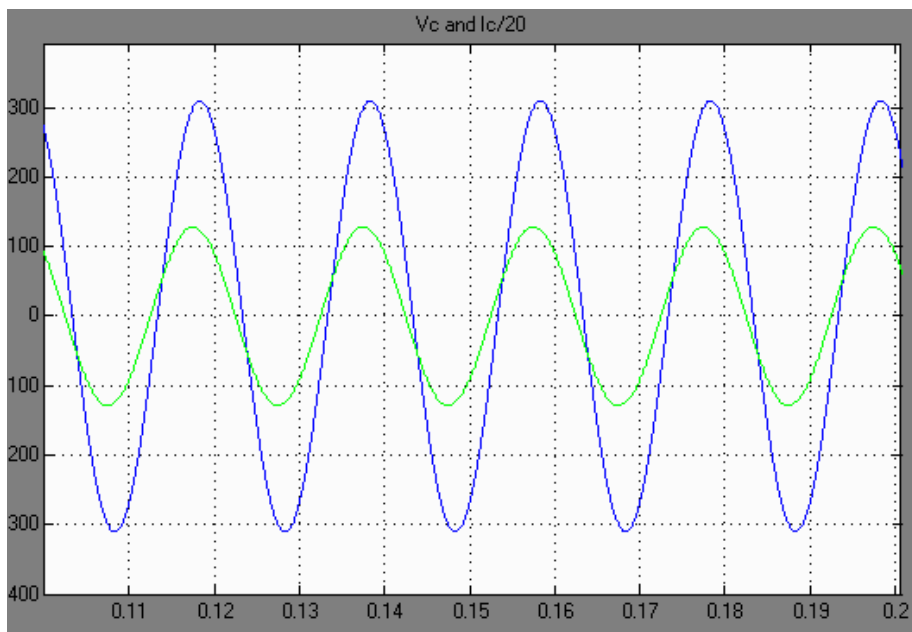


(a)

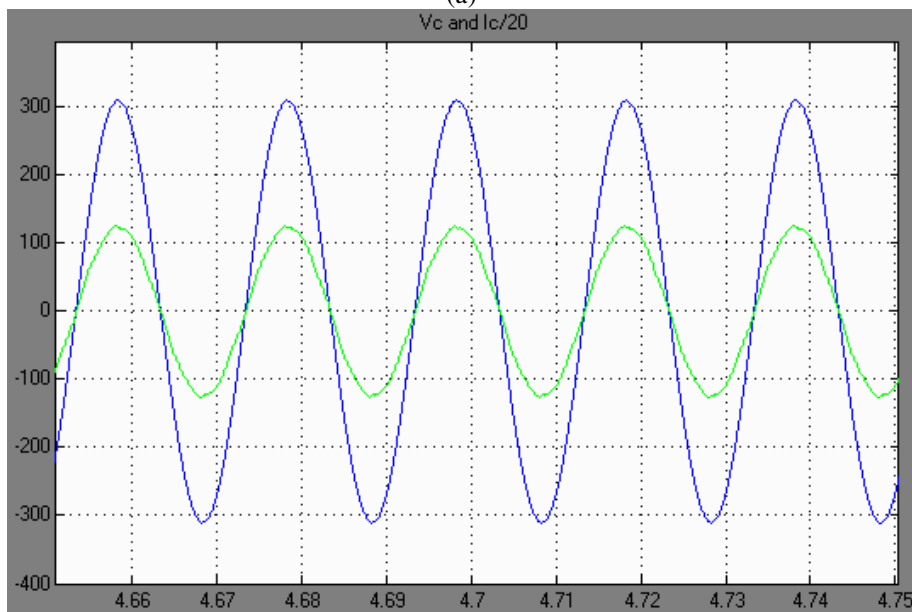


(b)

Figure 3.14 current and voltage waveform phase b (a) before compensation (b) after compensation.



(a)



(b)

Figure 3.15 current and voltage waveform phase c (a) before compensation (b) after compensation.

In figure 3.13, 3.14 and 3.15, the voltage and current waveform in the circuit are given.

Figure 3.17 shows the line current of the reactor. This current is not purely sinusoidal and it contains some amount of harmonics.

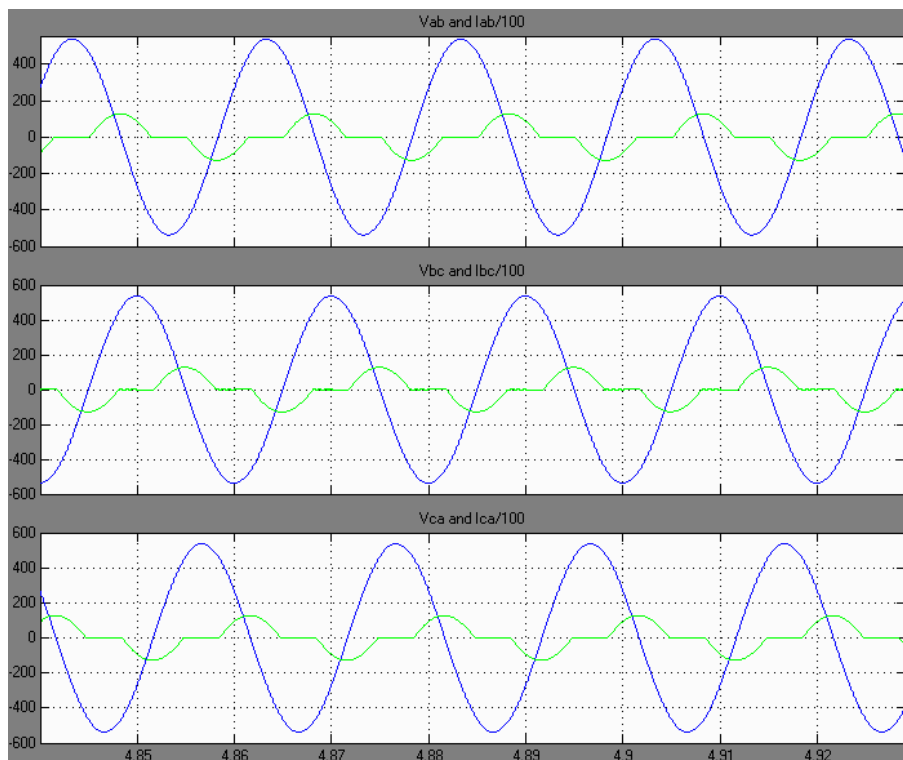


Figure 3.16 Phase to phase voltages and phase currents of TCR.

The waveforms given in figure 3.16 are obtained while the firing angle is 120° .

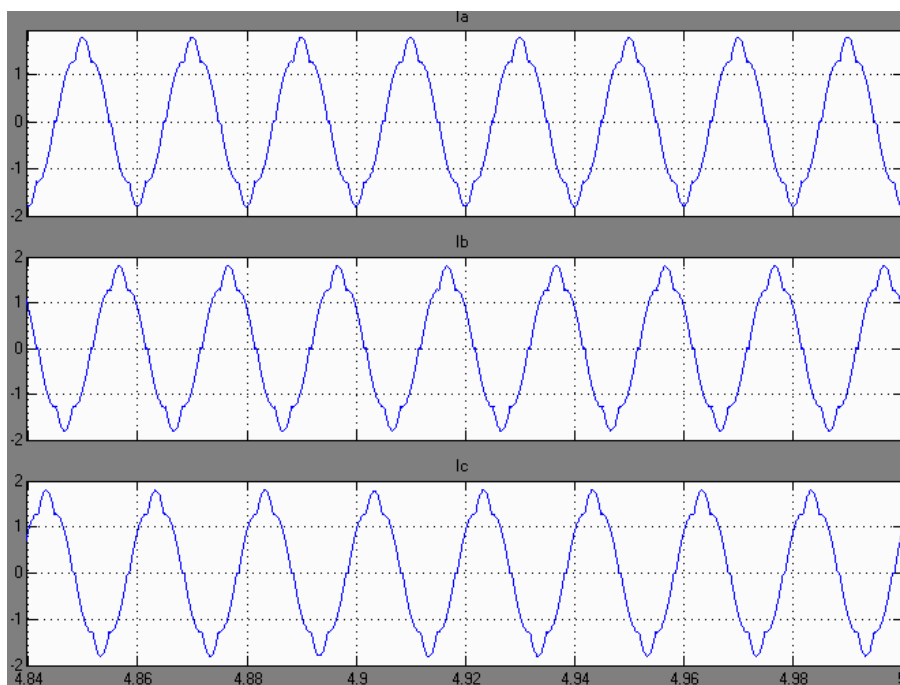


Figure 3.17 Line currents of TCR unit.

Same as in PSCAD, the waveform of line currents of TCR are shown in figure 3.17, these currents are not purely sinusoidal because TCR currents are not purely

sinusoidal. If the firing angles change from 90 to 180, TCR current waveform becomes less sinusoidal.

3.2.2 Unbalanced Condition

It is clear that the peak values of currents have different values before compensation and they are sinusoidal as shown 3.18(a).

The TCR circuit injects some harmonics in the line and they appear in the line currents as shown 3.18(b).

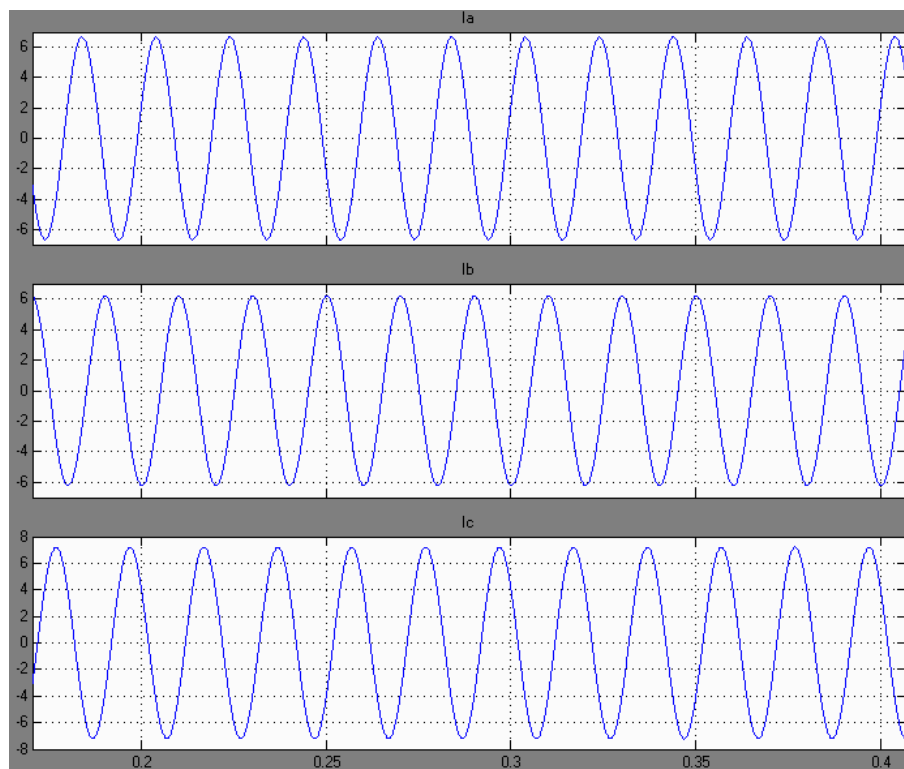
The loading condition is set to the values below;

$$C_a = 17 \mu F$$

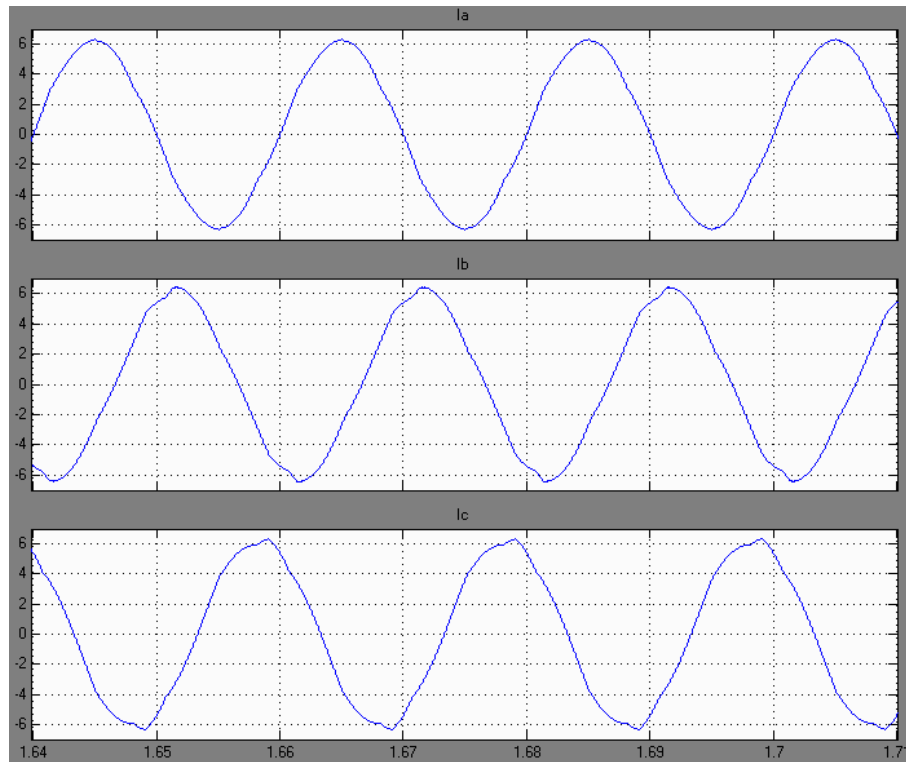
$$C_b = 27 \mu F$$

$$C_c = 37 \mu F$$

(3-3)



(a)



(b)

Figure 3.18 in unbalanced system, per phase current waveform (a) before compensation (b) after compensation.

In figure 3.18 (a), the current waveforms are shown on source. These currents amplitude are different from each other because of unbalanced load. So value of line currents of TCR has to be different at each phase for compensation as shown figure 3.19.

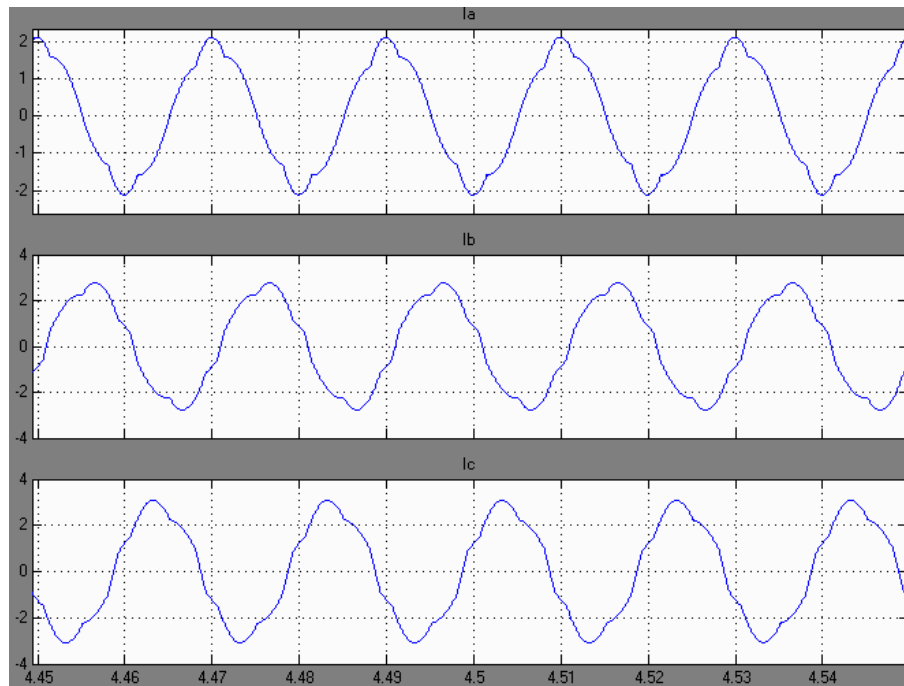


Figure 3.19 In unbalanced system, line currents of TCR unit.

Here, it can be noted that the load generates reactive power at different value for phases so TCR unit absorbs this value of reactive power. This value of reactive power is adjusted by means of firing angle as can be seen in figure 3.20.

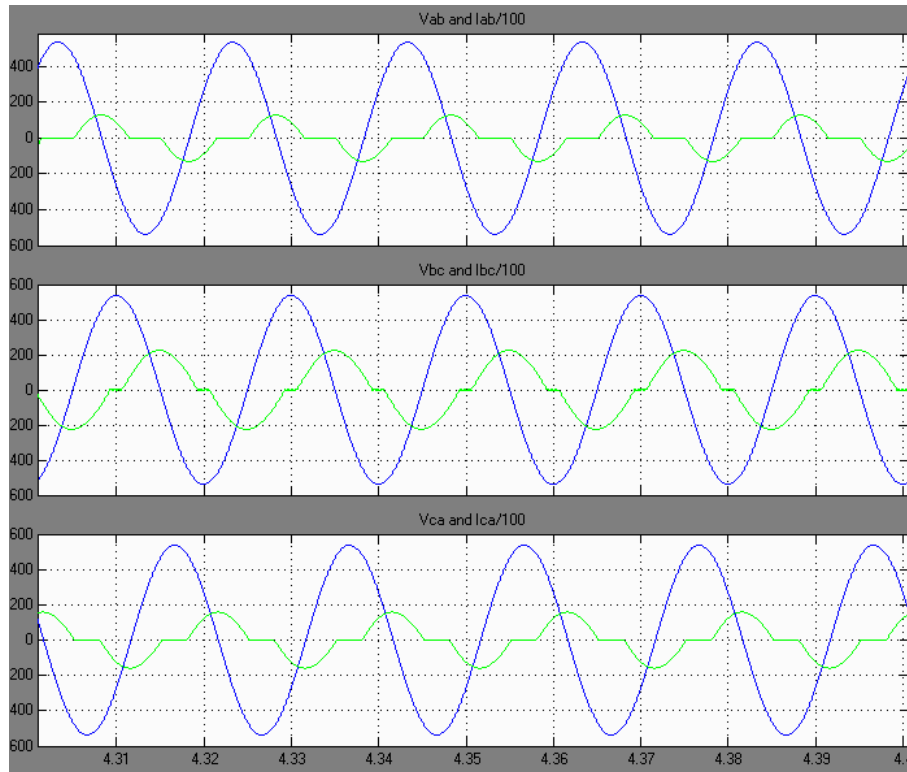


Figure 3.20 Phase to phase voltages and phase current of TCR unit.

3.3 Harmonic Analysis

The current flowing through the reactor becomes discontinuous by increasing the firing delay angle and eventually reducing the conduction angle. Therefore, TCR generates current harmonics (Miller, 1982). If the firing pulses of the back to back connected thyristors are balanced and the compensation system is in a steady state, all the odd harmonics of the fundamental frequency are generated. The RMS value of the n^{th} harmonic (I_n) of the TCR fundamental currents are given in equation (3-4).

$$I_n = \frac{4}{\pi} \frac{V}{X_L} \left[\frac{\sin(n+1)\alpha}{2(n+1)} + \frac{\sin(n-1)\alpha}{2(n-1)} - \cos\alpha \frac{\sin n\alpha}{n} \right] \quad (3-4)$$

Here, $n=3, 5, 7, 9, \dots$

In Equation (3-2), V is the line voltage and X_L is the reactance of TCR in full conduction.

The harmonic analysis of TCR phase and line currents are carried out for different firing angles, such as 90, 120, 150 and 165 degrees. The variation of total harmonic distortion as a function of firing angle is obtained.

When the firing angle is equal to 90, TCR phase current and its FFT:

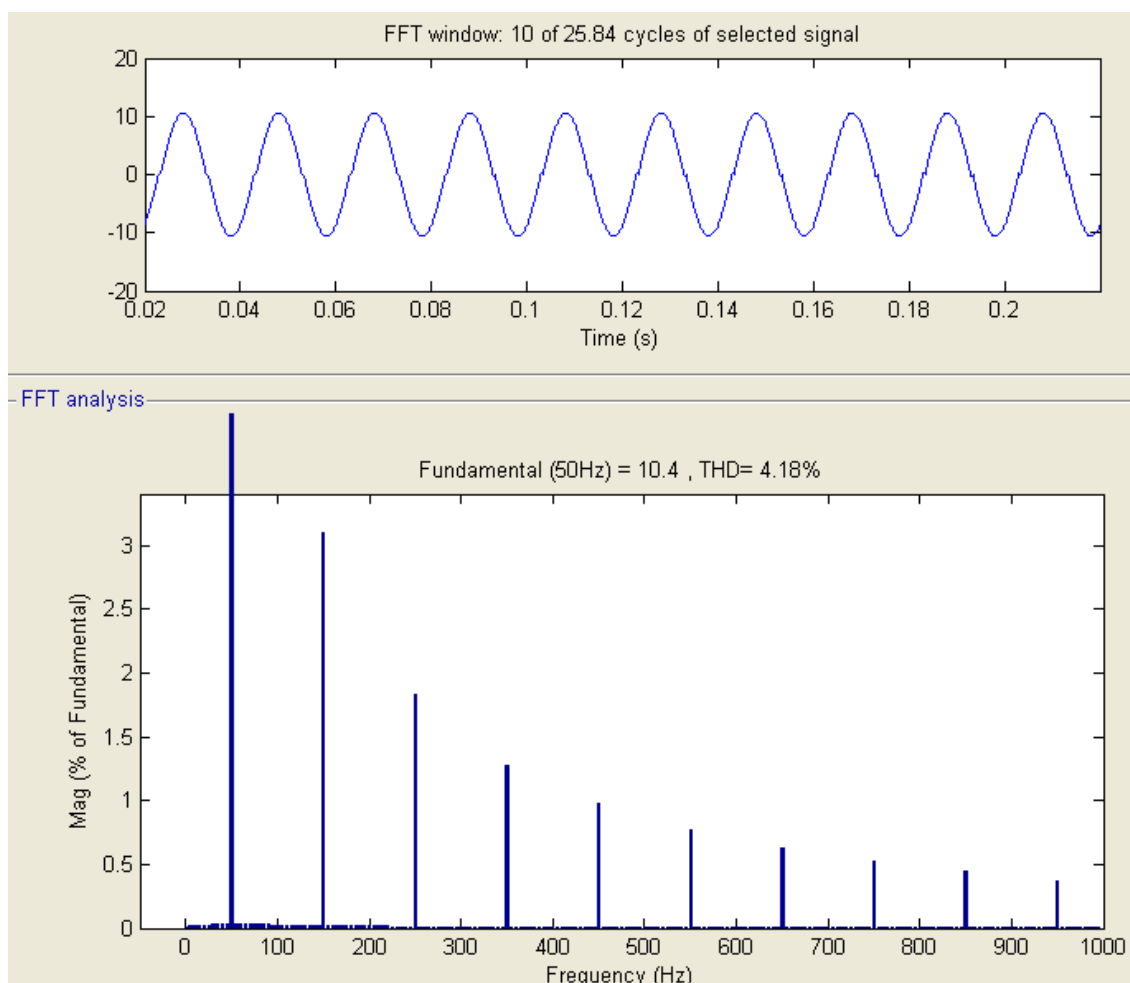


Figure 3.21 Harmonic analysis of TCR phase current when angle is equal to 90.

When the firing angle equals 90 degree, harmonic analysis of phase current of TCR is shown figure 3.21.

When the firing angle equals 90 degree, the waveform of current is sinusoidal on reactor so its harmonics amplitudes is low as shown figure 3.21. it is clear that TCR generates the all the odd harmonics of the fundamental frequency. This current is phase current of TCR. In delta connected TCR, all odd harmonics except 3rd harmonic and multiples in line currents of TCR are observed.

When the firing angle is equal to 90, TCR line current and its FFT:

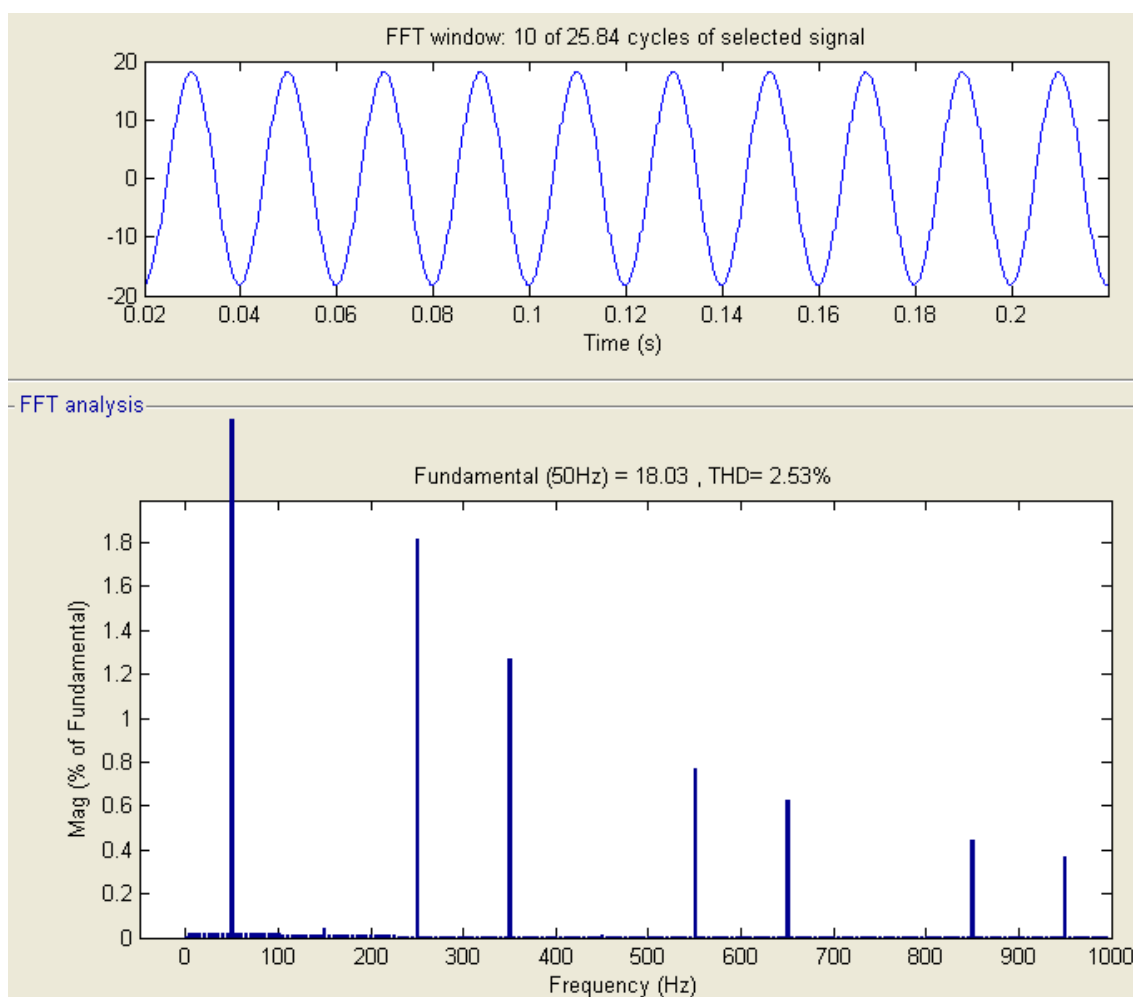


Figure 3.22 Harmonic analysis of TCR line current when angle is equal to 90.

When the firing angle equals 90 degree, harmonic analysis of line current of TCR is shown figure 3.22.

It is clear that all odd harmonics except for 3rd harmonics and multiples appear as shown figure 3.22.

When the firing angle is equal to 120, TCR phase current and its FFT:

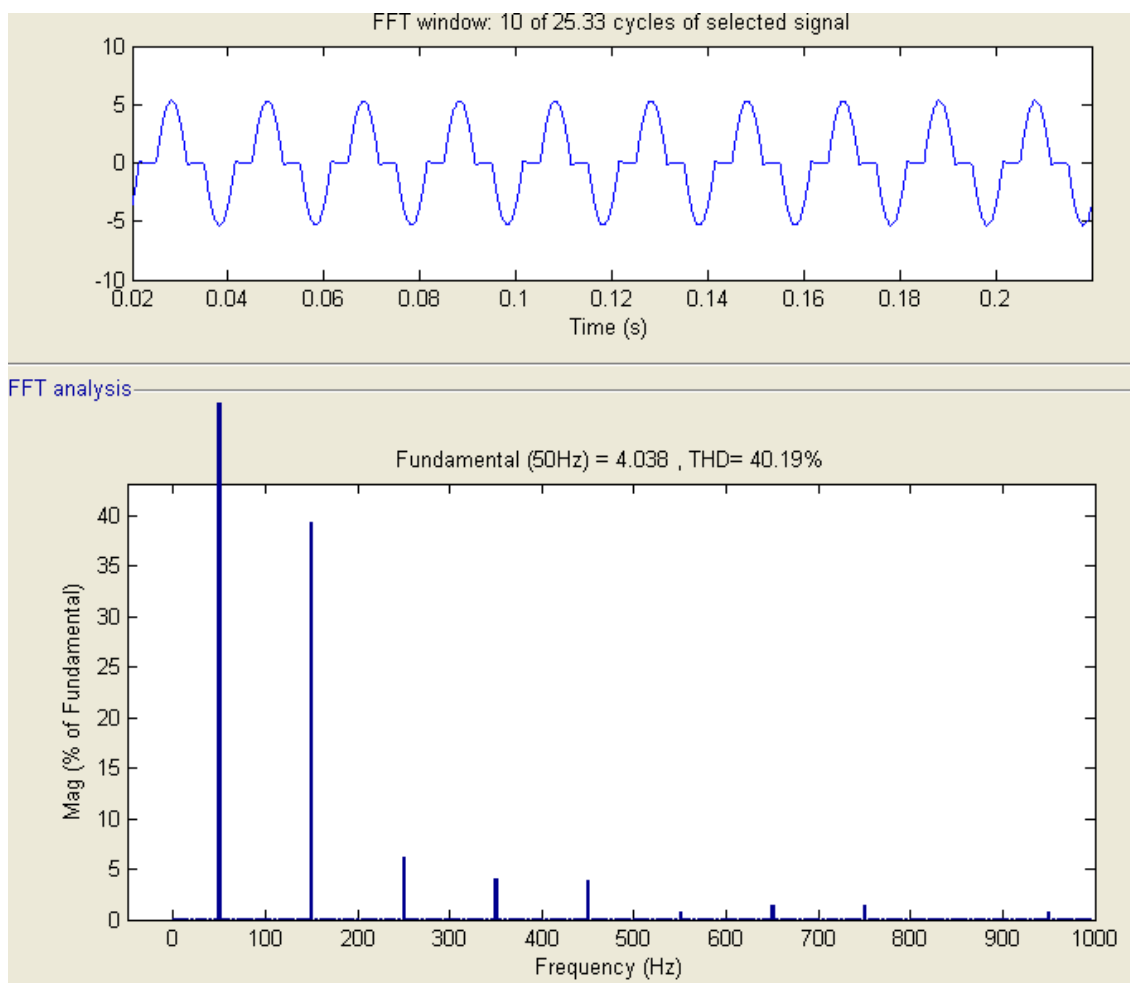


Figure 3.23 Harmonic analysis of TCR phase current when angle is equal to 120.

When the firing angle equals 120 degree, harmonic analysis of phase current of TCR is shown figure 3.23. It is clear that when firing angle is 120 degree, harmonic distortions level increase as shown figure 3.23. So appearance of the phase current waveform of TCR is far away from sinus form, hence, change of harmonic distortion level.

In delta connected TCR, all odd harmonics can be seen as shown figure 3.23.

When the firing angle is equal to 120, TCR line current and its FFT:

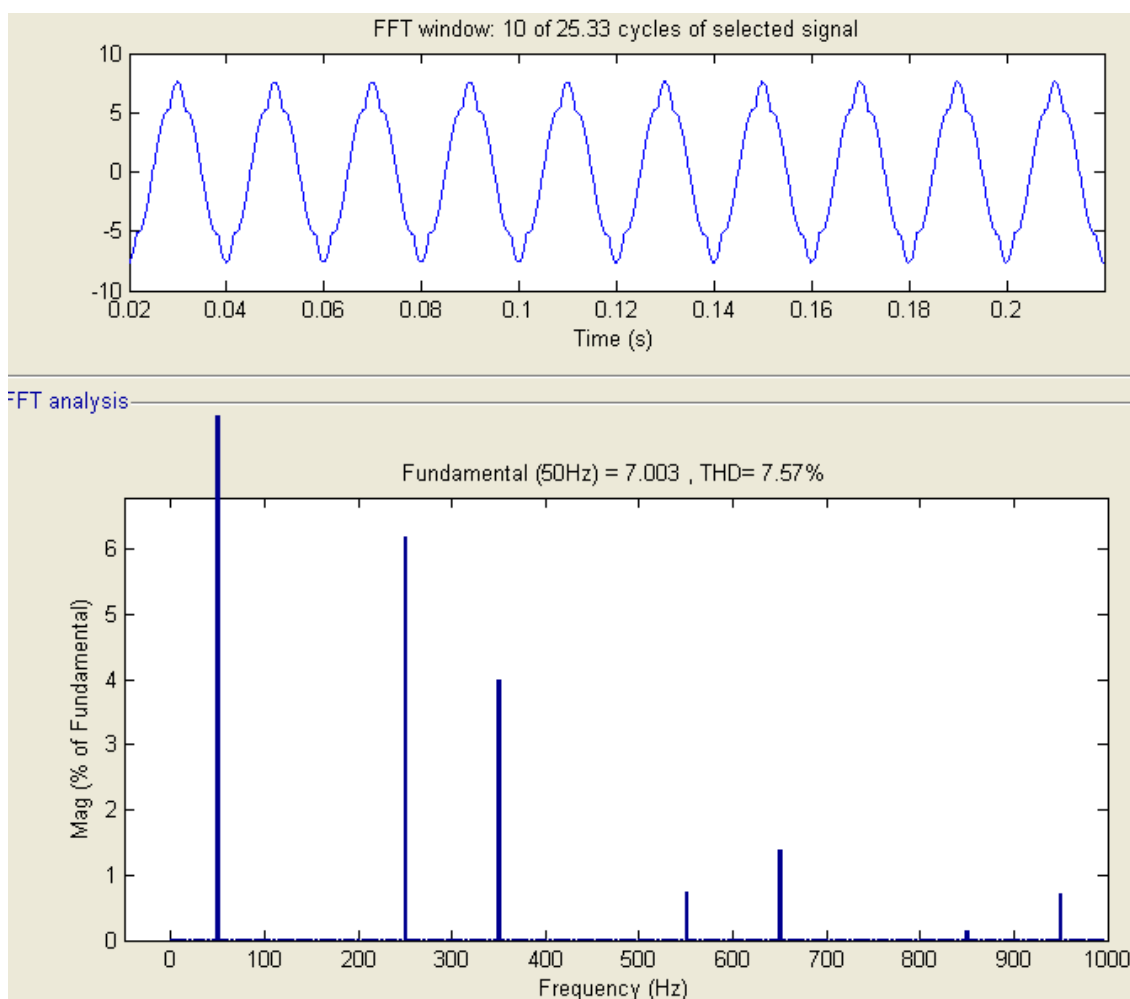


Figure 3.24 Harmonic analysis of TCR line current when angle is equal to 120.

When the firing angle equals 120 degree, harmonic analysis of line current of TCR is shown figure 3.24.

It is clear that all odd harmonics except for 3rd harmonics and multiples are observed as shown figure 3.24 at the same time rise amplitude of harmonics.

When the firing angle is equal to 150, TCR phase current and its FFT:

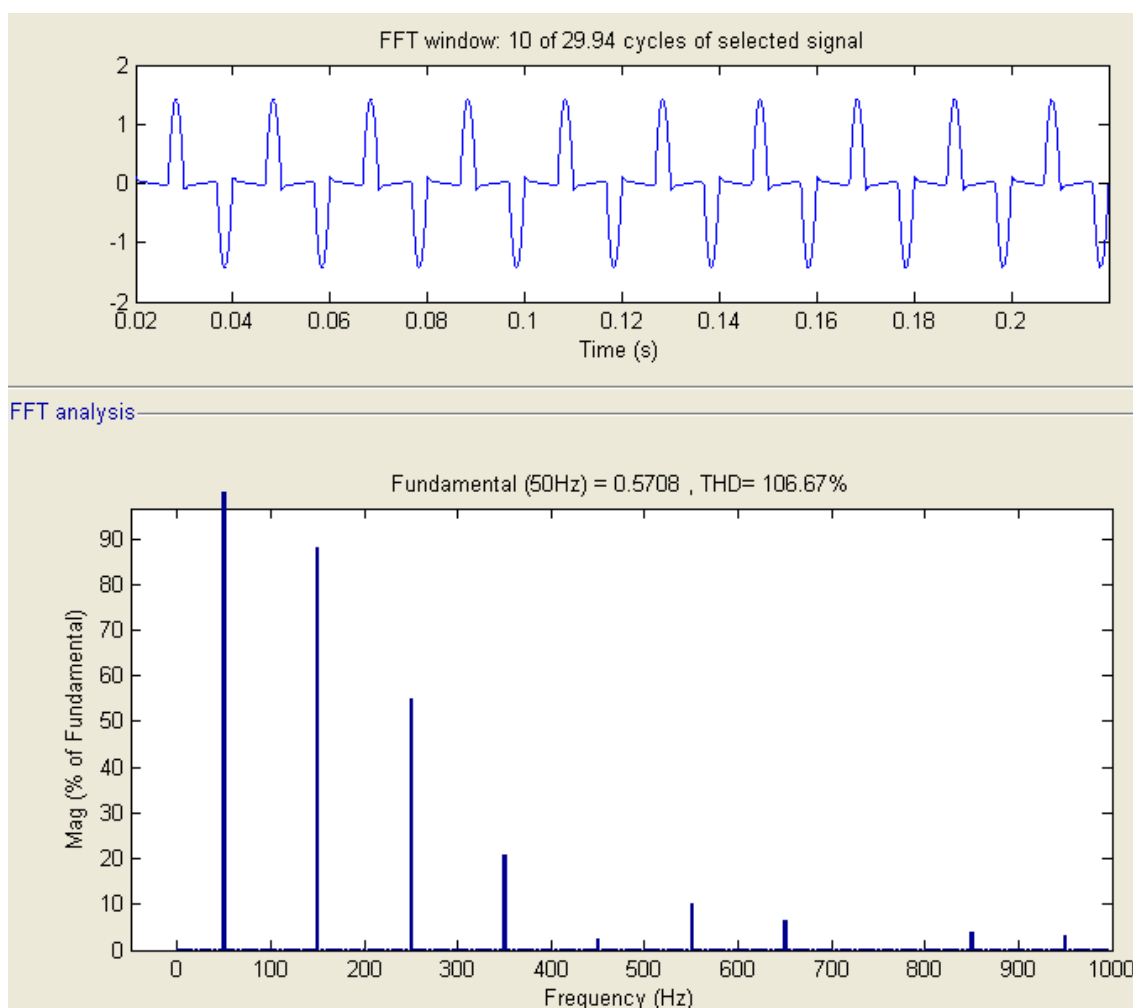


Figure 3.25 Harmonic analysis of TCR phase current when angle is equal to 150.

When the firing angle equals 150 degree, harmonic analysis of phase current of TCR is shown figure 3.25. It is clear that when firing angle is 150 degree, harmonic distortions level increase as shown figure 3.25. So appearance of the phase current waveform of TCR is distant from sinus form, hence, change of harmonic distortion level.

In delta connected TCR, all odd harmonics appear as shown figure 3.25.

When the firing angle is equal to 150, TCR line current and its FFT:

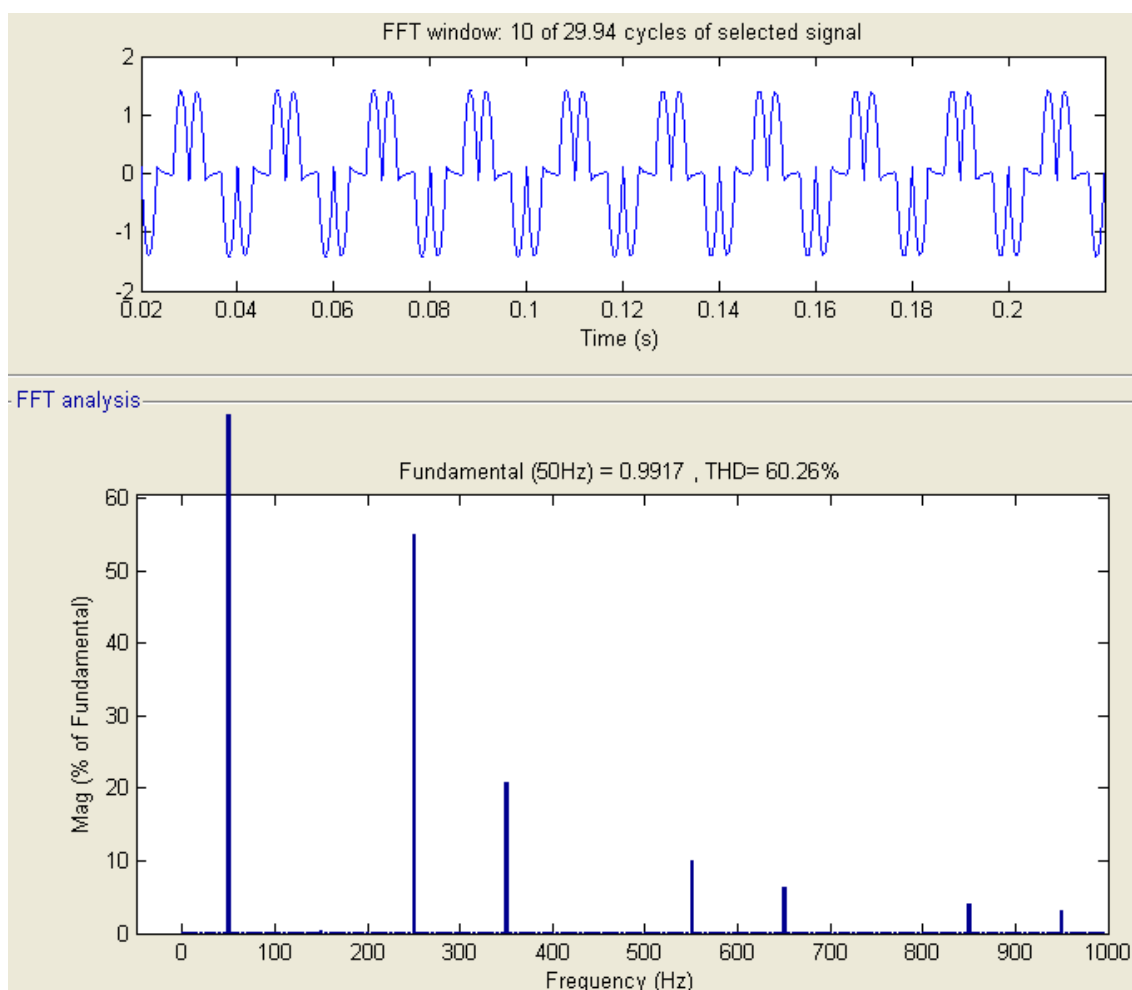


Figure 3.26 Harmonic analysis of TCR line current when angle is equal to 150.

When the firing angle equals 150 degree, harmonic analysis of line current of TCR is shown figure 3.26.

It is clear that all odd harmonics except for 3rd harmonics and multiplies appear as shown figure 3.26 at the same time rise amplitude of harmonics.

When the firing angle is equal to 165, TCR phase current and its FFT:

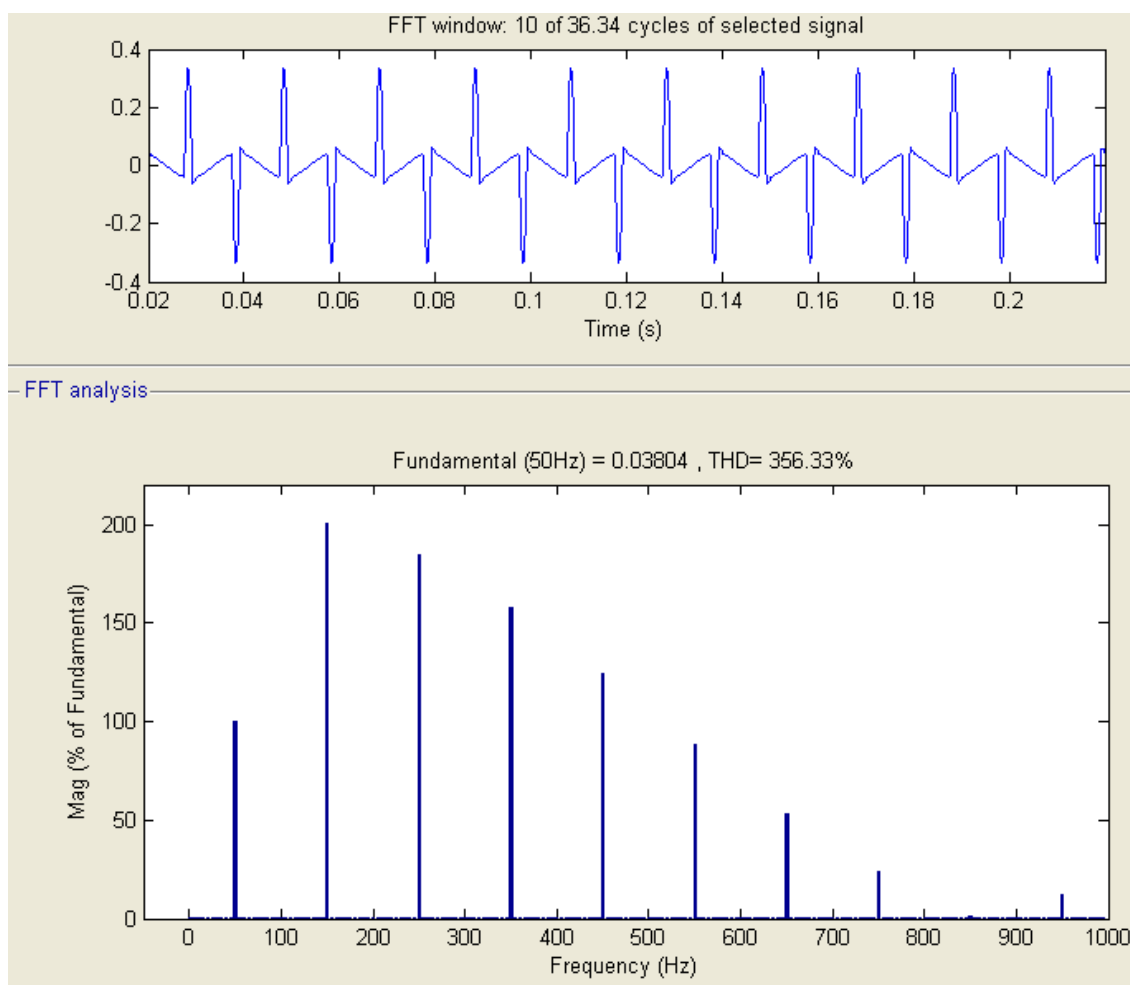


Figure 3.27 Harmonic analysis of TCR phase current when angle is equal to 165.

When the firing angle equals 165 degree, harmonic analysis of phase current of TCR is shown figure 3.27. The amplitude of odd harmonics of fundamental frequency is bigger than amplitude of fundamental frequency. Because appearance of the phase current waveform of TCR is so far away from sinus form, hence, change of harmonic distortion level.

In delta connected TCR, all odd harmonics can be seen as shown figure 3.27.

When the firing angle is equal to 165, TCR line current and its FFT:

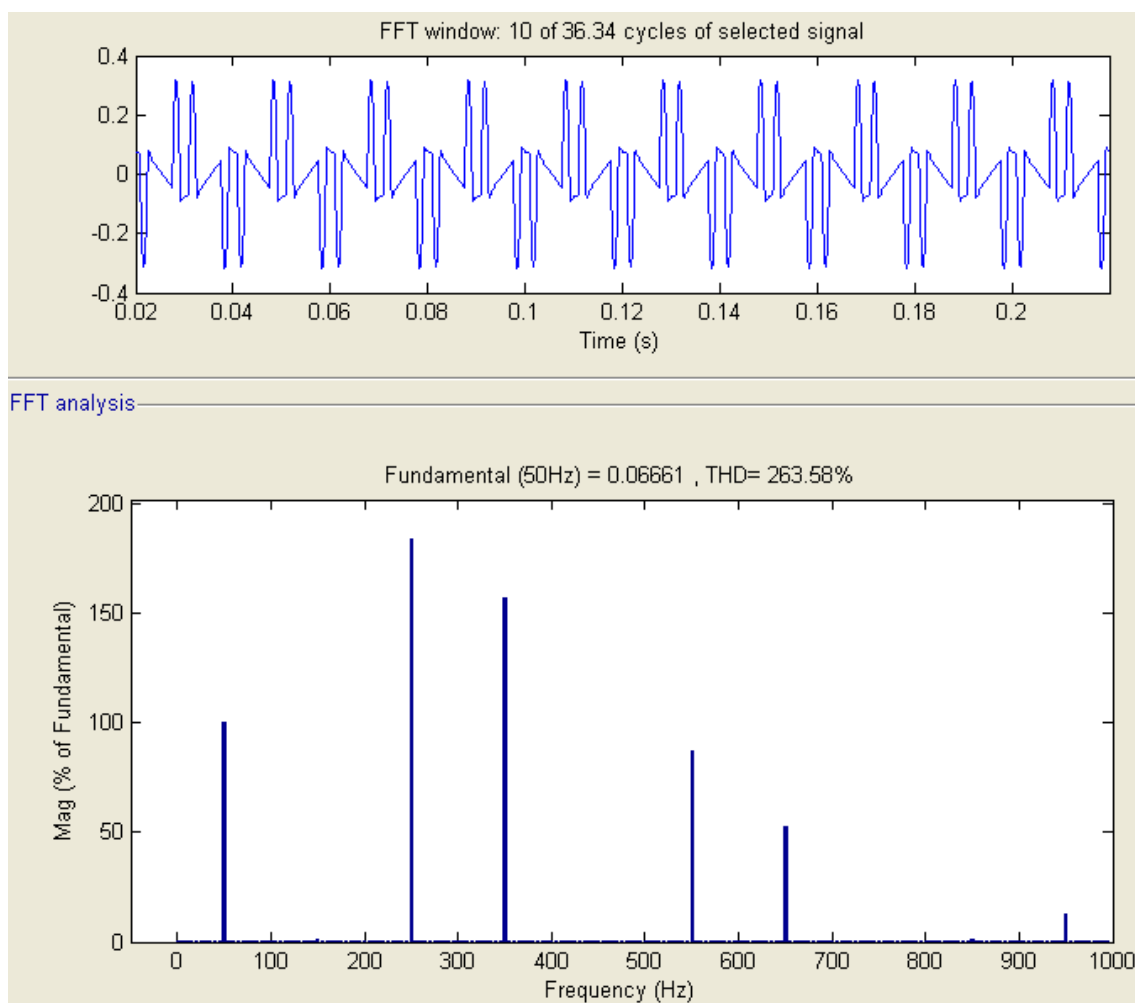


Figure 3.28 Harmonic analysis of TCR line current when angle is equal to 165.

It is clear that when the system is balanced, all the triple harmonics circulate in the closed delta (TCR connected delta) and are absent from the line currents. All the other harmonics are present in the line currents and their amplitudes are increase when firing angle is increase as shown figures 3.22, 3.24, 3.26, 3.28.

3.4 Current And Voltage Measurement Sensors And Circuits

TCR model is obtained in PSCAD and MATLAB. This model shows that the implementation needs the three phase voltage and current measurements. The voltage and current sensors are used for this purpose.

This sensors output is not convenient for analog-digital converters which can do sampling between 0-5V so the signal is needed update between this levels. Because of this level, we create these shaping circuits:

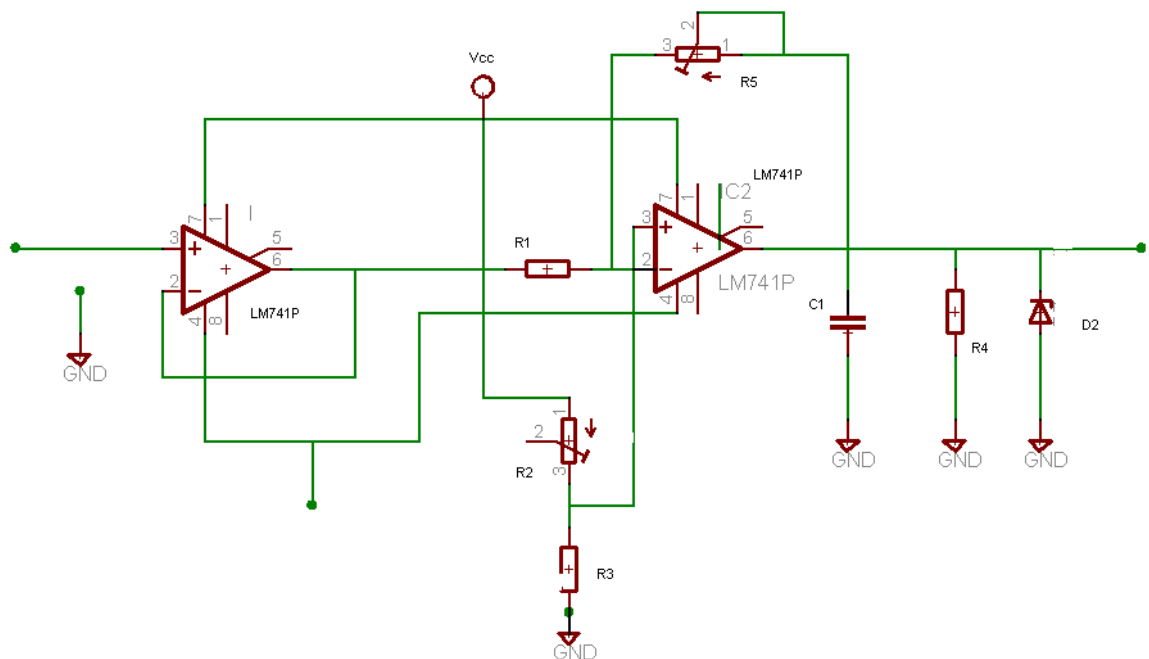


Figure 3.29 Signal shaping circuit.

Firstly the signal enters the buffer circuit which output can be minimizing with gain ($R5/R1$). This signal is adding with offset value which is adjustment by voltage divider resistance ($R2, R3$). Between the 0-5V signal is filtration from noise by capacitor.

3.5 Pulse Drive Circuit

We are using ezdsp2812 processing form Texas instrument. Our programs outputs (pulse) drive thyristor but these pulses do not connect directly from DSP to thyristor. So we must create pulse drive circuit between DSP and thyristor.

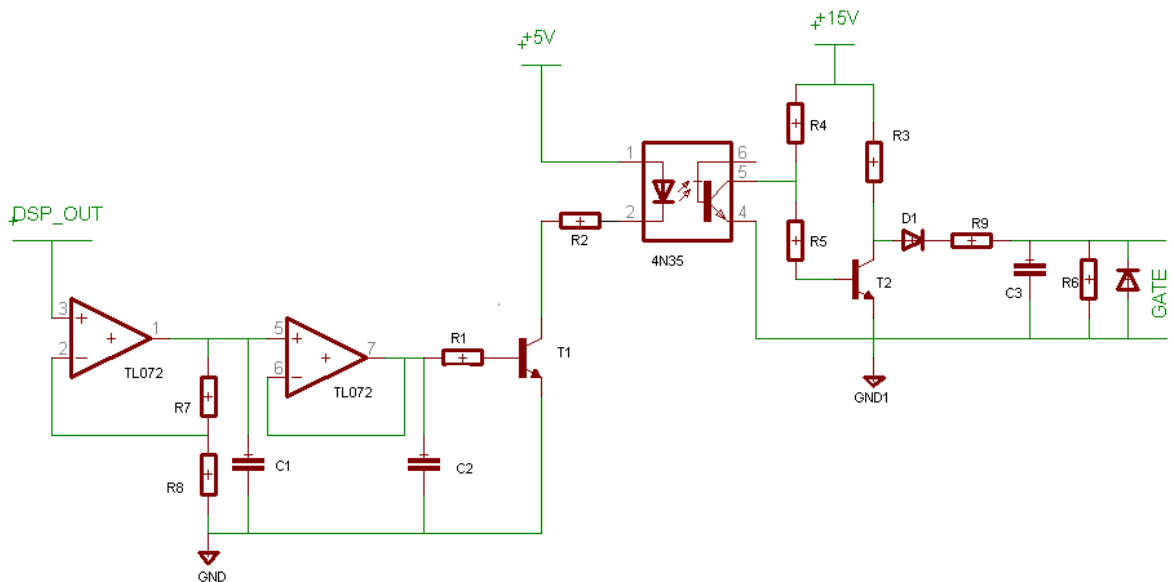


Figure 3.30 Pulse drive circuit .

In figure 3.30, we use 4N35 for isolation between DSP and thyristor side. DSP signals amplify from 3.3V to 5 V with rate of $\left(1 + \frac{R7}{R8}\right)$. And this signal enters the buffer circuit and its output enters the gate of transistor. When this transistor is active, optocoupler (4N35) output is active.

3.6 Zero Crossing Detection

The zero crossing circuit is given in Figure 3.31. The input of the circuit is supplied by the phase voltage passed through a center tapped transformer. The output of the circuit provides pulses at the zero crossing of voltage.

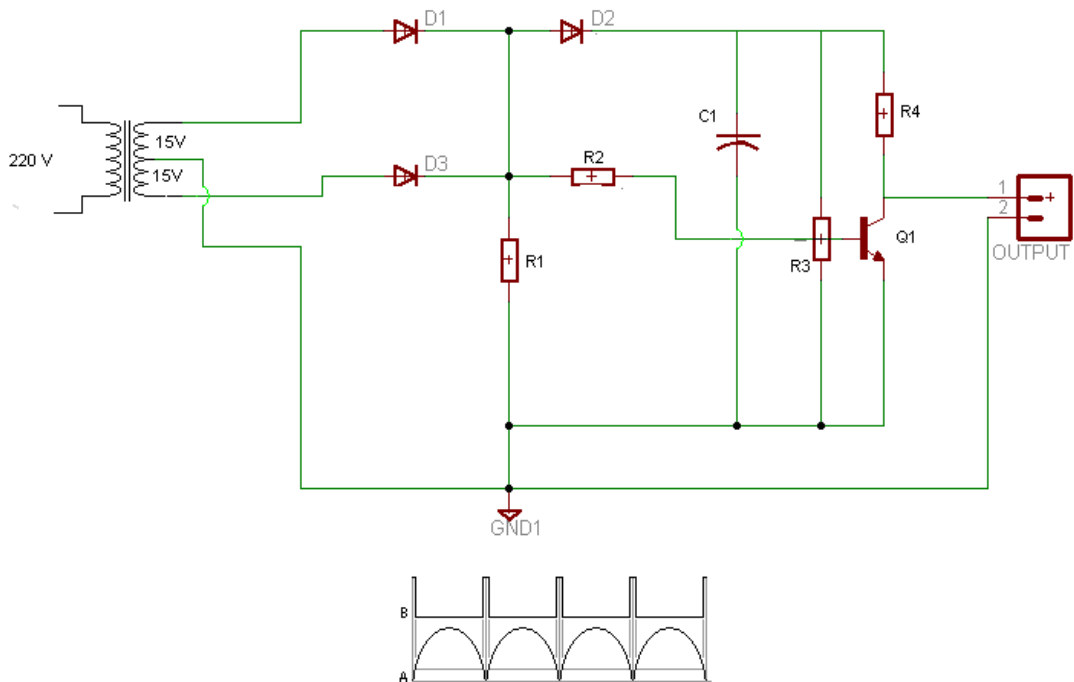


Figure 3.31 Zero crossing detection circuit .

The circuit is sensitive to threshold level present. R1 is used to ensure that the voltage falls to zero. C1-stray capacitance should be selected at a reasonable value to operate the circuit properly. The measured waveform is given in figure 3.32.

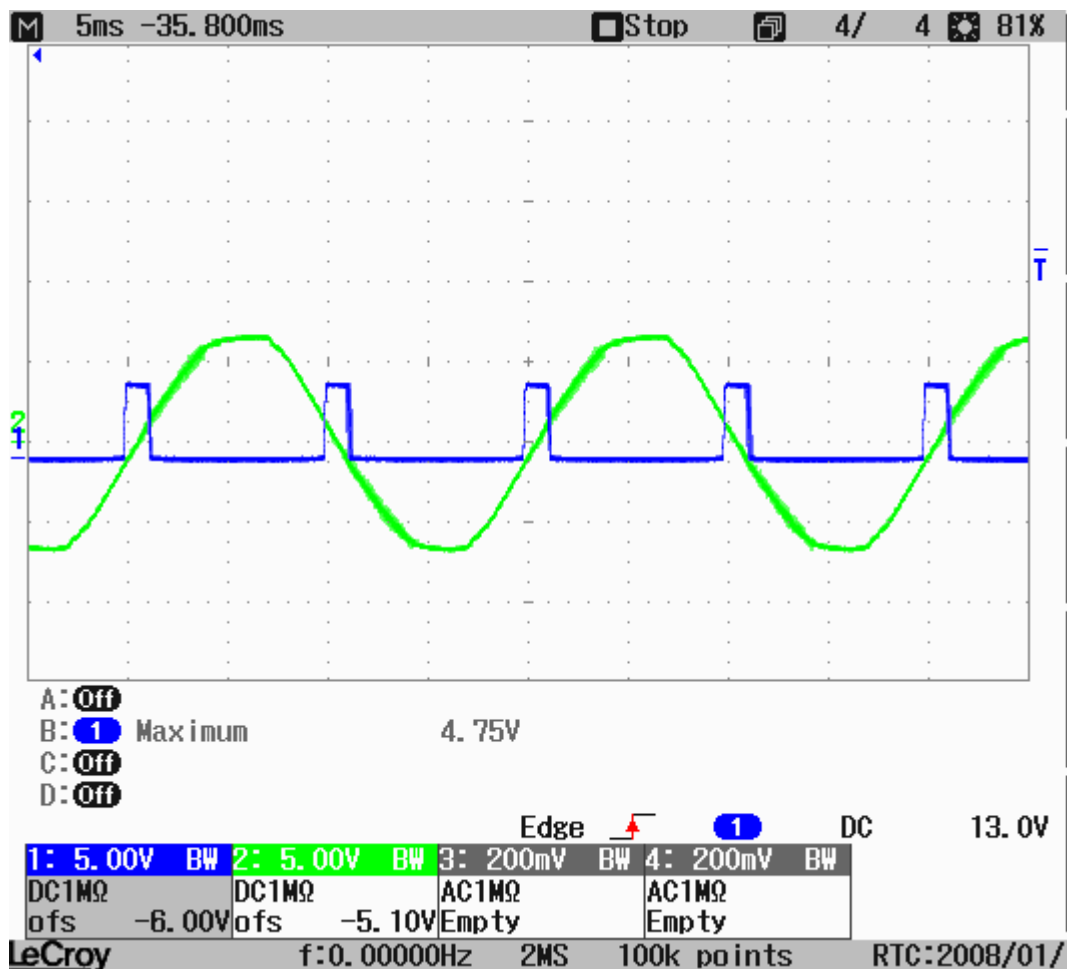


Figure 3.32 Phase voltage and zero crossing detection circuits output.

In figure 3.33 is used with its drive circuit desired before. Figure 3.33 shows that the negative cycles are not fired properly in time as shown in figure 3.34. The reasons of that the zero crossing detection needs to give sufficient delay to the pulses to capture the negative cycles.

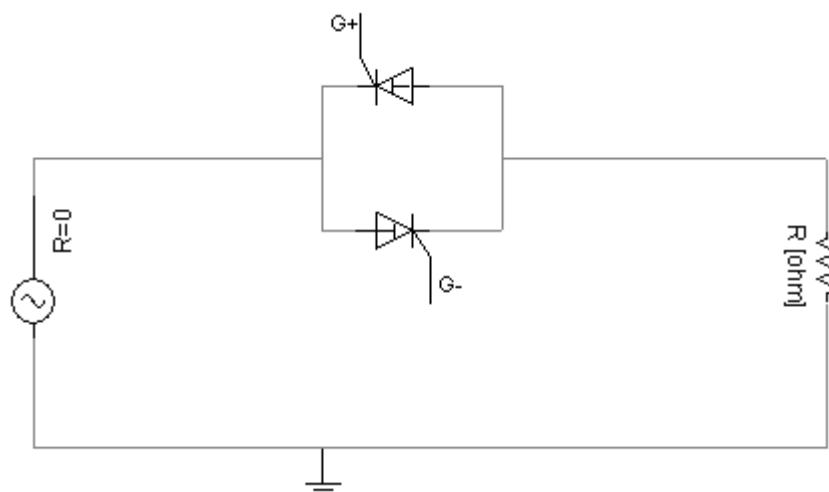


Figure 3.33 Single phase system.

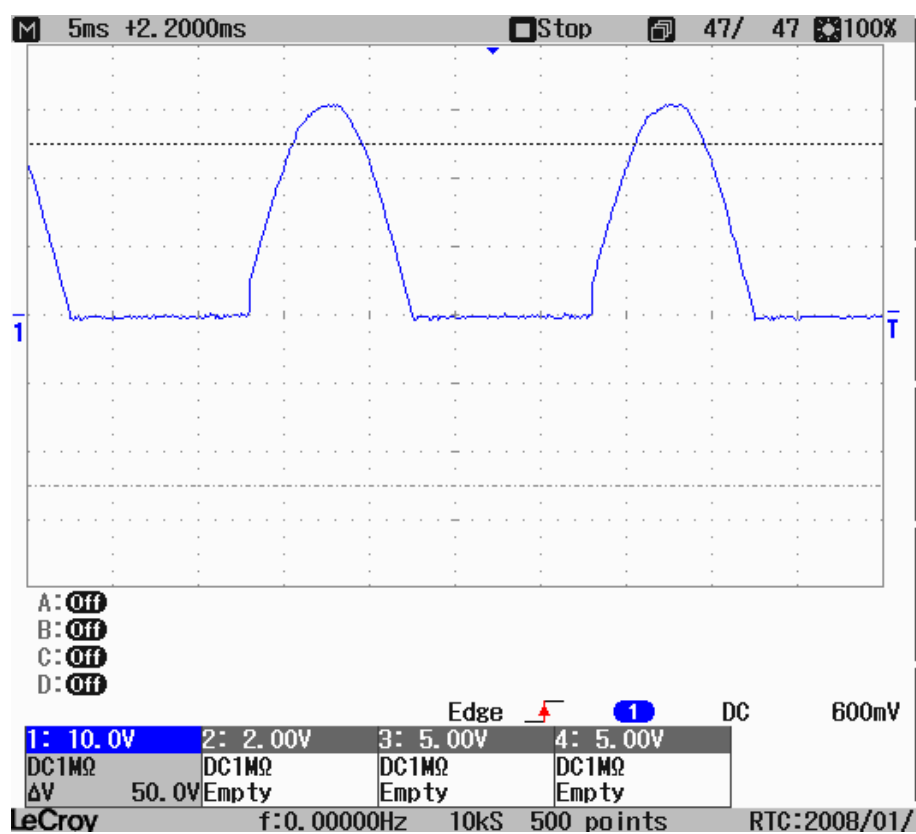


Figure 3.34 Voltage waveform on R.

3.7 Phase Delay Circuit In PSPICE

The firing angle of a Thyristor is usually generated due to a reference. This reference in some applications is the zero crossing of supply voltage. The following circuit (figure 3.35) generates sinusoidal voltage with a phase difference according to its input. This phase difference is adjusted with R1 and C3. When the circuit is combined with a zero crossing circuit, the output of zero crossing circuit will have a pulse having delay adjustable delay.

The phase delay circuit is analyzed in PSPICE before implementation. All the circuit parameters are set forth due to the simulation result. figure 3.36 shows the simulation result of the circuit.

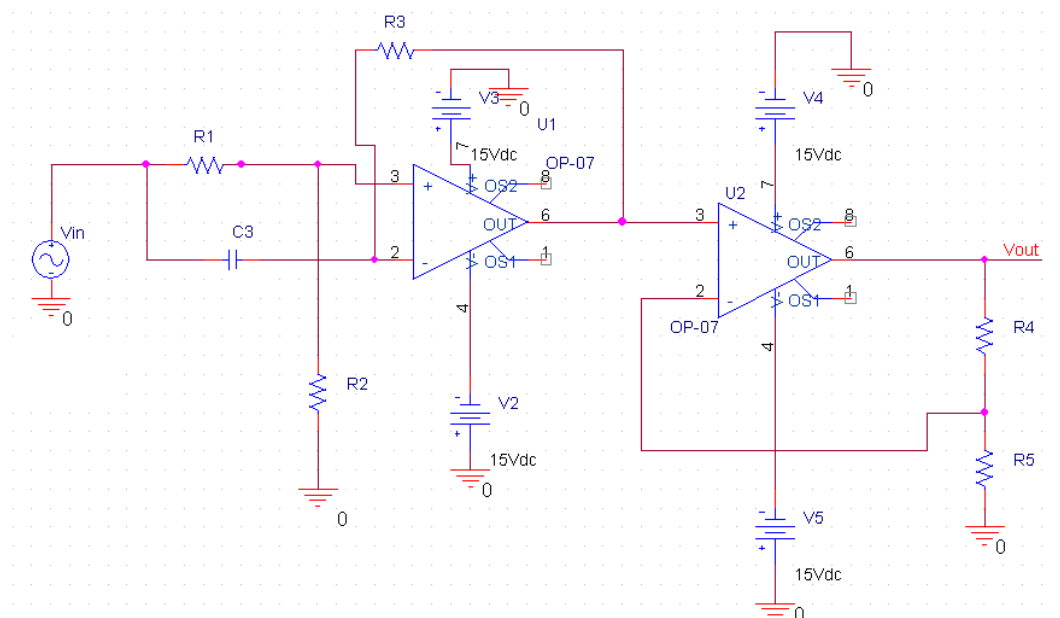


Figure 3.35 Phase delay circuit.

In figure 3.35, this circuit's input is 4.5 Volt because of transformer's turns ratio (220/4.5 V). First opamp is for delay second opamp is for amplifier 4.5 V to 5 volt which is a standard voltage level for processing. This circuit output and input in PSPICE is shown figure 3.36.

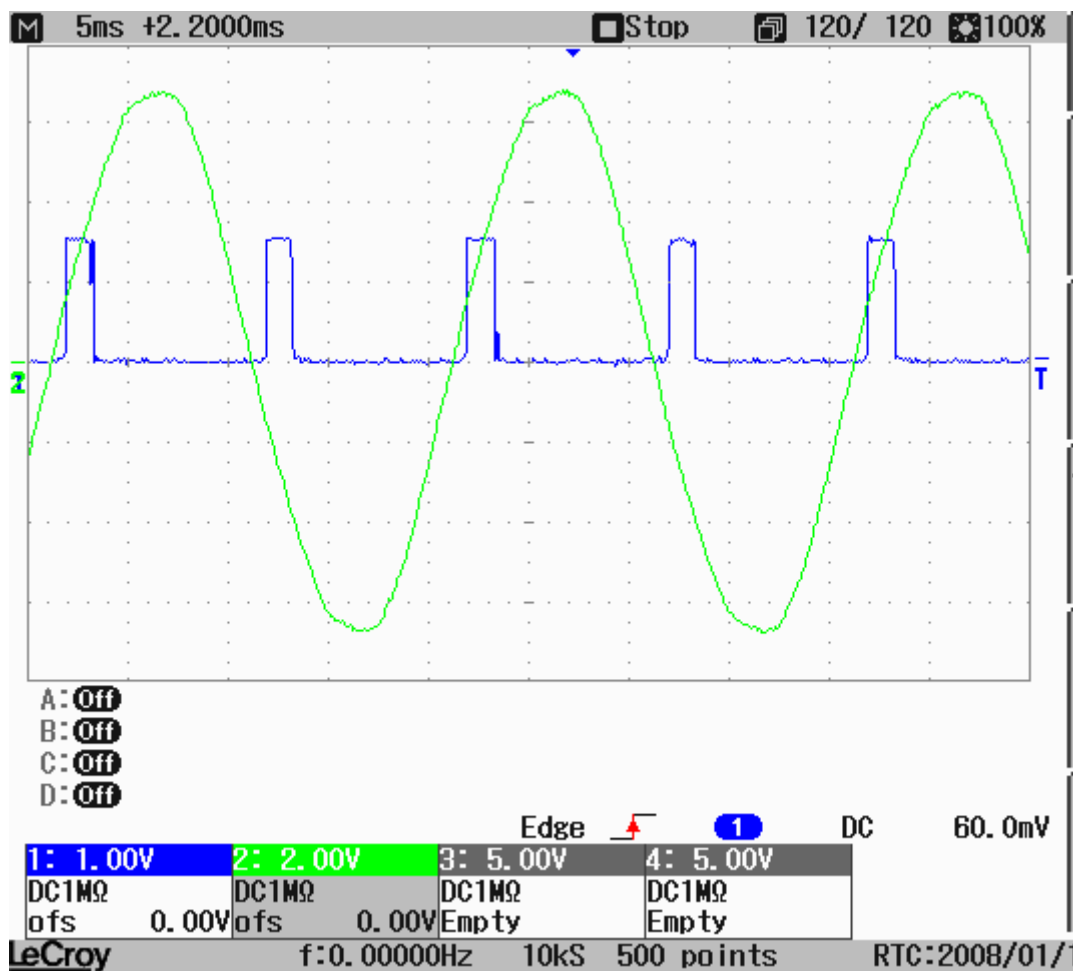


Figure 3.38 Zero crossing circuit with phase delay input and output

Figure 3.39 shows the load voltage of an AC/AC converter. This circuit is given in figure 3.33. The thyristors are fired at zero delay.

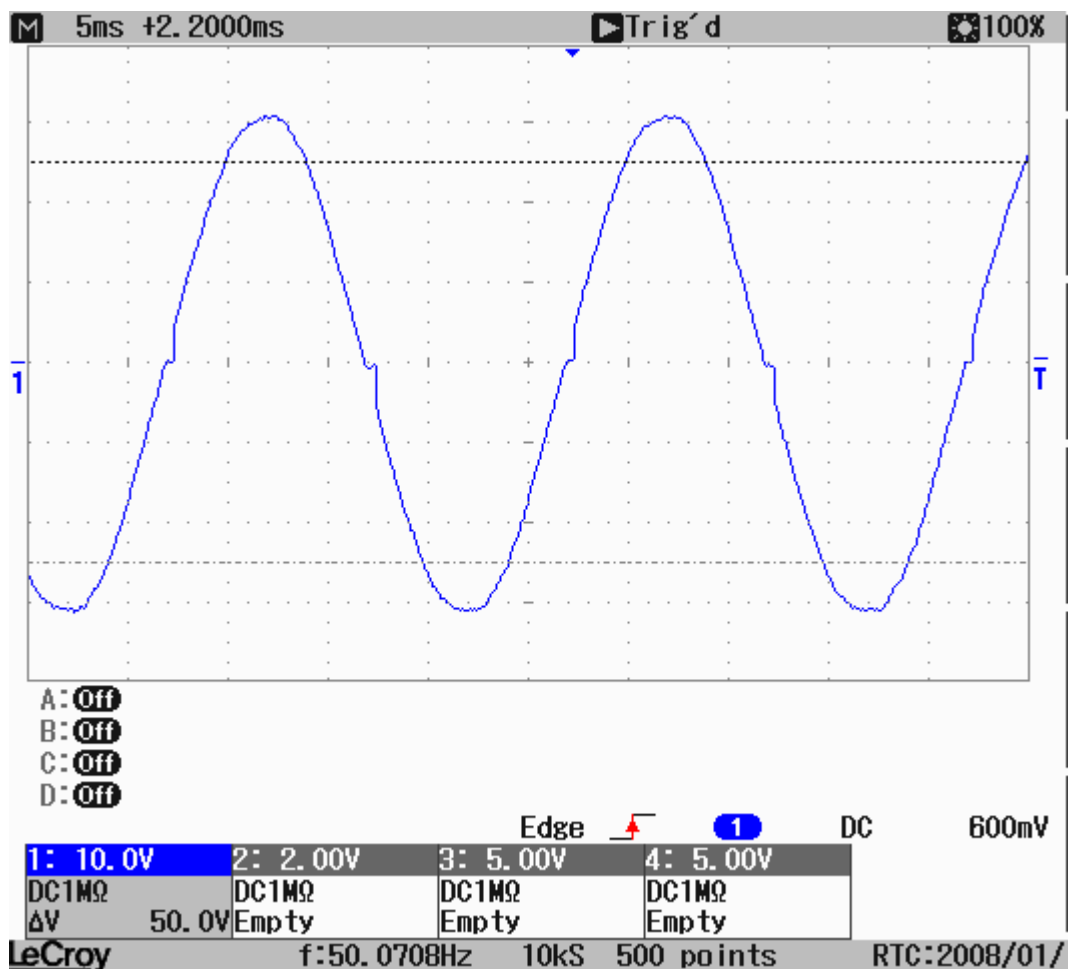


Figure 3.39 Voltage waveform on R.

As a result, the voltages are delayed and its zero crossing is found. Figure 3.39 shows the output voltage (voltage across the R) of AC to AC converter give figure 3.33.

CHAPTER FOUR

EXPERIMENTAL RESULTS OF TCR

The circuit given in figure 4.1 (b) is implemented in the laboratory for the TCR. The load R is variable load varying between 0 and 3kW. The capacitors are also varied between 0 and 3 kVAR. The TCR circuit (0-3kVAR) is controlled to obtain the unity power factor at supply side.



(a)

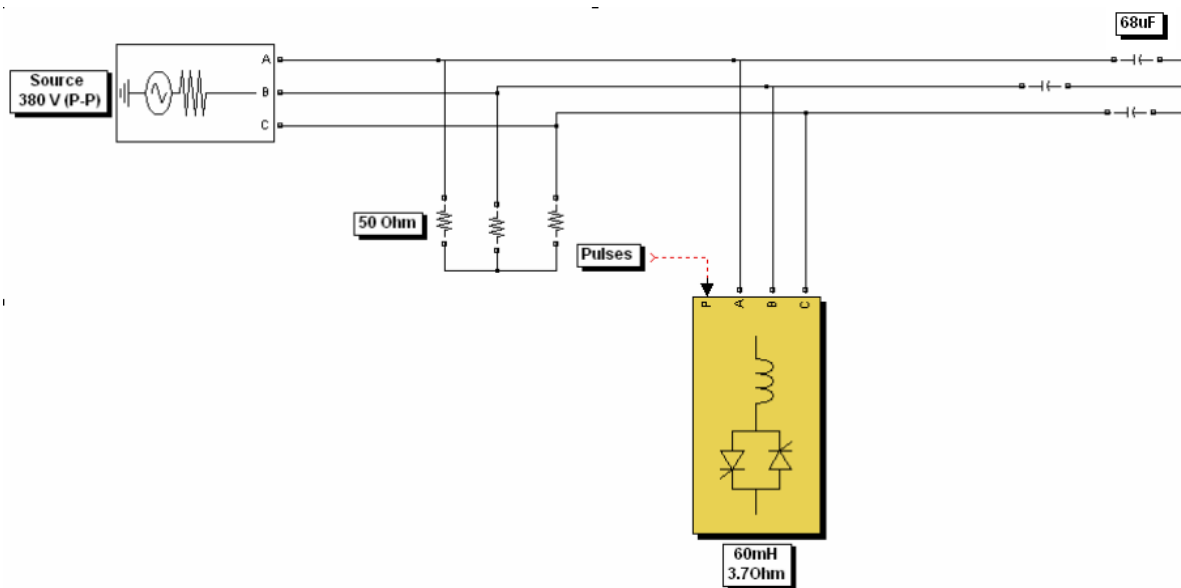


Figure 4.1 (a) Experimental TCR unit (b) schematic of the system.

Figure 4.2 shows supply voltage and supply current at leading power factor. This loading condition is obtained with balanced operation as being shown in figures 4.3 and 4.4.

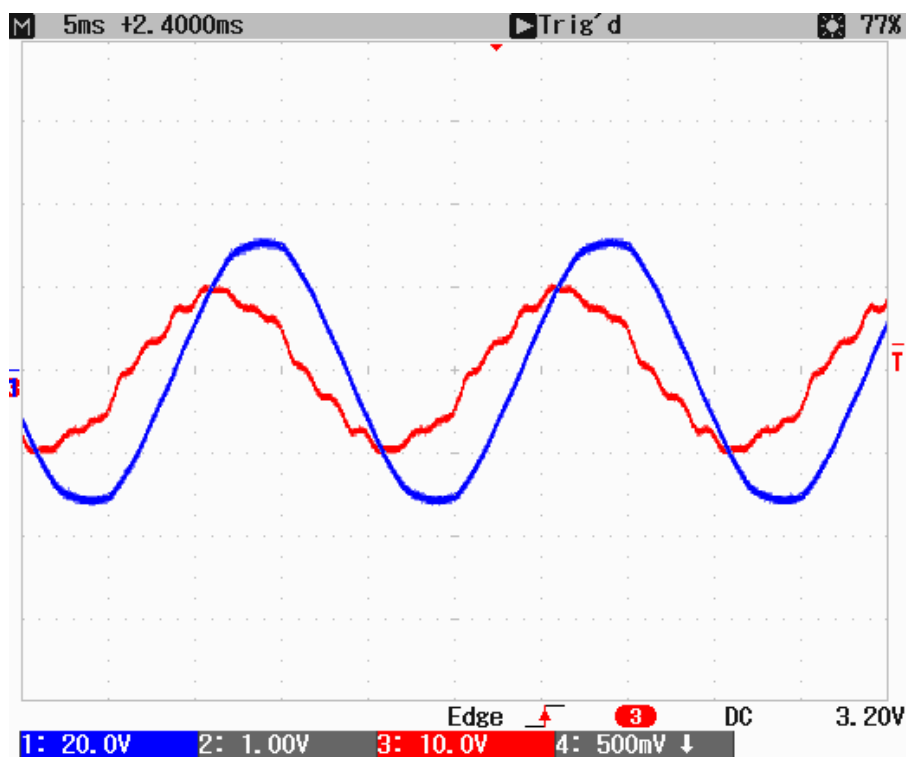


Figure 4.2 $V_a - I_a$ (before compensation in source).

Because of RC load, the current is leading to voltage. This capacitive loading is compensated by the TCR. The loading conditions in the industry are usually changing. Therefore, the value of inductance is automatically set by the TCR unit in order to get zero phase shift between voltage and current.

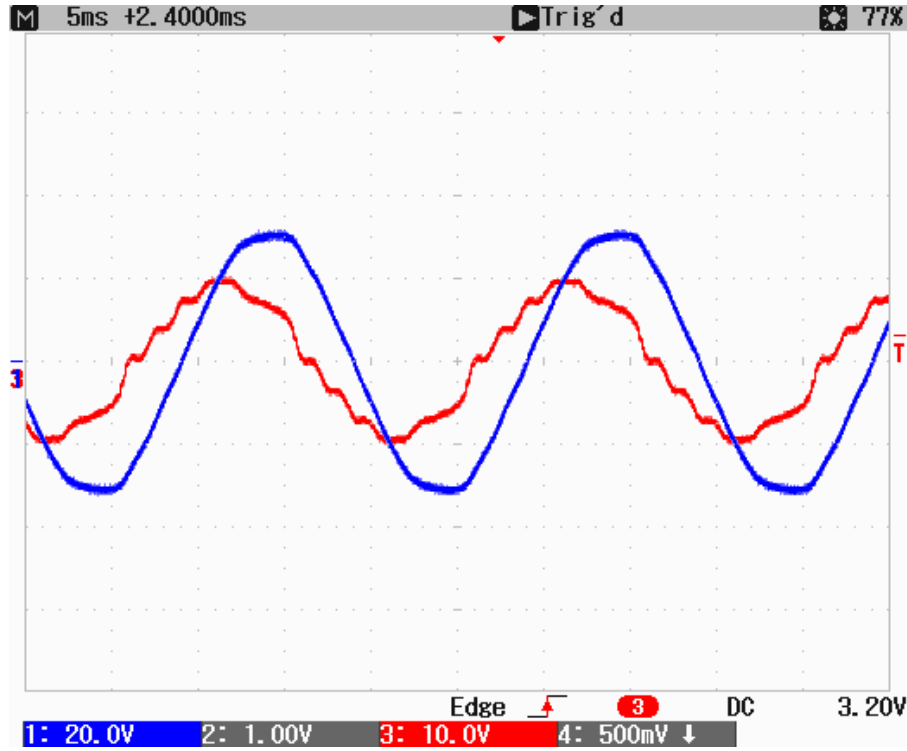


Figure 4.3 $V_b - I_b$ (before compensation in source).

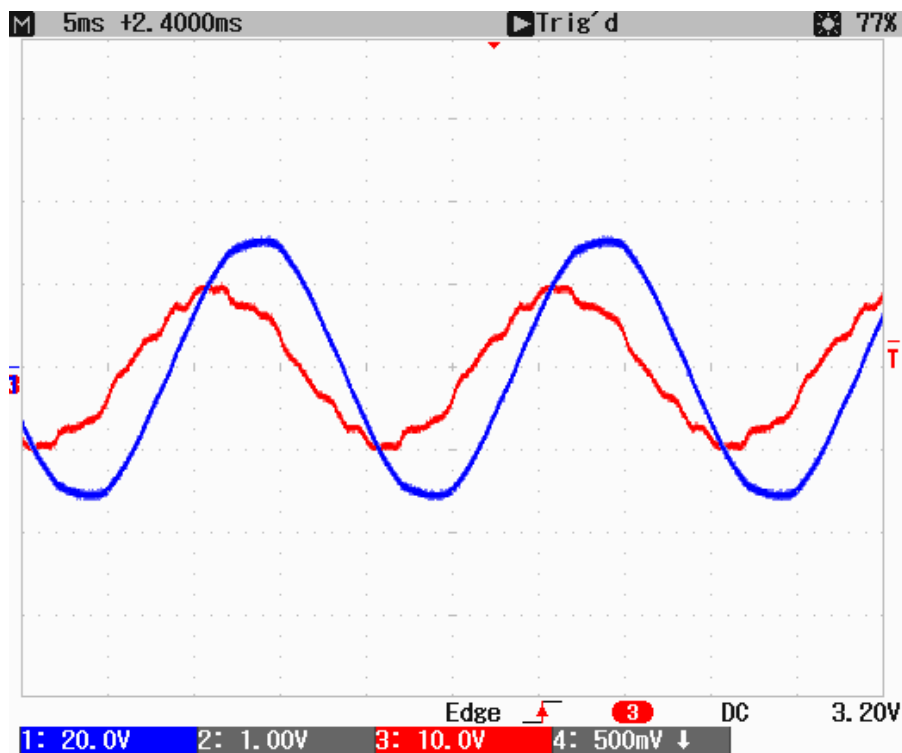


Figure 4.4 $V_c - I_c$ (before compensation in source).

When the DSP based circuit is operated for compensation, the current and voltage are brought to the position in phase. Figures 4.5, 4.6 and 4.7 show the measured results over all phases.

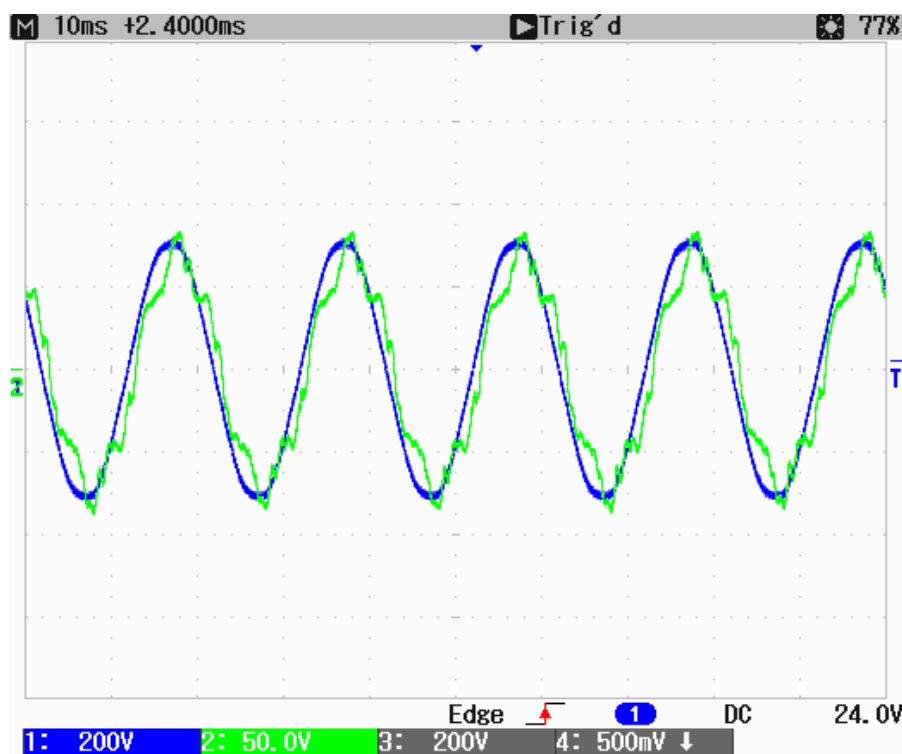


Figure 4.5 $V_a - I_a$ (after compensation in source).

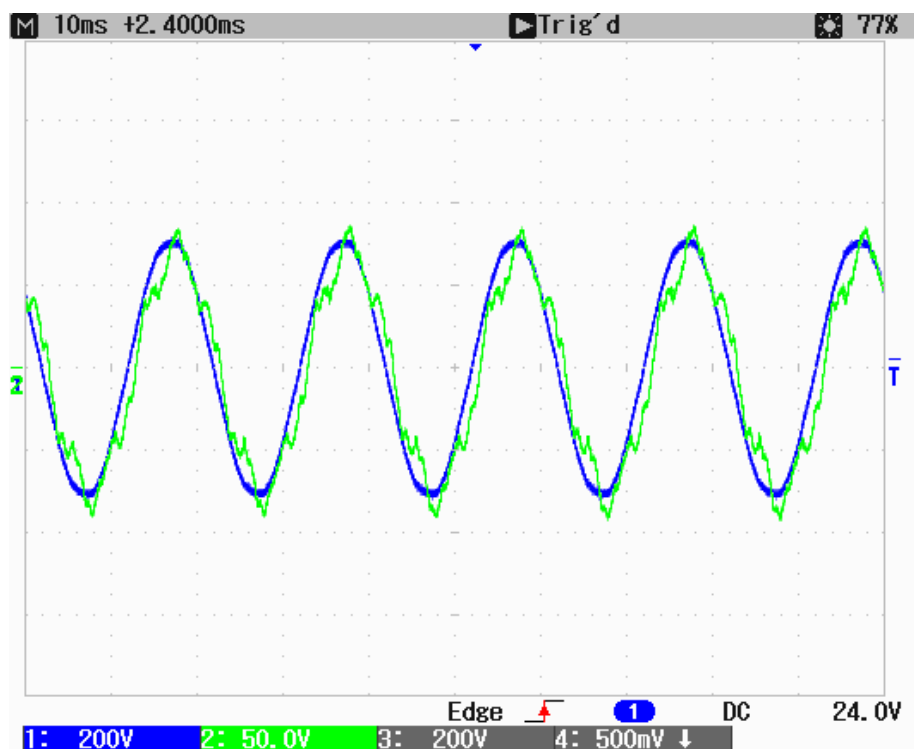


Figure 4.6 $V_b - I_b$ (after compensation in source).

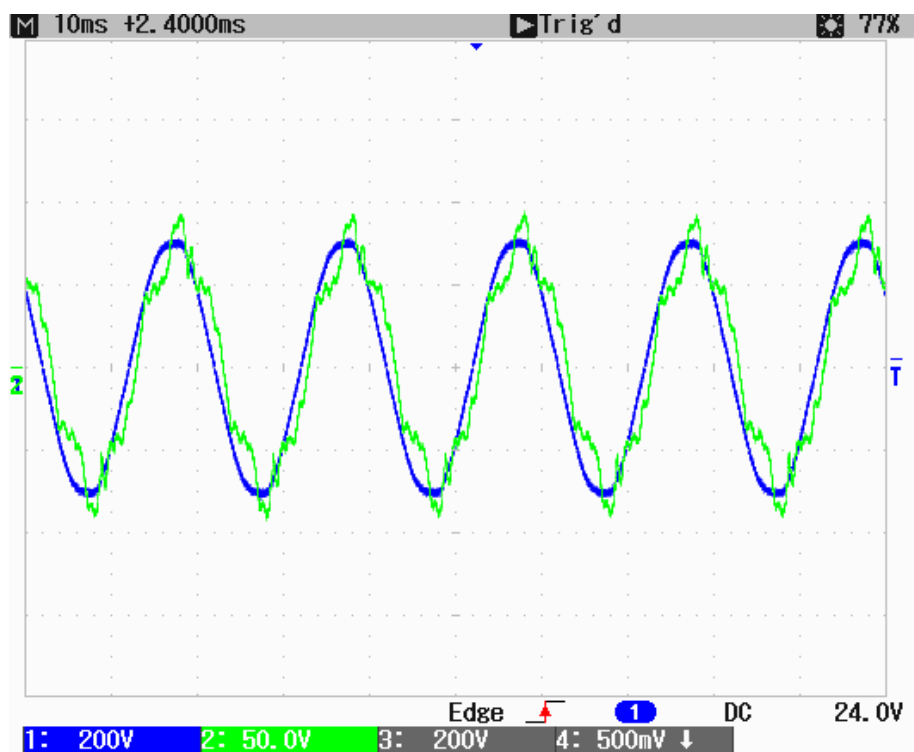


Figure 4.7 $V_c - I_c$ (after compensation in source).

TCR circuit is connected in parallel with compensation capacitors designed with reactive power measurement relay. The circuit is given in figure 4.8.

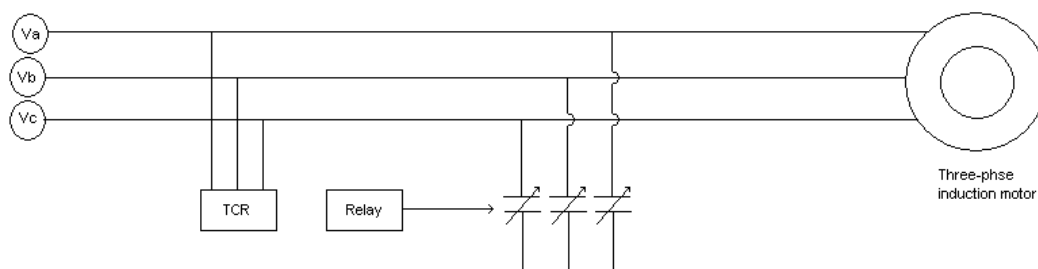


Figure 4.8 New system for compensation.

Three phase motor is started up and its reactive power is compensated by the discrete capacitors controlled by a relay. The excessive reactive power is drawn by TCR circuit successfully such that supply power factor is unity.

Here, discrete capacitors steps value is 0.5, 1, 1.5 and 2.5 kVAR and power of induction motors 4kW.

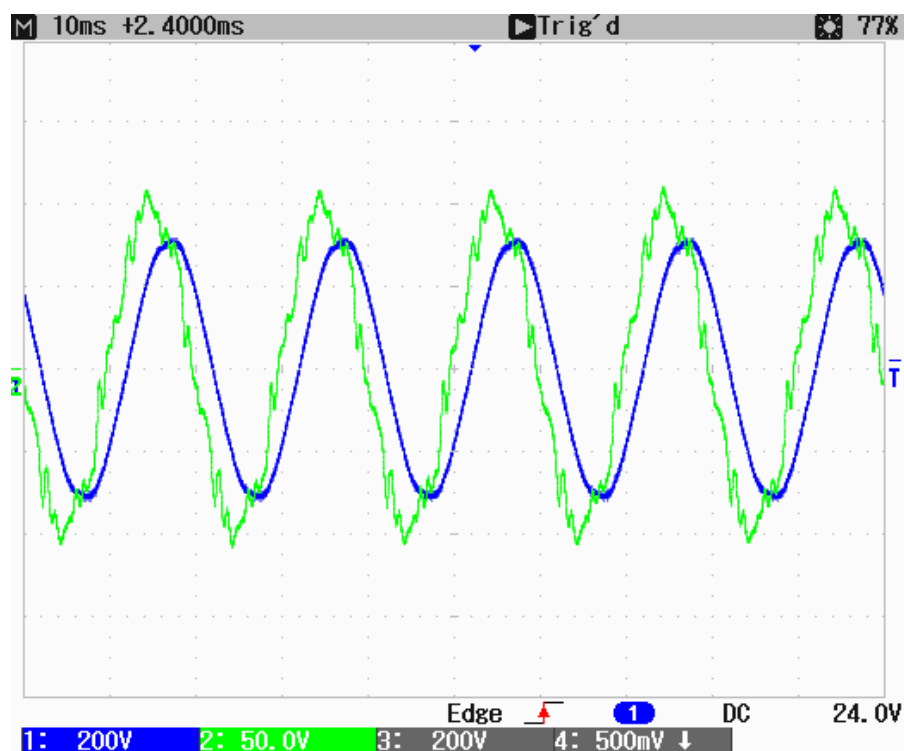


Figure 4.9 $V_a - I_a$ (only with changeable capacitor bank)

The induction motor absorb the reactive power and discrete capacitors generate reactive power but capacitive reactive power is not equal to inductive reactive power so the current is leading from the voltage as shown figures 4.9, 4.10 and 4.11.

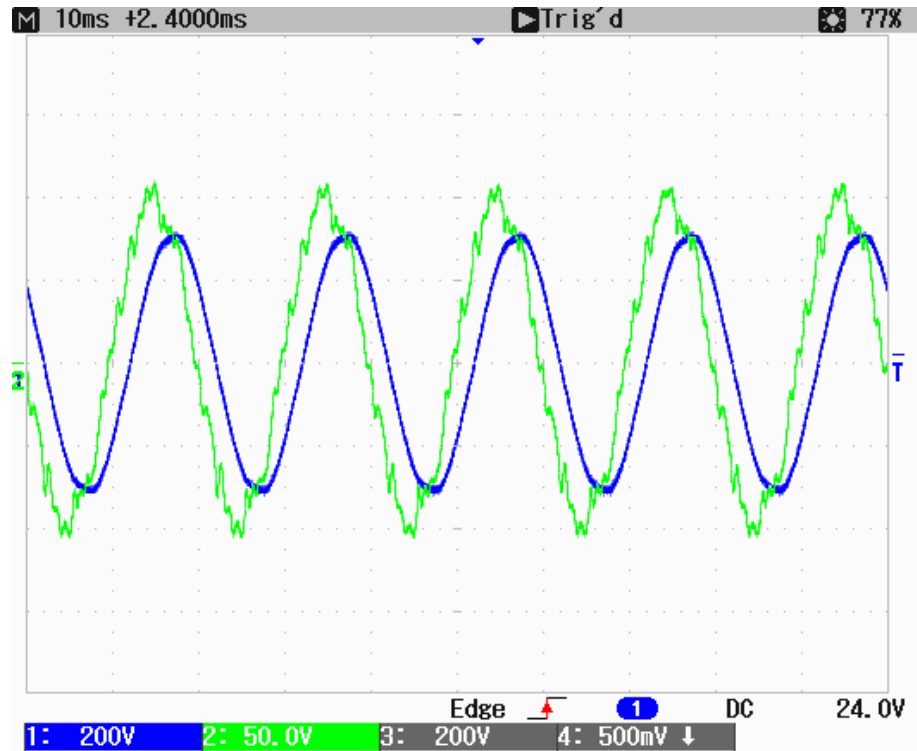


Figure 4.10 $V_b - I_b$ (only with changeable capacitor bank).

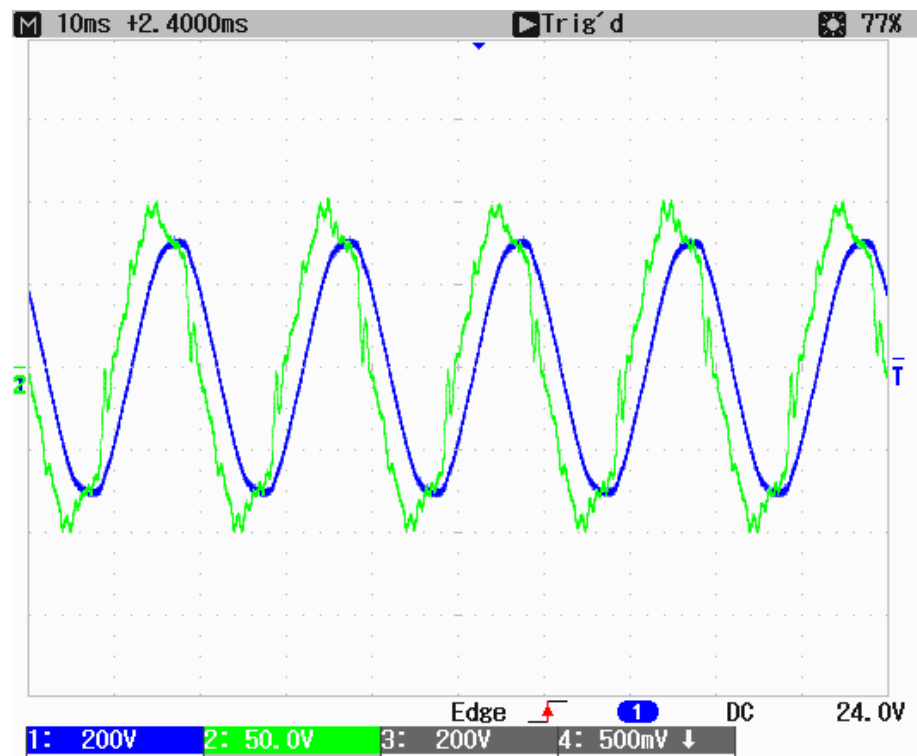


Figure 4.11 $V_c - I_c$ (only with changeable capacitor bank).

Figures 4.9, 4.10 and 4.11 show the phase voltages and currents and supply side. When the TCR unit is operated the currents of all phases are brought to be in phase with voltages. These results are given in figures 4.12, 4.13 and 4.14.

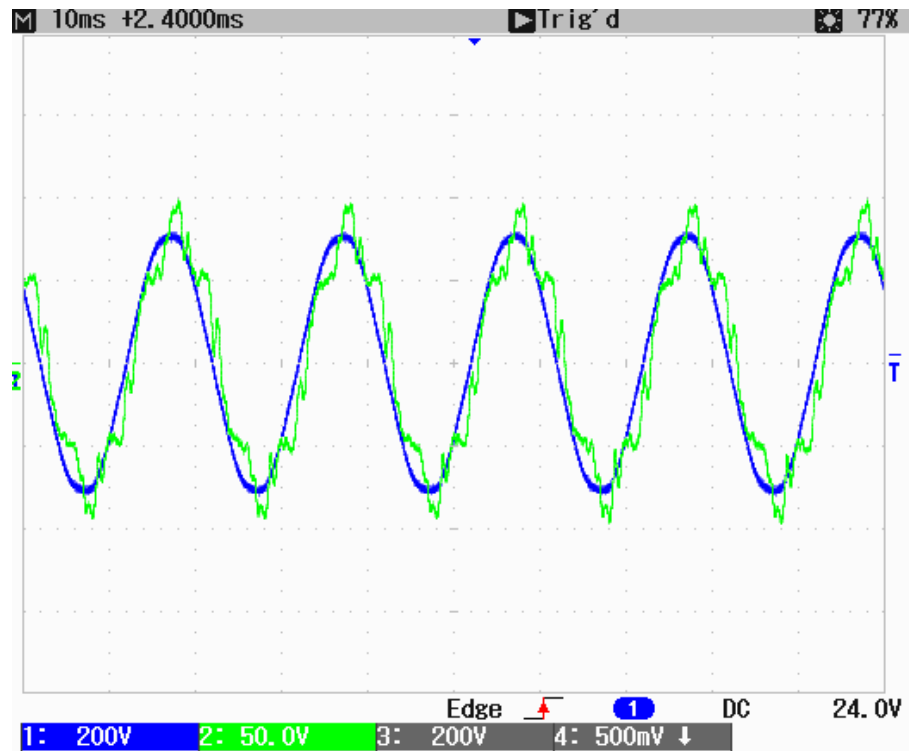


Figure 4.12 $V_a - I_a$ (changeable capacitor bank, tcr, motor).

The TCR absorbs excessive capacitive reactive power from the system. The voltages and currents are in phase as shown figures 4.12, 4.13 and 4.14.

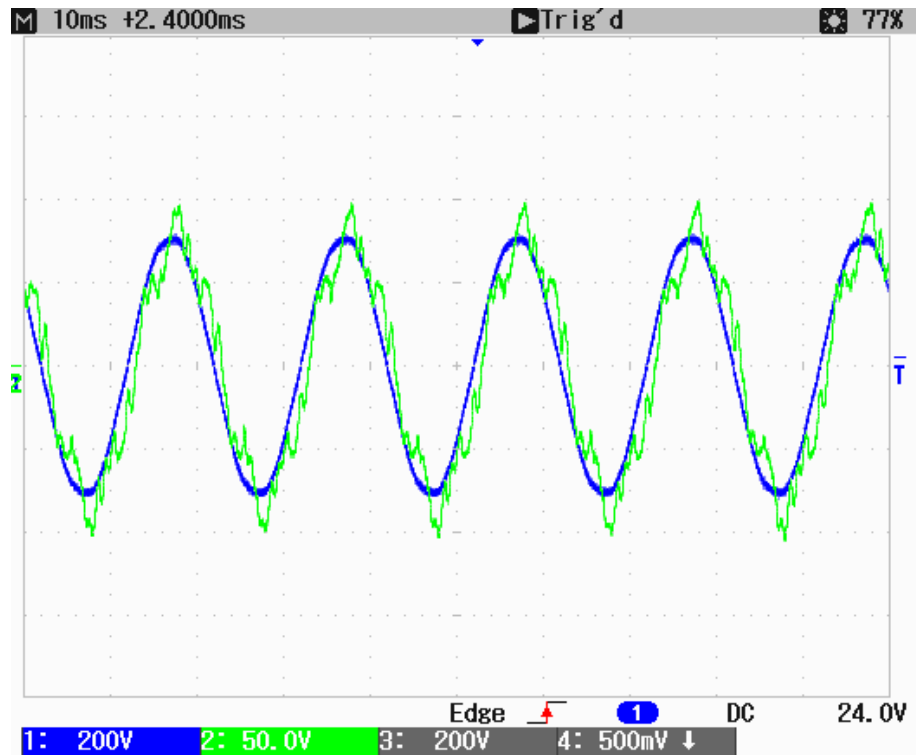


Figure 4.13 $V_b - I_b$ (changeable capacitor bank, tcr, motor).

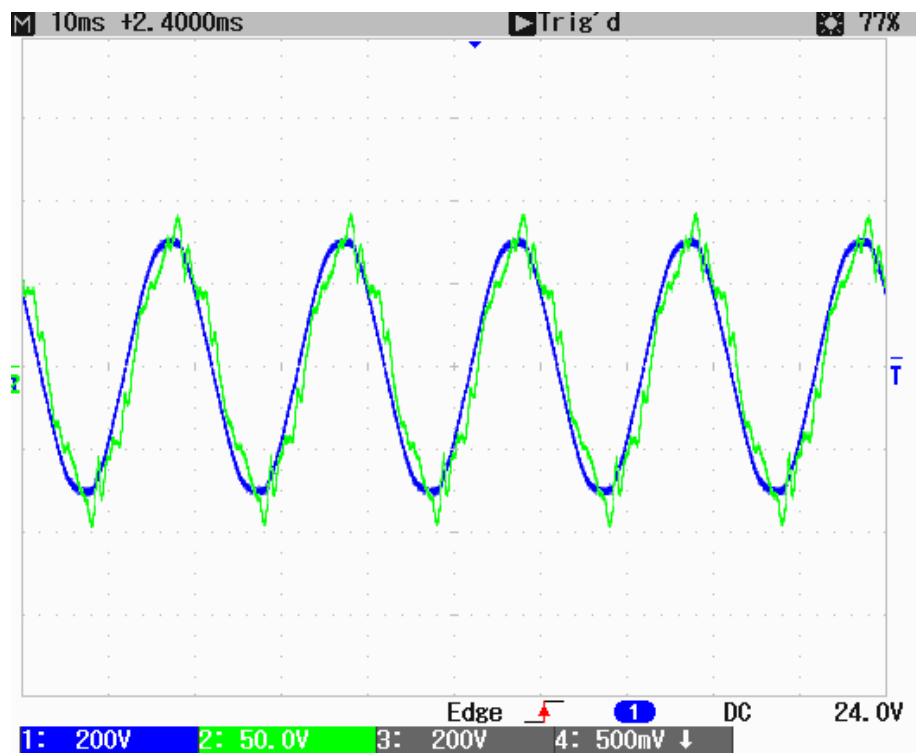


Figure 4.14 $V_c - I_c$ (changeable capacitor bank, tcr, motor).

According to value of reactive power, the firing angles of inductance of TCR are set. Thyristors drive with these angles and the system is compensated these angle. The phase currents in the inductances of TCR unit are recorded and given in figure 4.15, 4.16 and 4.17.

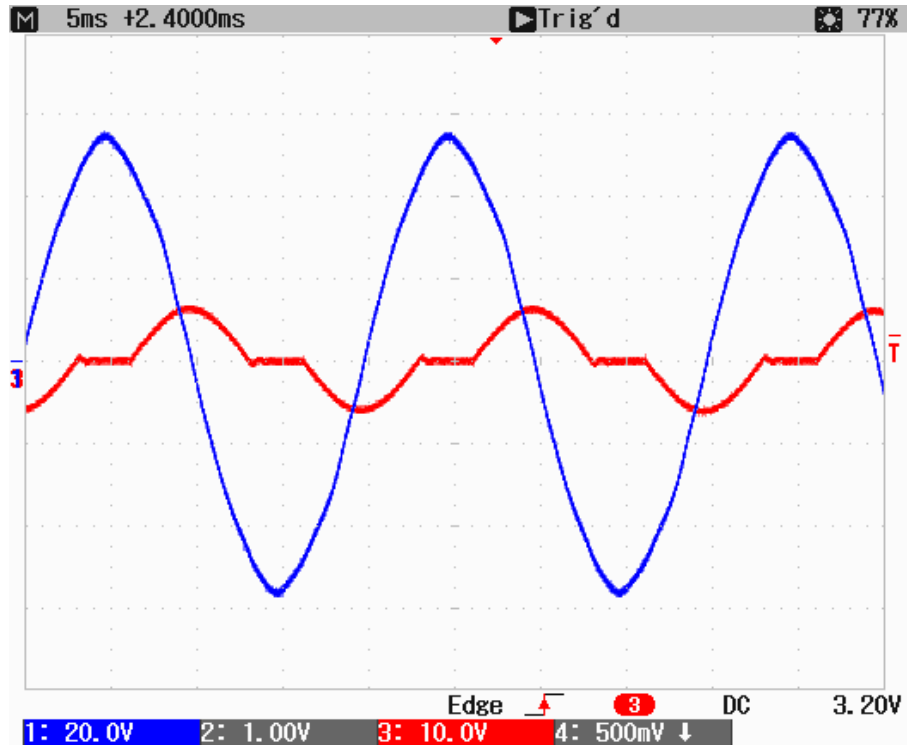
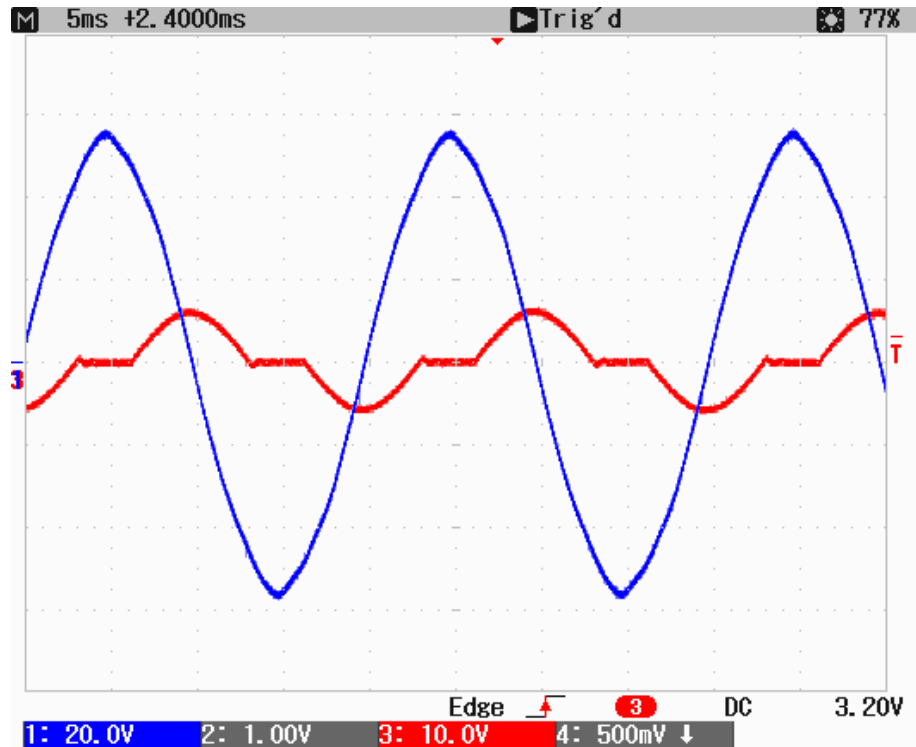
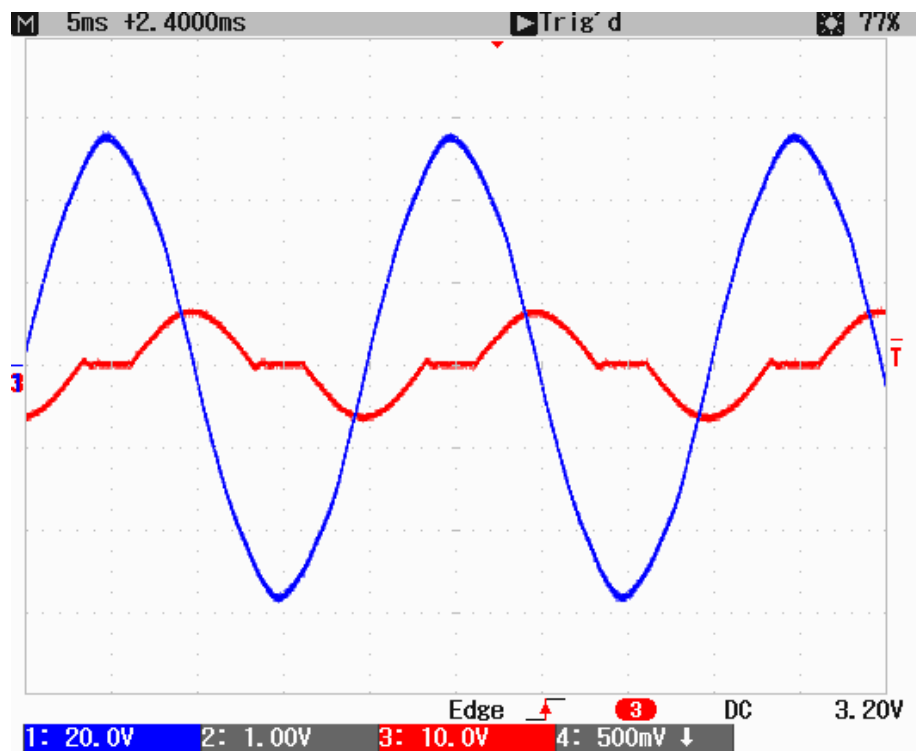


Figure 4.15 $V_{ab} - I_{atcr}$.

This system is balanced so peak value of per phase of inductance of TCR equal to each other as shown figure 4.15, 4.16 and 4.17.

Figure 4.16 $V_{bc} - I_{bcr}$.Figure 4.17 $V_{ca} - I_{ctcr}$.

The operating phase delay is set by the closed loop control in order to get unity power factor.

CHAPTER FIVE

PASSIVE FILTER ANALYSIS

It is clear that if the harmonics exist in the power system, the voltage and currents do not have sinusoidal waveforms in time.

The harmonic filters are built using capacitors, inductors and resistors that provides path for harmonic currents to circulate. Each harmonic filter could contain many such elements, each of which is used to deflect harmonics of a specific frequency.

A harmonic filter is used to eliminate the harmonic distortion caused by the loads. Harmonics are currents and voltages that are continuous multiples of the fundamental frequency of 50 Hz such as 100 Hz (2nd harmonic) and 150 Hz (3rd harmonic). Harmonic currents provide power that cannot be used and also takes up electrical system capacity. Large quantities of harmonics can lead to malfunctioning of the system that results in downtime and increase in operating costs. Figure 5.1 shows a general circuit including harmonic source, filter circuit and the grid.

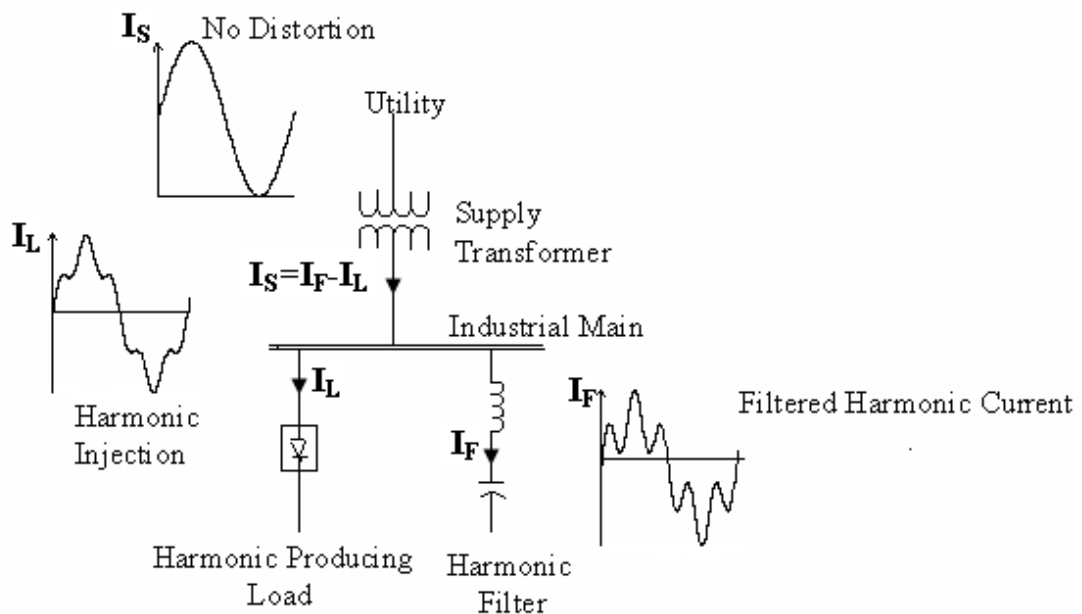


Figure 5.1 General system, load, source and passive filter.

The series resonance frequency of the passive filter can be calculated by using equation (5-1).

$$w_0 = \sqrt{\frac{1}{LC}} \quad (5-1)$$

The filtering application can yield the following advantages in terms of power quality.

- Protects electrical systems
- Increases system capacity
- Decreases system losses
- Reduces transformer loading
- Reduces total harmonic distortion and etc.

In this thesis, electrical arc furnaces located in Aliaga is analyzed in order to identify the effectiveness of passive filter harmonic filters and TCR circuits. The industries use both TCR and passive filters to reduce the effects these harmonics in power system.

5.1 Passive Filter Analysis In PSCAD

5.1.1 Passive Filter Analysis Of Plant1 In PSCAD

The arc furnace named as Plant1 here is represented by the harmonic current sources at different frequencies. The block diagram is depicted in figure 5.2.

System of Plant1 is established in PSCAD. Harmonic filters are connected to each phase. Harmonic orders are 2nd, 3rd and 4th. All harmonic current amplitude is 1000 Amp. Harmonic current frequencies are 100, 150 and 200 Hz.

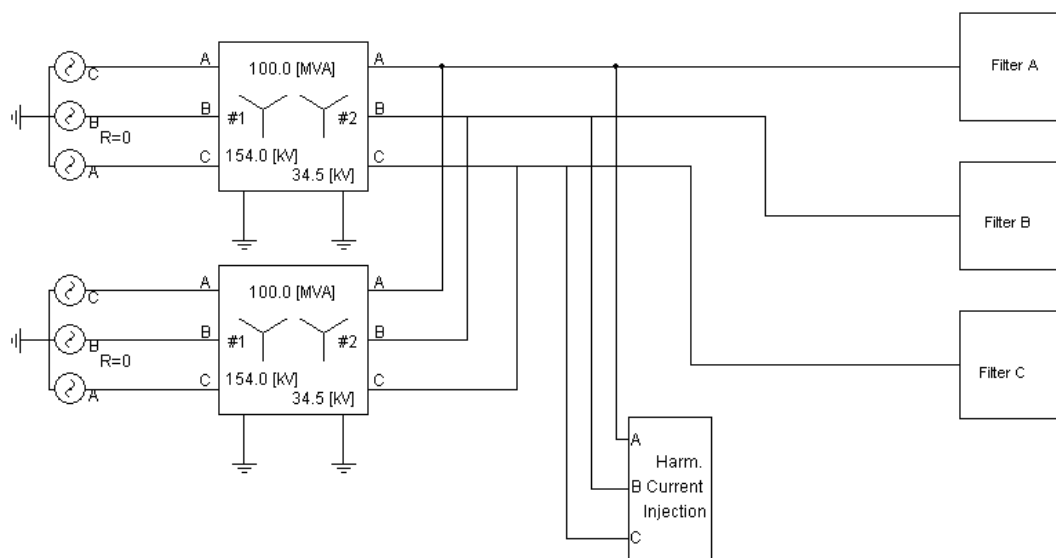


Figure 5.2 Schematic of the system.

The detail of harmonics filters connected to each phase is given in figure 5.3.

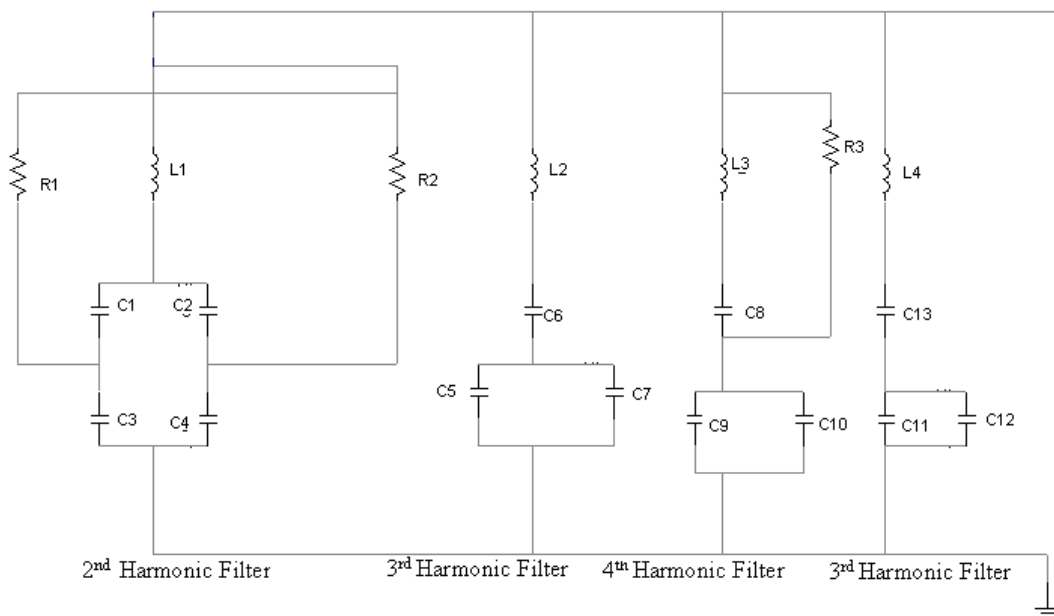


Figure 5.3 Filters of Plant1.

It is expected that 2nd, 3rd and 4th harmonics order filters provide the low to impedances of 100 Hz, 150 Hz and 200 Hz harmonic currents. So the harmonic currents are not flowing through the source.

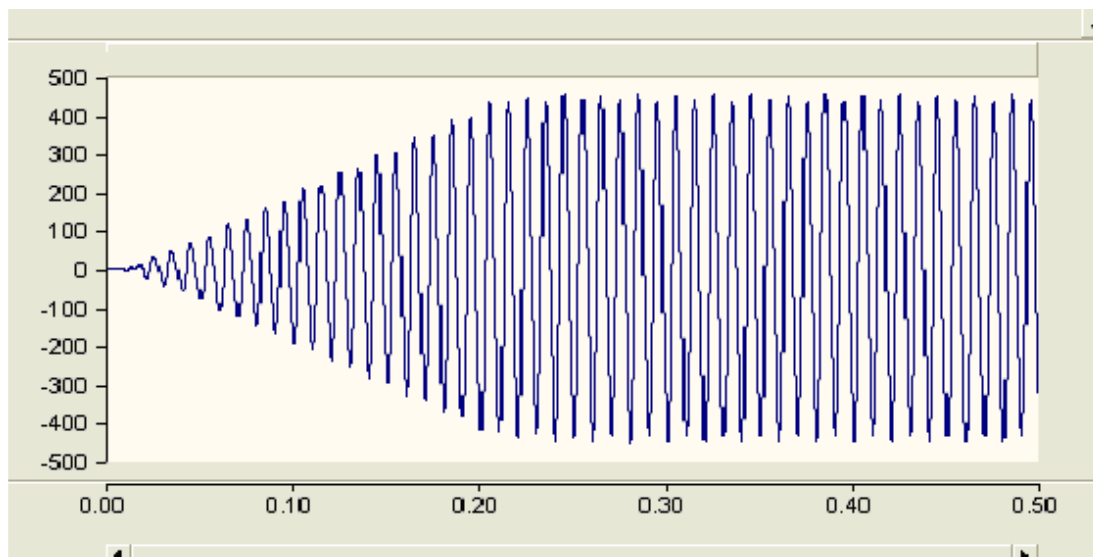


Figure 5.4 2nd Harmonic filter current.

2nd harmonic current is injected to the system at a value of 1000 Amp. But it is clear that the 2nd harmonic filter takes 500 Amp from load as shown figure 5.4. The rest of 2nd harmonic current flows through the source. The filter designed for 2nd

harmonic does not show low impedance good enough to eliminate its effect in the source.

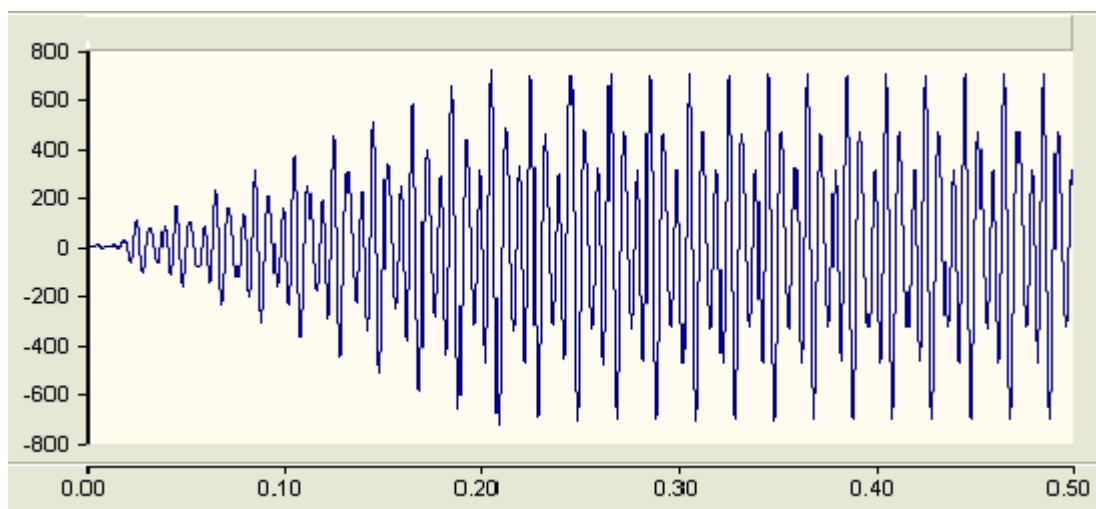


Figure 5.5 3rd Harmonic filter current.

In the system there are two 3rd harmonic filters. It is expected that the 3rd harmonic current equally shares in both of them. Here, 3rd harmonic order filter absorb about 600 Amp of 1000 Amp as shown figure 5.5.

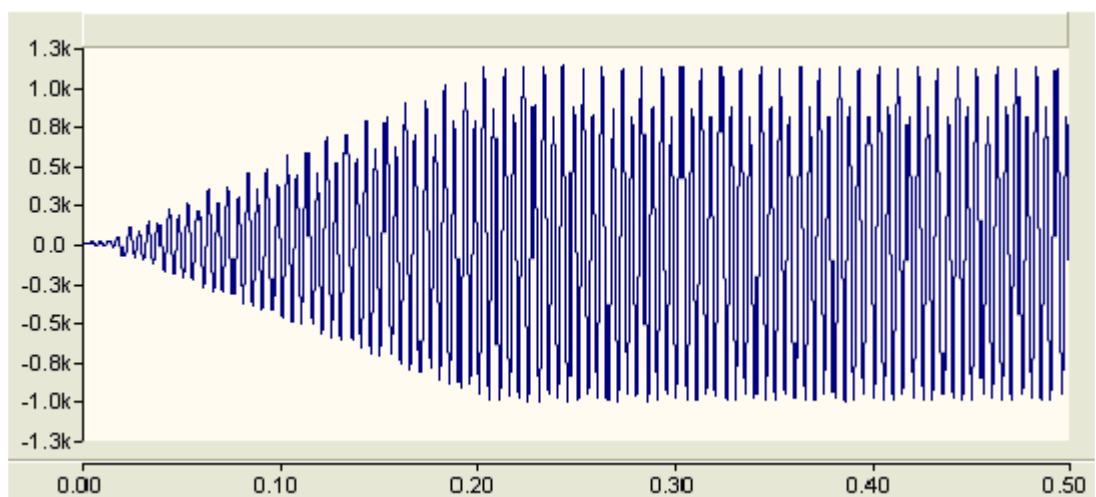


Figure 5.6 4th Harmonic filter current.

The magnitude of 4th harmonic current is 1000 Amp in the system and 4th harmonic filter absorb all of this harmonic current as shown as figure 5.6. It is clear that 4th harmonic filters parameters are set well.

5.1.2 Passive Filter Analysis Of Plant2 In PSCAD

The second plant named as Plant2 in Aliaga region is analyzed for harmonic currents. 2nd, 3rd and 4th order harmonic passive filters have been used in this plant. Therefore these harmonics are represented by related current sources and details of passive filter elements are included in the program of PSCAD. The schematic of the system is given in figure 5.7.

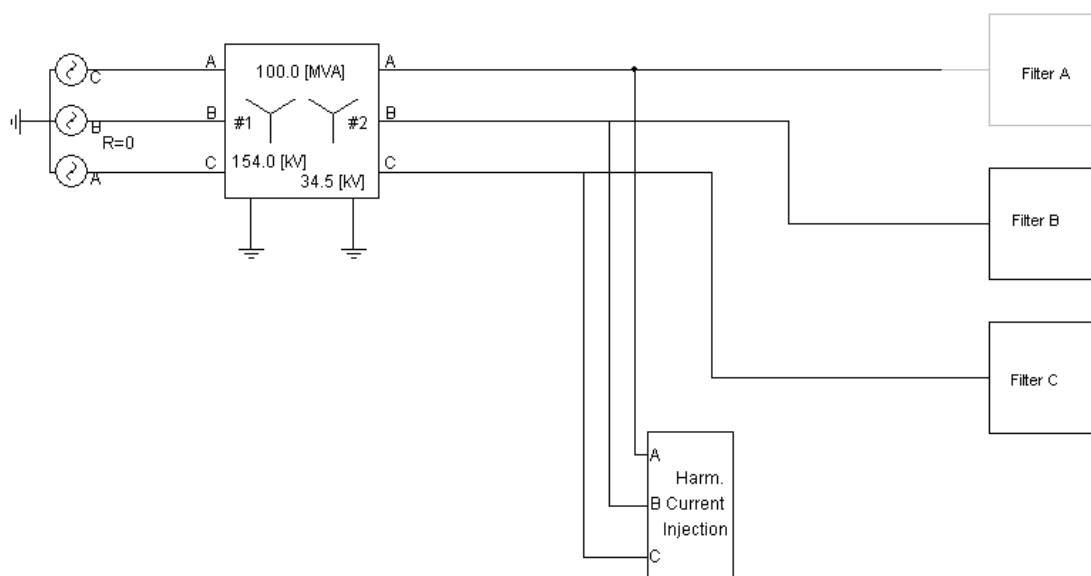


Figure 5.7 Schematic of the system.

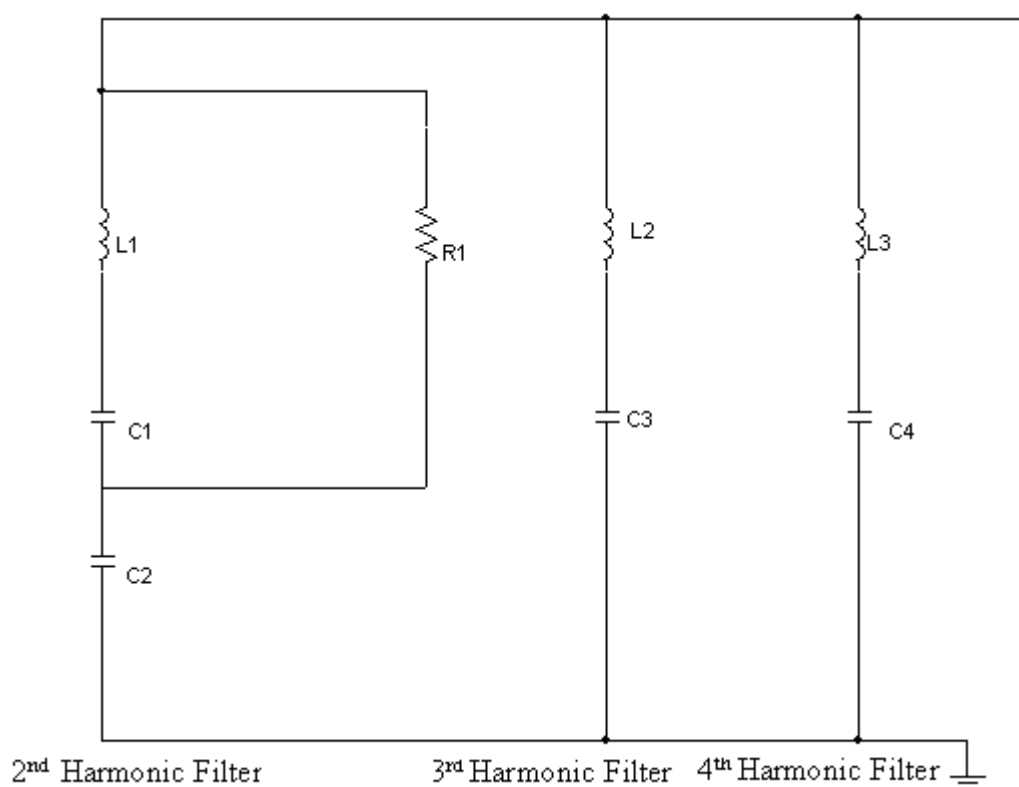


Figure 5.14 Filters of Plant2.

2nd harmonic current is injected to system at the value of 1000 Amp. And all of this current is absorbed by 2nd harmonic filter as shown figure 5.9.

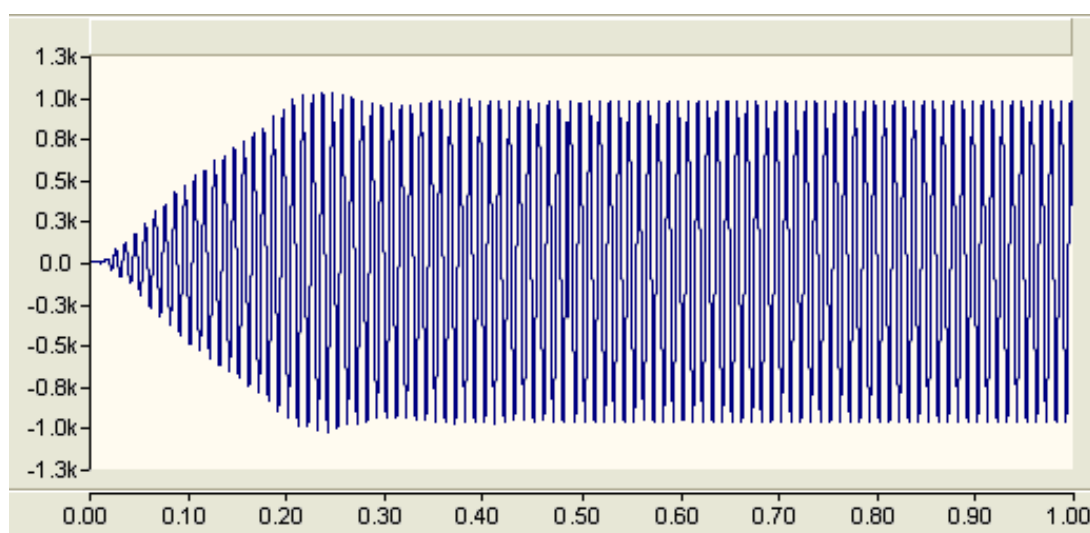


Figure 5.9 2nd Harmonic filter current.

3rd harmonic current is injected to system at the value of 1000 Amp. And all of this current is absorbed by 3rd harmonic filter as shown figure 5.10.

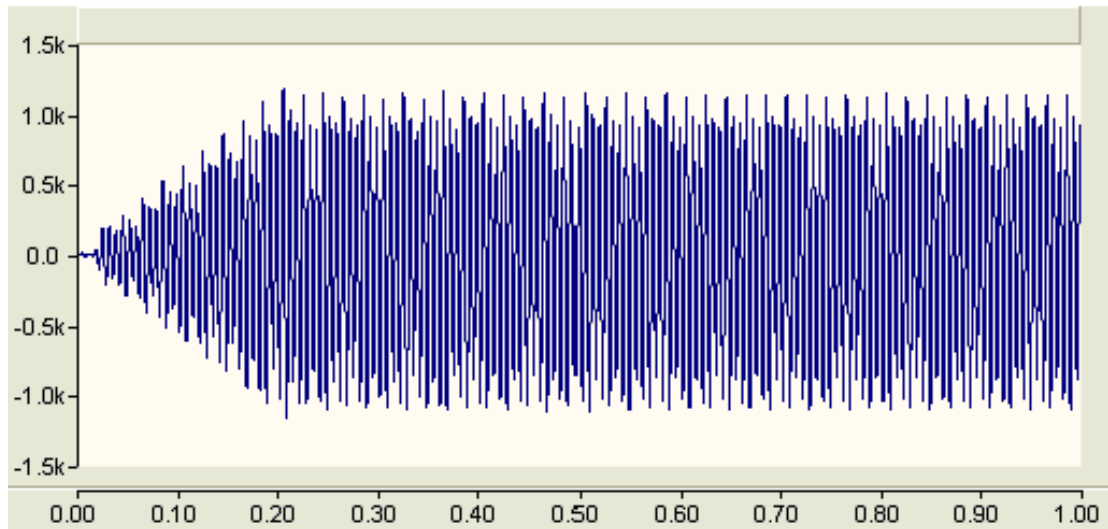


Figure 5.10 3rd Harmonic filter current.

4th harmonic current is injected to system at the value of 1000 Amp. And all of this current is absorbed by 4th harmonic filter as shown figure 5.11.

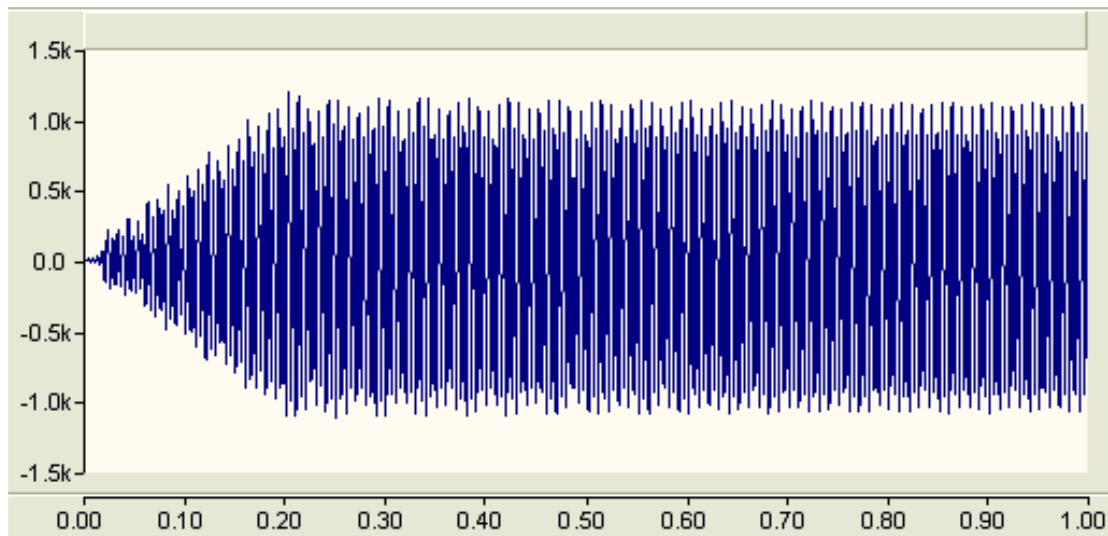


Figure 5.11 4th Harmonic filter current.

As a result of simulation of Plant2, in this plant the filters design are done better as shown figures 5.9, 5.10 and 5.11. Since harmonic current is injected by the load are not allowed to the source.

5.2 Frequency Response Of Passive Filters In Plant1 And Plant2

The simulation results of PSCAD show that some of passive filters are not designed properly to eliminate the harmonic currents in the source. Therefore, the frequency response of the circuits is investigated using MATLAB, since the PSCAD does not have this facility.

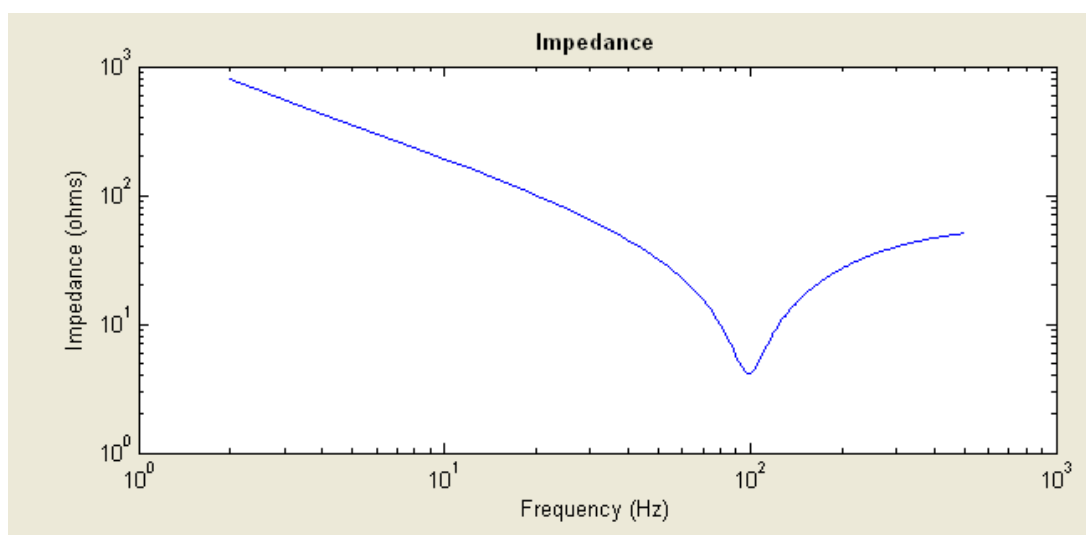


Figure 5.12 Impedance of 2nd harmonic filter.

The frequency response of 2nd harmonic filter shows that the minimum value of appears at 100 Hz with magnitude of 4 Ohm as shown figure 5.12. Since the minimum value is not small enough to take all current at 100 Hz, some value of it go to the source.

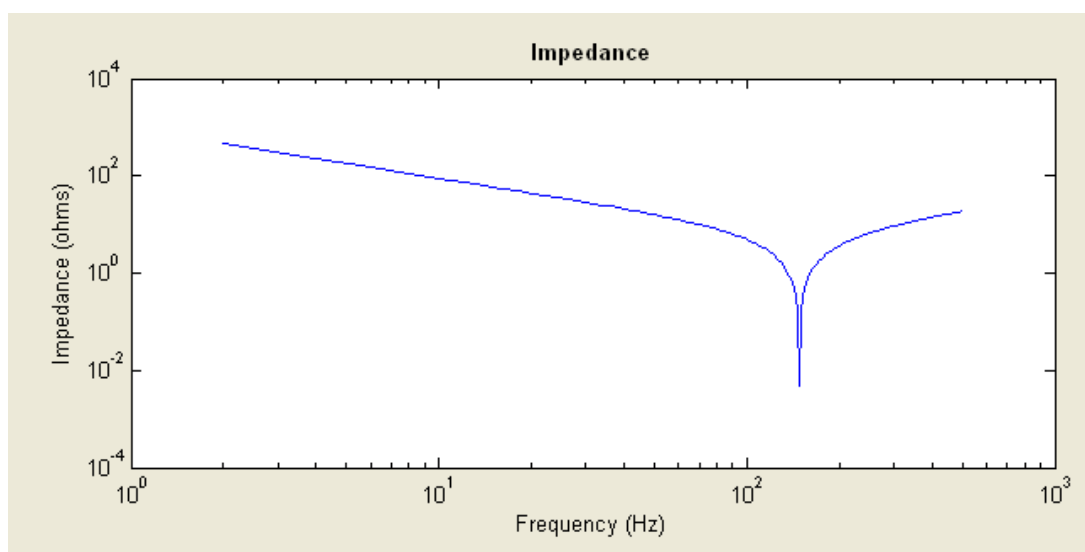


Figure 5.13 Impedance of 3rd harmonic filter.

The frequency response of 3rd harmonic filter shows that the magnitude of impedance is almost zero at 150 Hz. Therefore, all currents at this frequency are absorbed by the filter and not allowed to go to source.

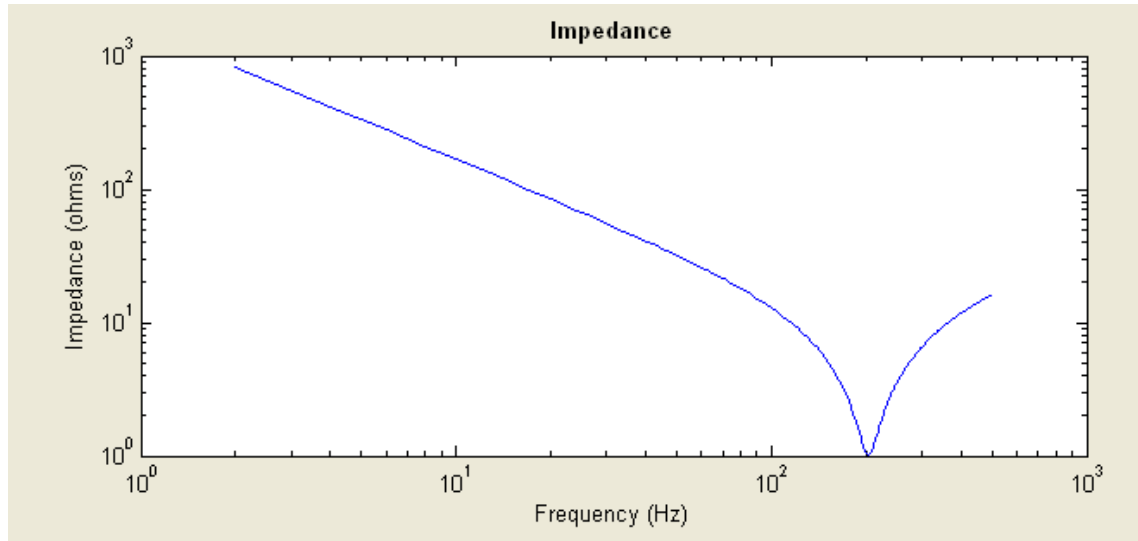


Figure 5.14 Impedance of 4th harmonic filter.

The frequency response of 4th harmonic filter shows that the magnitude of impedance is almost 1 Ohm and filter is taken almost all harmonic current at 200 Hz.

The second harmonic filter of Plant1 is redesigned by changing the resistor in parallel with L-C. The selected values are 120, 300, 400 and 600 Ohms. It should be noted that there two parallel resistance identical. Therefore the equivalent resistances are 60, 150, 200 and 300 Ohms.

Figures 5.15, 5.16, 5.17, 5.18 show the frequency response of the filters at the value of resistance. It is clear that the minimum impedance at 100 Hz decreases as the value of resistance increases.

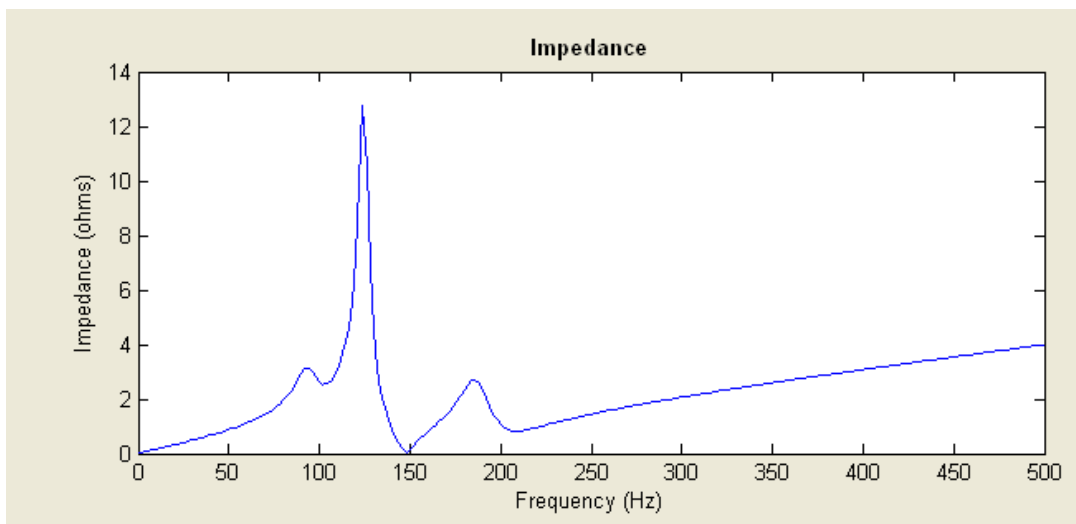


Figure 5.15 Impedance of all filter.

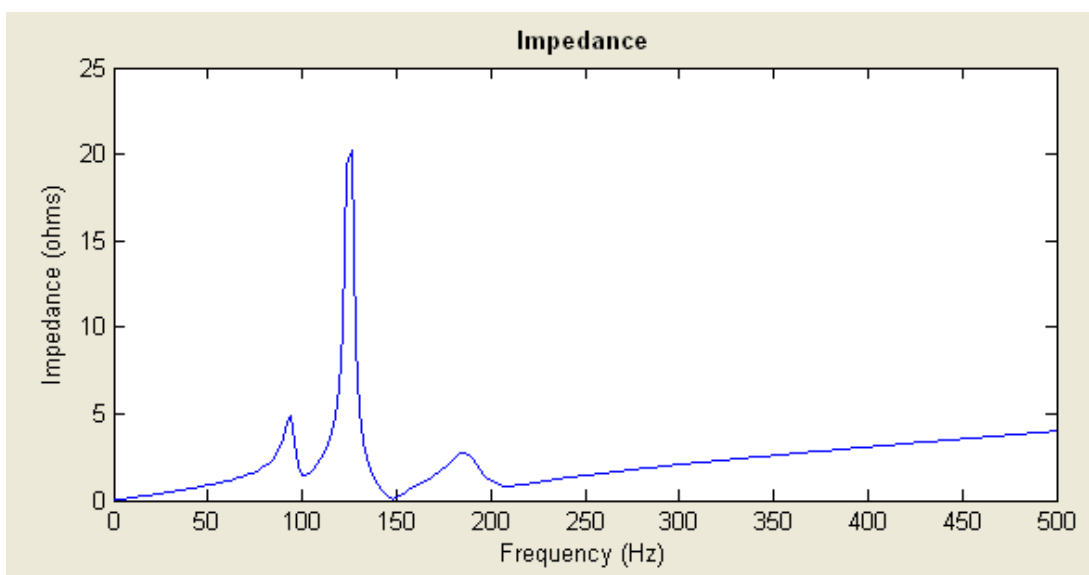


Figure 5.16 Impedance of all filter, Res = 150.

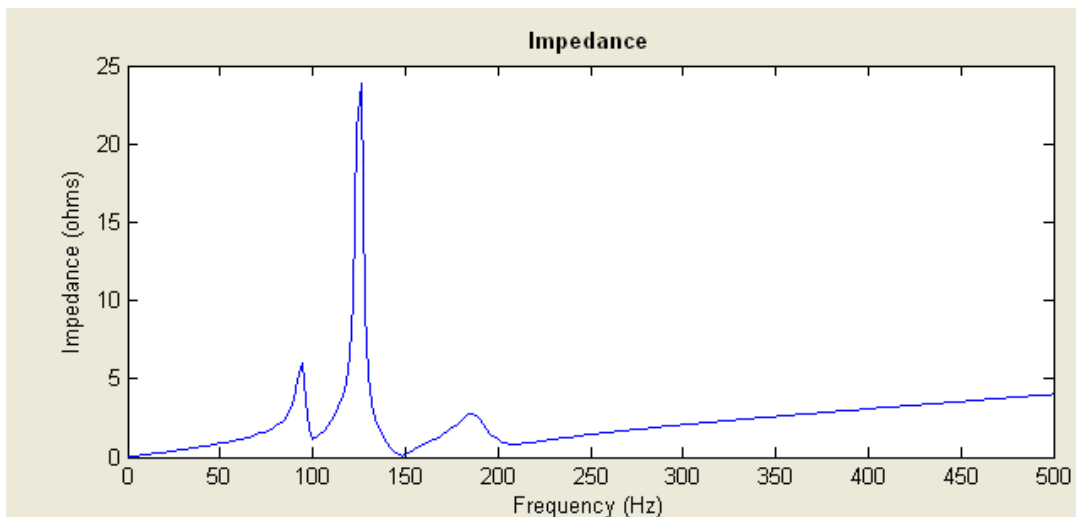


Figure 5.17 Impedance of all filter, Res = 200.

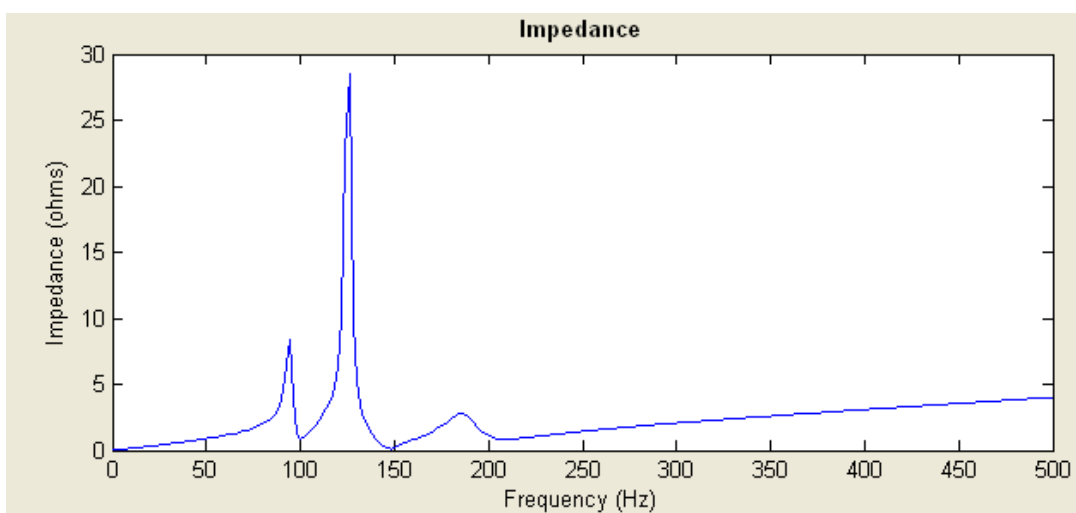


Figure 5.18 Impedance of all filter, Res = 300.

The frequency response of passive harmonic filter in Plant2 is also obtained in MATLAB and give in figure 5.18. It is clear that the minimum impedances at 100, 150 and 200 Hz are very low and proper to filter out the harmonics.

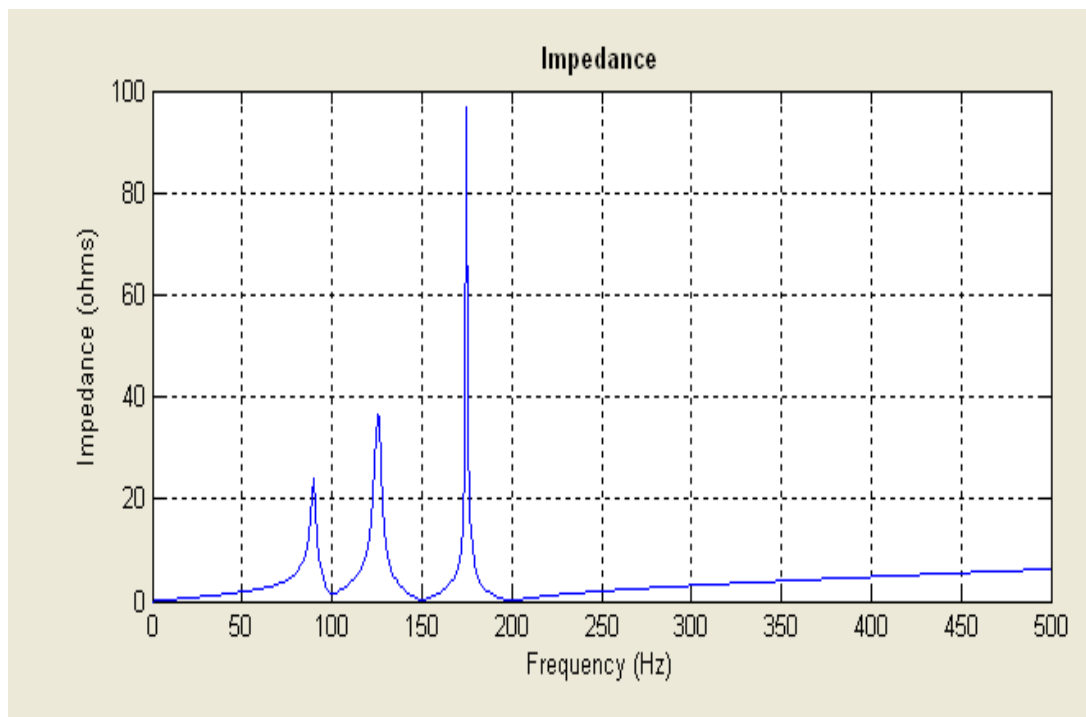


Figure 5.19 Impedance of all filter.

CHAPTER SIX

CONCLUSION

Thyristor controlled shunt compensators operate essentially as variable reactance (capacitive and inductive impedance). Functionally they can be divided into two classes: the first one is dynamic load balancing and power factor correction, the second one is terminal voltage balancing and voltage regulation.

The dynamic load balancing and power factor correction, which is the scope of this thesis, eliminates the negative sequence component (balancing) and the reactive part of positive sequence component (power factor correction).

When static compensation and dynamic compensation are compared, if the reactive power of the load is changing rapidly, fast response compensators are required. Therefore, the TCR compensators are preferred in these applications. Also if the load is unbalanced, the compensation is carried out by changing for each phase separately susceptances of TCR.

Thyristor control reactor is connected in delta so this structure generates harmonics, these harmonics are odd harmonics. They are available in phase current of TCR. In the line current of TCR, all the odd harmonics appear except triple harmonics and multiples of them.

REFERENCES

- Acha E., Agelidis V.G., Anaya-Lara O., & Miller T.J.E. (2002). *Power electronic Control in Electrical Systems*. Newnes.
- Dixon J., Moran L., Rodriguez J., & Domke R. (2005). Reactive power compensation technologies: State-of-the-art review. *Proceedings of the IEEE*, Vol.93, No.12, Page(s):2144-2164.
- Farias V. J. , de Oliveira J. C., Silveria J. C. P., & Miskulin M. S. (1991). Performance analysis of static TCR compensators for load balancing under asymmetrical voltages. *Transmission and Distribution Conference, Proceedings of the 1991 IEEE Power Engineering Society*, 22-27 Sept. 1991 Page(s):953 – 958
- Gyugyi L., & Taylor E. R. (1980). Characteristics of static, Thyristor-Controlled shunt compensators for power transmission system applications. *IEEE Transactions on Power Apparatus and Systems*, Vol. PAS-99, No. 5.
- Lee W., & Kim T. (2007). Control of the Thyristor-controlled Reactor for reactive power compensation and load balancing. *Industrial Electronics and Applications, ICIEA . 2nd IEEE Conference on*, page(s): 201–206.
- Miller T.J.E. (1982). *Reactive power control in electric systems*. USA: John Wiley&Sons.
- Mayordomo J. G., Izzeddine M., & Asensi R. (2002). Load and voltage balancing in harmonic power flows by means of static VAr compensators. *IEEE Transactions on Power Delivery*, Vol.17, No.3.
- Montano J.C., Gutierrez J., Castilla M., & Lopez A. (1993). Effect of harmonic distortion of the supply voltage on the optimum gating angle of a TCR-type compensation. *Power electronics Congress*, page(s):123-128.

Rashid, M. H. (2001). *Power Electronics Handbook*. California:Academic Press.

Tosato F., Quaia S., & Rabach G. (1989). Reactive power compensation by TCR technology : Simulation for large electrical loads control. *Electro technical conference*.